Structure-function relationships in the cytochrome bc_1 complex from *Saccharomyces cerevisiae*

Dissertation zur Erlangung
des Doktorgrades der Naturwissenschaften

vorgelegt beim Fachbereich 14
Chemische und Pharmazeutische Wissenschaften
der Johann Wolfgang Goethe-Universität
in Frankfurt am Main

von
Hildur Pálsdóttir
aus Reykjavík

Frankfurt am Main 2004
(DF1)

vom Fachbereich Chemische und Pharmazeutische Wissenschaften der
Johann Wolfgang Goethe-Universität als Dissertation angenommen.

Dekan : Prof. Dr. H. Schwalbe

Gutachter : Prof. Dr. H. Michel
Prof. Dr. B. Ludwig

Datum der Disputation

Diese Doktorarbeit wurde vom 15. August 2000 bis zum 30. Juli 2004 unter Leitung von Prof. Dr. Hartmut Michel und Dr. Carola Hunte im Abteilung für Molekulare Membranbiologie am Max-Planck Institute für Biophysik in Frankfurt am Main durchgeführt.

Eidesstattliche Erklärung

Hiermit versichere ich, dass ich die vorliegende Arbeit selbständig angefertigt habe und keine weiteren Hilfsmitten und Quellen als die hier aufgeführten verwendet habe.

Hildur Pálsdóttir
Berkeley, den 21. Oktober 2004

"Complex III is what the others want to be"

in memory of Matti Saraste

PUBLICATIONS

Palsdottir, H. and Hunte, C. (2003) Purification of the cytochrome bc_1 complex from yeast. In: Membrane Protein Purification and Crystallization - A practical guide. C. Hunte, G. von Jagow, and H. Schagger, Eds. Academic Press, Elsevier Science (USA), pp. 191-203.

Palsdottir, H., Lojero, C. G., Trumpower, B. L., and Hunte, C. (2003) Structure of the yeast cytochrome bc_1 complex with a hydroxyquinone anion Q_o site inhibitor bound. J Biol Chem 278: 31303-31311.

Hunte, C., Palsdottir, H., and Trumpower, B. L. (2003) Protonmotive pathways and mechanisms in the cytochrome bc_1 complex. FEBS Letters 545: 39-46.

Kessl, J. J., Lange, B. B., Merbitz-Zahradnik, T., Zwicker, K., Hill, P., Meunier, B., Palsdottir, H., Hunte, C., Meshnick, S., and Trumpower, B. L. (2003) Molecular basis for atovaquone binding to the cytochrome bc_1 complex. J Biol Chem 278: 31312-31318.

Ritter, M., Palsdottir, H., Abe, M., Mäntele, W., Hunte, C., Miyoshi, H., and Hellwig, P (2004). Direct Evidence for the Interaction of Stigmatellin with a Protonated Acidic Group in the bc_1 Complex from *Saccharomyces cerevisiae* As Monitored by FTIR Difference Spectroscopy and ^{13}C Specific Labeling. Biochemistry 43: 8439-8446.

Palsdottir, H. and Hunte, C. Lipids in membrane protein structures. Biochim Biophys Acta (*in press*).

TABLE OF CONTENTS

LIST OF FIGURES

LIST OF TABLES

ZUSAMMENFASSUNG

Das Hauptaugenmerk der hier vorgelegten Dissertation richtete sich auf die Aufklärung von Struktur-Funktions-Beziehungen in der Ubihydrochinon : Cytochrom *c* Oxidoreduktase, dem Cytochrom-bc_1-Komplex, aus *Saccharomyces cerevisiae*.

Der Cytochrom-bc_1-Komplex ist eine essentielle Komponente von Elektronentransportketten in Eukaryoten und Prokaryoten, wo er an verschiedenen bioenergetischen Prozessen wie der Atmungskette, der Photosynthese und der Stickstoffixierung beteiligt ist. Der Mechanismus dieses Enzyms ist in seinen Grundzügen charakterisiert und mit dem Model des modifizierten Q-Zyklus beschrieben. Jedoch sind Regulationsprozesse und insbesondere der molekulare Mechanismus der Ubichinoloxidation immer noch unverstanden. Weitere ungeklärte Punkte betreffen die Bewegung des Rieske-Proteins, die Verzweigung des Elektronentransfers, die Besetzung der Ubichinol-oxidierenden Bindungstasche und den Verlauf von Protonentransferwegen.

Die Fragestellung wurde mittels einer Kombination biophysikalischer Techniken, vor allem der Röntgenkristallographie, untersucht. Die aus den Proteinstrukturen gewonnen Informationen wurden mit funktionellen Aussagen aus kinetischen Studien und den Daten spektroskopischer Experimente, insbesondere der FTIR-Differenzspektroskopie, ergänzt.

Um den molekularen Mechanismus der Katalyse in der Q_o-Bindungsstelle zu untersuchen, wurde der Bindungsmodus des Q_o-Inhibitors HHDBT mittels der Röntgenkristallographie bestimmt (Palsdottir *et al*, 2003). Diese 2.5 Å Kristallstruktur (PDB-Eintrag: 1P84) erlaubte wichtige Rückschlüsse auf den Katalysemechanismus. Vorherigen kristallographischen Arbeiten am UHDBT-Inhibitorkomplex waren nicht erfolgreich und führten nicht zu einer hochaufgelösten Struktur. Unter Verwendung von Heptyl-HDBT, das eine kürzere Alkyl-Kettenlänge aufweist, wurden erfolgreich dreidimensionale Kristalle des Komplexes gezüchtet.

Die Bindung von Heptyl-HDBT an das Enzym wurde durch kinetische Studien in Kollaboration mit Prof. B. Trumpower charakterisiert. Eine wesentliche Information dabei war, dass dieses Hydroxychinon in seiner ionisierten Form bindet, entgegen vorherigen Behauptungen, eine ionisierte Verbindung könne nicht in der katalytischen Substrattasche binden (Zhang *et al*, 1999). Demnach weisen unsere Studien darauf hin, dass die pH-Abhängigkeit der alkyl-HDBT Inhibierung durch eine dissoziierbare

Gruppe im Komplex, vermutlich den Liganden des [Fe-2S]-Zentrums His181, bewirkt wird und nicht durch eine Verringerung der Inhibitoreffizienz durch Deprotonierung der Hydroxylgruppe. Die strukturelle Ähnlichkeit zu Ubichinol und die kompetitive Hemmung der Q_o-Bindungsstelle erlauben es, HHDBT als Substratanalogon zu betrachten.

Die Konformationsänderungen an der Bindungsstelle unterstützen den zuvor postulierten Protonentransferweg und offenbaren die Plastizität der katalytischen Bindungsstelle. $Glu272^{Copb}$ ist ein primärer Ligand der Hydroxylgruppe von Stigmatellin, wie im röntgenkristallographischen Strukturmodell gezeigt wurde (Hunte *et al.*, 2000). Die Seitenkette rotiert von der Bindungsstelle weg, wenn die Hydroxylgruppe des Stigmatellins durch die Carbonylgruppe von HHDBT ersetzt wird (Palsdottir *et al.*, 2003). Die beobachtete Rotation von Glu272 bestätigte den vorgeschlagenen Protonentransferweg, zusammen mit der wichtigen Beobachtung, dass das Glu272-Carboxylat in der neuen Orientierung über ein Wassermolekül direkt mit dem Häm-Propionat A verbunden ist. Vom Propionat A aus können Protonen über ein kurzes Netzwerk von Wasserstoffbrücken, das strukturelle Wassermoleküle einbindet, zum Intermembranraum transferiert werden (Palsdottir *et al.*, 2003). Aus dem beobachteten Bindungsmodus des Hydroxychinon-Anions und dem Protonentransferweg wurde ein katalytischer Mechanismus abgeleitet, der sich mit dem Modell einer einfachen Besetzung der Ubichinol-Oxidationstasche in Einklang bringen lässt. Die aus der Struktur hergeleiteten funktionellen Rückschlüsse werden diskutiert (Palsdottir *et al.*, 2003).

Um das vorgeschlagene mechanistische Modell zu überprüfen, wurde die FTIR-Spektroskopie in Kollaboration mit Dr. P. Hellwig eingesetzt (Ritter *et al.*, 2004). Diese Studie zeigte zum ersten Mal, dass die Bindung der Inhibitoren HHDBT und Stigmatellin den Protonierungszustand und/oder die Orientierung von sauren Seitenketten beeinflusst. Des weiteren wurde die Interaktion der Stigmatellin Carbonylgruppe mit dem Enzym nachgewiesen.

In Zusammenarbeit mit Prof. M. Ullmann wurden elektrostatische Berechnungen an den atomaren Koordinaten des Cytochrom-bc_1-Komplexes mit gebundenem HHDBT in der Q_o-Bindungsstelle durchgeführt. Vorläufige Ergebnisse dieser theoretischen Untersuchung, besonders im Hinblick auf die Protonierungswahrscheinlichkeit funktionell relevanter Aminosäurereste wurden diskutiert (*Diplomarbeit, A. Klingen*).

Bei einem Vergleich von Cytochrom-bc_1-Komplex Strukturen von Hefe und Rind, mit verschiedenem Besetzungsgrad der Chinon-Bindungsstellen wurde die Plastizität der Q_o-Bindungsstelle beobachtet. Die Bindung des Q_o-Bindungsstellen Inhibitors verursacht folgende Konformationsänderungen in den Cytochrom *b* Domänen: die cd_1 Helix und der *ef* Loop einschließlich der Seitenkette des Tyr279 bewegen sich und führen zu einer Aufweitung der Bindungstasche. Diese Konformationsänderungen gehen mit einer Domino-ähnlichen Verschiebung des Wasserstoffbrückennetzwerkes einher. Die Reorientierung der Aminosäurereste in Abhängigkeit der Besetzung der Q_o-Bindungsstelle wurde unter funktionellen Gesichtspunkten diskutiert.

Ein weiteres Ergebnis der Doktorarbeit war die Optimierung der Proteinreinigung im Hinblick auf eine geringere Delipidierung der Proteinprobe und eine vergrößerte Kapazität. Dabei wurde, verglichen zu den früheren Präparationen, die Ausbeute verbessert sowie die spezifische Enzymaktivität des gereinigten Proteins erhöht. Der Lipid-Gehalt wurde durch die geringere Exposition des Proteins gegenüber Detergenz-haltigen Medien erhöht. So konnten zwei neue Phospholipidmoleküle reproduzierbar in unterschiedlichen Datensätzen identifiziert werden. Die Position eines dieser Phospholipide an der Oberfläche der Q_o-Bindungsstelle ist der äußeren Lipidschicht der Doppelmembran zuzuordnen und erlaubte zusammen mit den zuvor identifizierten Phopholipiden von der Matrixseite eine vertikale Positionierung des Komplexes in der Membran. Darüber hinaus wird die Bindung eines Cardiolipins an der Dimergrenzfläche beschrieben.

Die in der Kristallstruktur identifizierten, spezifisch gebundenen Phospholipide, die an Interaktionsflächen von Proteinuntereinheiten auftreten, weisen auf eine wichtige Rolle für die strukturelle Integrität des Komplexes hin. Eine vergleichende Analyse der Lipidbindungsstellen in Strukturen homologer Proteine wurde durchgeführt und zeigte, dass sie Spezies-übergreifend konserviert sind (Palsdottir und Hunte, *in Druck*). Eine Überlagerung der Strukturen des Cytochrom-bc_1-Komplexes aus Hefe und Huhn zeigte konservierte Bindungsstellen für die spezifisch gebundenen Lipid- und Detergenzmoleküle. Vielleicht noch erstaunlicher sind die lipidangereicherten Kavitäten, die beim Vergleich der Strukturen von mitochondrialen Cytochrom-bc_1-Komplexen mit den Röntgenkristallstrukturen des Cytochrom-b_6f-Komplex beobachtet wurden. Eine Analyse des Bindungsmodus von fest gebundenen Lipiden in Membranproteinstrukturen wurde durchgeführt. Es wurden hierbei

spezifische Bindungsmuster für die Stabilisierung der Interaktionen zwischen den Phosphodiestergruppen und den Seitenketten der Aminosäurereste identifiziert. Eine bevorzugte Stabilisierung der Phospholipide auf der negativen Seite der Membranen wurde beobachtet. Ein erster Versuch wurde unternommen, um spezifische Motive für Lipidkopfgruppenbindung zu identifizieren.

Es wurden Prüfstrategien entwickelt, um sowohl den Cytochrom-bc_1-Komplex als auch das Fv-Fragment auf seine Qualität zu überprüfen. Ein *magnetic beads pull down assay* wurde für den analytischen Test der Bildung des Ko-Komplexes aus Antikörper-Fv-Fragmenten und Cytochrom-bc_1-Komplexes etabliert. Es wurde eine detaillierte strukturelle Charakterisierung des Rieske-Epitops, das von dem Fv-Fragment erkannt wird, durchgeführt. Die Spezies-Spezifität in der Erkennung der antigenen Determinante wurde experimentell bestätigt. Daraufhin wurde ein Projekt in Zusammenarbeit mit der Arbeitsgruppe von Herrn Prof. B. Ludwig (*Diplomarbeit, T. Kleinschroth*) initiiert, mit der Aufgabe das Epitop der Hefe auf ein bakterielles Rieske-Protein zu übertragen. Das Ziel dieses Projekts ist die Konstruktion eines bakteriellen Cytochrom-bc_1-Komplexes, der sich zur Fv-Fragment-vermittelten, dreidimensionalen Kristallisation eignet.

Die Röntgenkristallstrukturen der Hefe Cytochrom-bc_1-Komplexe mit gebundenen HHDBT oder Stigmatellin in der Q_o-Bindungsstelle sind wertvoll, um Einsichten in den molekularen Mechanismus und die molekulare Architektur des katalytischen Zentrums zu erhalten. Außerdem ist die strukturelle Analyse dieser hoch konservierten Enzyme wichtig, um die molekularen Ursachen menschlicher Krankheiten zu verstehen, die auf Mutationen im Cytochrom *b* zurückzuführen sind. Ebenfalls von großer Bedeutung sind diese Strukturen für die gezielte Entwicklung von Pestiziden oder pharmazeutischen Wirkstoffen, die gegen das aktive Zentrum der Komplexe in Parasiten oder Pilzen gerichtet sind. Zielorganismen entwickeln oft eine Resistenz gegenüber diesen Wirkstoffen.

Basierend auf dem HHDBT Bindungsmodus in der Q_o-Bindungsstelle wurde die Interaktion mit dem Antimalariawirkstoff Atovaquone modelliert. Die strukturellen Grundlagen von dessen Spezies-spezifischer Wirkung können so diskutiert werden. Weiterhin dienen Sequenzanalysen in Kombination mit strukturellen Studien der Untersuchung von auftretenden Resistenzen gegenüber der Inhibitoren der Q_o-Bindungsstelle (Kessl *et al*., 2003).

Die Röntgenstrukturen des Cytochrom-bc_1-Komplexes bieten die Grundlage für detaillierte Struktur-Funktions-Studien zur Beschreibung der molekularen katalytischen Vorgänge. Sie fördern aufregende Entdeckungen für das tiefere Verständnis der fundamentalen Prozesse des Lebens, welche durch diesen Typ der Enzyme katalysiert werden.

ABSTRACT

This dissertation is a study of the structure and function of the cytochrome bc_1 complex from the yeast *Saccharomyces cerevisiae*. This enzyme operates in all kingdoms of life and is a cornerstone in bioenergetic electron transfer chains, where it carries out tasks as diverse as respiration, photosynthesis, and nitrogen fixation. This homodimeric multisubunit membrane protein has been studied extensively for several decades and the enzyme mechanism is described with the modified protonmotive Q cycle. Still, the molecular and kinetic description of the catalytic cycle is not complete and questions remain regarding the bifurcation of electron transfer at the quinol oxidation (Q_o) site, substrate occupancy, pathways of proton conduction, and the nature of the Rieske protein domain movement.

We used competitive inhibitors to study the molecular architecture at the Q_o site with X-ray crystallography. The structure of the enzyme with the substrate analog 5-*n*-heptyl-6-hydroxy-4,7-dioxobenzothiazole (HHDBT) bound at the Q_o site was determined at 2.5 Å resolution. Spectroscopic studies showed that HHDBT is negatively charged when bound at the active site. Mechanistic interpretations from inhibitor binding are in line with single occupancy model for quinol oxidation and structural analysis supports the proposed proton transfer pathway. For functional insight into the enzyme mechanism, redox-sensitive protonation changes were studied by Fourier transform infrared spectroscopy.

The protein purification procedure was optimized for less delipidation and the isolated enzyme was more active. Furthermore, two new phospholipids were identified in the X-ray structures, including a cardiolipin. Strikingly, conserved lipid binding cavities were observed in structural comparison with homologous enzymes. The functional role of tightly bound phospholipids will be discussed.

Finally, the Q_o site is a target for various compounds of agricultural and pharmaceutical importance. Importantly, the X-ray structures permit detailed analysis of the molecular reasons for acquired resistance to and treatment failure of Q_o site inhibitors, such as atovaquone, that is used to treat malaria and pneumonia, as discussed herein.

1. INTRODUCTION

1.1 Biological energy conversion and oxidative phosphorylation

The enzymes that drive cellular energy production are highly conserved throughout the kingdoms of life. Before the atmosphere was enriched with O_2, the early anaerobic life forms displayed a large repertoire of energy transduction mechanisms (see Schopf, 1994; Berry, 2002). Less variation is observed in the building blocks that construct the molecular machines that carry out oxidative phosphorylation and oxygenic photosynthesis. The organelles that host these essential bioenergetic processes, namely mitochondria and chloroplasts, are suggested to be remnants of ancient bacteria, which were engulfed and integrated by endosymbiosis (see Margulis, 1981). The endosymbiosis hypothesis is supported by the remarkable similarity of the photosynthetic machinery of cyanobacteria and plant chloroplasts. Likewise, the mitochondrial enzymes involved in oxidative phosphorylation are highly conserved (see Saraste, 1999; Schultz and Chan, 2001).

Regardless of metabolic diversity, the common principle in bioenergetics is the establishment of a chemiosmotic gradient across biological membranes. The conceptual breakthrough of a protonmotive force, first proposed in the chemiosmotic hypothesis by Mitchell (1961), terminated the search for an organic compound linking oxidation of metabolites and ATP production. Instead the protonmotive force was proposed to comprise electrogenic separation of charges and a pH gradient across insulating membranes.

In aerobic life, the great majority of cellular energy is produced by oxidative phosphorylation which yields adenosine triphosphate (ATP). In eukaryotes, mitochondria are specialized for this task. An outer membrane and a highly folded inner mitochondrial membrane enclose the enzyme-saturated matrix (Fig. 1B). The respiratory electron transfer chain resides in the inner mitochondrial membrane and is typically composed of four multisubunit membrane protein complexes (complexes I-IV) (Fig. 1C). Electron transfer through these membrane bound enzymes is achieved by cofactors of distinct redox midpoint potentials (E_m), that are configured to harvest the free energy from oxidation of metabolites in a process that facilitates proton translocation.

Cytosolic oxidation of carbohydrates, commonly known as glycolysis, terminates in the dehydrogenase catalyzed decarboxylation of pyruvate to acetylCoA (AcCoA), a reaction that takes place in the mitochondrial matrix. AcCoA is also a terminal product of fatty acid oxidation. Enzymes of the citric acid cycle (*i.e.* Krebs cycle) oxidize AcCoA to CO_2 in stepwise reactions, and thereby reduce three nicotinamide adenine dinucleotide (NADH) and one flavin adenine dinucleotide ($FADH_2$) per cycle. NADH is the substrate for Complex I (NADH:ubiquinone oxidoreductase), whereas $FADH_2$ is intrinsic to the only membrane bound component of the citric acid cycle, or Complex II (Succinate:ubiquinone oxidoreductase, SQR). Complex I and II reduce the lipophilic two electron-two proton carrier, ubiquinol, which is the substrate of the third respiratory complex, the cytochrome bc_1 complex [E.C.1.10.2.2, Ubiquinol: cytochrome *c* oxidoreductase]. Complex III reduces the soluble cytochrome *c* in the intermembrane space, which is the substrate of Complex IV, or cytochrome *c* oxidase, that finally reduces oxygen to H_2O. Electron transfer through Complexes I, III and IV is coupled to translocation of protons across the inner mitochondrial membrane. The established gradient of protons drives ATP production by the thermodynamically feasible backward flow through Complex V, the reversible F_1-F_0 ATP synthase.

The yeast *Saccharomyces cerevisiae* is a suitable model organism to study the respiratory chain. It is easy to cultivate, the genome has been sequenced (Goffeau *et al*., 1996) and it is accessible to genetic manipulation. Furthermore, it is facultative anaerob organism, and therefore it is possible to grow respiratory deficient variants on fermentable carbon sources.

In *S. cerevisiae*, Complex I is lacking, but its function in reducing ubiquinone is supplemented by alternative NADH dehydrogenases (de Vries and Grivell, 1988; Marres *et al*., 1991; Small and McAlister-Henn, 1998). These alternative dehydrogenses, however, do not translocate protons (see Joseph-Horne *et al*., 2001).

1.2 The cytochrome bc_1 complex catalysis

Cytochrome *bc* complexes are versatile enzymes found in most niches of life, where they operate in tasks as diverse as respiration, bacterial nitrogen fixation, denitrification, and together with the bacterial reaction center in light driven electron transfer (see Berry *et al.*, 2000). In thylakoids and cyanobacterial plasma membrane, a homologous enzyme, cytochrome b_6f complex, functions in oxygenic photosynthesis.

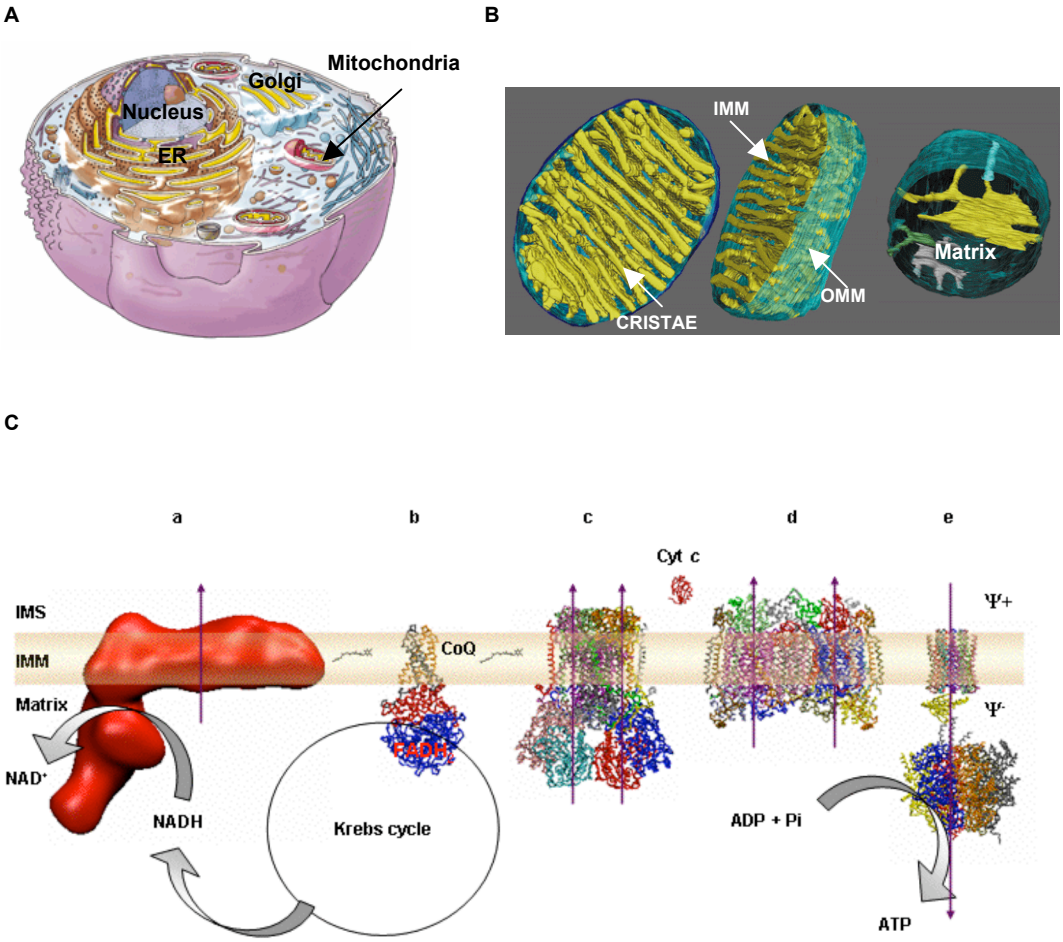

Fig.1 Oxidative phosphorylation in mitochondria. ***A,*** *schematic overview of an eukaryotic cell.* ***B****, mitochondria, the organelles responsible for cellular energy production, exhibit different shapes and sizes. 3D imaging of mitochondrial morphology has extended the schematic "baffle model" to include more complex invaginations of the inner mitochondrial membrane (IMM). Shown are electron microscopy tomographic reconstructions of dendritic mitochondrion from chick cerebellum (Frey and Mannella, 2000). The highly folded IMM forms cristae (Palade, 1952), which increase the surface area for respiration to take place.* ***C,*** *structural overview of oxidative phosphorylation (OXPHOS). Except for Complex I, the components of OXPHOS have been structurally characterized by X-ray crystallography:* ***a)*** *structural insight and subunit assignment in Complex I relies so far on electron microscopy and single particle analysis (e.g. Zickermann et al., 2003; Peng et al., 2003; Friedrich and Bottcher, 2004). Shown here is a single particle reconstruction of complex I from the obligate aerob fungi, Y. lipolytica (kindly provided by M. Bostina),* ***b)*** *X-ray structure of the mitochondrial Complex II is not available, shown here is a monomer from the X-ray structure of the homologous enzyme from E. coli (pdb entry 1NEK),* ***c)*** *Complex III from S. cerevisiae mitochondria (pdb entry 1KB9),* ***d)*** *Complex IV from bovine heart mitochondria (pdb entry 1V54),* ***e)*** *Complex V from S. cerevisiae mitochondria (pdb entry 1QO1). In the intermembrane space (IMS) the soluble electron carrier cytochrome c (cyt c) (from pdb entry 1KYO) is shown. The lipophilic electron carrier CoQ diffuses within the IMM and connects complexes I, II and III. The Krebs cycle products NADH and* $FADH_2$ *fuel the respiratory chain. The purple arrows show the direction of proton translocation across the membrane.*

The protonmotive Q cycle was first proposed to describe cytochrome bc_1 complex catalysis by Mitchell (1975, 1976). Subsequently, extensive research into the enzyme mechanism has yielded a reaction scheme termed 'the modified protonmotive Q cycle' (*e.g.* Crofts and Meinhardt, 1983; Crofts and Wang, 1989; Trumpower, 1990; Crofts, 2003). The overall chemical equation is well understood. In short, quinone is reduced at the Q_i site with uptake of protons from the matrix. In contrast, protons are released on the intermembrane side when quinol is oxidized at the Q_o site (see Fig. 2). Despite decades of research efforts to understand the enzyme mechanism, detailed molecular and kinetic description of the reaction cycle, especially at the Q_o site, is still lacking.

Quinol oxidation involves the highly debated bifurcated electron transfer reaction. One electron is passed via the high potential electron transfer chain, from the [2Fe-2S] cluster to heme c_1. Surprisingly, the second electron travels a thermodynamically less favorable route and is recycled within the enzyme. It is transferred via the two *b* type hemes to reduce quinone at the Q_i site. The resulting stable semiquinone at the Q_i site, is fully reduced after a second quinol molecule is oxidized at the Q_o site.

1.3 Isolation of the cytochrome bc_1 complex and supercomplex formation

The first methods to purify the cytochrome bc_1 complex were based on bile salt detergent solubilization and differential ammonium sulfate precipitation (Rieske, 1976; Siedow *et al.*, 1978; Yu *et al.*, 1974). Also, chromatographic approaches, such as hydroxyapatite chromatography with Triton X-100 (Engel *et al.*, 1980; Riccio *et al.*, 1977) and anion-exchange chromatography of dodecyl-maltopyranoside solubilized protein (Berry and Trumpower, 1985) were successfully applied. The latter procedure has been modified and optimized for preparations from diverse sources, including animals (Ljungdahl *et al.*, 1987), plants (Berry *et al.*, 1991), bacteria (Montoya *et al.*, 1999), and fungi (Hunte *et al.*, 2000; Palsdottir and Hunte, 2003).

Although the components of the respiratory chain are active as isolated complexes, there is growing evidence for their supramolecular organization in the membrane, the 'respirasome' (Schägger and Pfeiffer, 2000). Early isolation protocols provided the first evidence that the respiratory chain assembles into supercomplexes. Complex II and III were co-purified (Yu *et al.*, 1974) and complex III and IV were

isolated together (Cruciat *et al*., 2000). Blue native polyacrylamide gel electrophoresis (BN-PAGE) of digitonin extracts suggested specific assemblies of OXPHOS system components in both bacterial and mitochondrial membranes (see Schägger, 2002). In disagreement with results from mutagenesis studies (Bruel *et al*., 1996), BN-PAGE analysis of mitochondrial membranes from yeast failed to reveal a stable supercomplex between complex II and complex III (Schägger and Pfeiffer, 2000). However, strong evidence for physical interactions between Complex II, III and IV comes from inhibitor titration studies. The observed absence of pool function for CoQ and cytochrome *c* under physiological conditions suggests that the respiratory chain forms a functional unit in yeast (Boumans *et al.*, 1998).

1.4 Structural characterization of the cytochrome bc_1 complex

From the total of 10 subunits, which construct a monomer in yeast, 3 carry redox centers and are essential for catalysis: cytochrome *b* with two *b*-type hemes, cytochrome c_1 with the *c*-type heme, and the Rieske protein, which contains an [2Fe-2S] iron-sulfur cluster. The first electron micrographs of the cytochrome bc_1 complex showed that the enzyme was a homodimer (see Weiss *et al*., 1987; Weiss *et al*., 1990). A functional unit in catalysis is composed of the soluble Rieske protein domain, which interacts with cytochrome *b* and cytochrome c_1 from the other monomer. X-ray structures of the enzyme at a resolution 3 Å or better were available by the late nineties (Xia *et al.*, 1997; Zhang *et al*., 1998; Iwata *et al*., 1998; Hunte *et al*., 2000). Importantly, the large-scale domain movement necessary for electron transfer from Rieske to cytochrome c_1 was first visualized in the X-ray structures (Zhang *et al*., 1998). The X-ray structure determination of the cytochrome bc_1 complex from *S. cerevisiae* was facilitated by the antibody Fv fragment 18E11 and yielded 2.3 Å resolution (Hunte *et al*., 2000), the highest resolution currently available.

The cytochrome *c* oxidase from the soil bacterium *Paracoccus denitrificans* was the first example of Fv fragment mediated 3-D crystallization (Ostermeier *et al.*, 1995; Iwata *et al.*, 1995). The antibody fragment Fv7E2 was first used to crystallize the four subunit enzyme and its versatility was manifest in subsequent structure determination of the two subunit catalytic core (Ostermeier *et al*., 1997). Further usefulness of antibody-based crystallization enhancers is illustrated in the recent Fab-mediated X-ray structure determination of the potassium channel KcsA (Zhou *et al.*,

2001), the voltage-dependent potassium channel KvAP (Jiang *et al*., 2003), and the ClC chloride channel (Dutzler *et al.*, 2003).

The yeast cytochrome bc_1-Fv18E11 co-complex crystallized in space group C2, with a monomer in the asymmetric unit. The recent structure determination to 2.97 Å resolution of the ternary complex with the substrate cytochrome *c* co-crystallized with the Fv-bc_1 co-complex, yielded a different crystal packing, with a dimer in the asymmetric unit (Lange and Hunte, 2002). Interestingly, a single cytochrome *c* was bound per dimer. The X-ray structure of the homodimeric yeast cytochrome bc_1 complex consists of nine subunits per monomer (Fig. 3) with 24 transmembrane helices (TM) (Table 1). The tenth and most basic subunit, Qcr10p, is removed during the anion exchange chromatography (Hunte *et al*., 2000). The bacterial enzyme is structurally simpler and consists only of the homodimeric catalytic core (see Berry and Huang, 2003). Similarly, other bacterial respiratory enzymes, for instance Complex I, are present in the minimal form, and supernumerary subunits appear to be acquired as recent events in the evolution of the mitochondrial counterparts (see Brandt *et al*., 2002). Many of the accessory, *i.e.* non-catalytic, subunits are non-essential, but rather appear to guide assembly and/or enforce stability. This function could be dictated by structure, rather than sequence-specific traits. For instance, the cytochrome bc_1 complex subunit 10 (Qcr10p) in the yeast and bovine enzymes, lack sequence similarity (Brandt *et al*., 1994). Still, both subunits contain one transmembrane helix and charged extramembraneous domains and are therefore suggested to serve similar structural roles.

Table 1 Subunit composition of the yeast cytochrome bc_1 complex.

Subunit	Abbr.	Topology	Function
Cytochrome *b*	Cobp	8 TM	Catalytic, essential
Cytochrome c_1	Cyt1p	1 TM, IMS	Catalytic, essential
Rieske	Rip1p	1 TM, IMS	Catalytic, essential
Core I	Cor1p	Matrix	Assembly, proteolytic protection, pI~6
Core II	Qcr2p	Matrix	Assembly, proteolytic protection, pI~6
Subunit VI	Qcr6p	IMS	Thermal stability, pI<4
Subunit VII	Qcr7p	Matrix	Biogenesis, essential, pI~6
Subunit VIII	Qcr8p	1 TM	Biogenesis, essential
Subunit IX	Qcr9p	1 TM	Thermal stability
Subunit X	Qcr10p	1 TM	Stability

pI values were only calculated for the peripheral subunits. Functional aspects regarding catalysis, assembly and stability are discussed in text. Nomenclature, i.e. abbreviations (Abbr.) for subunits, was adapted from the Yeast Protein Database (YPD).

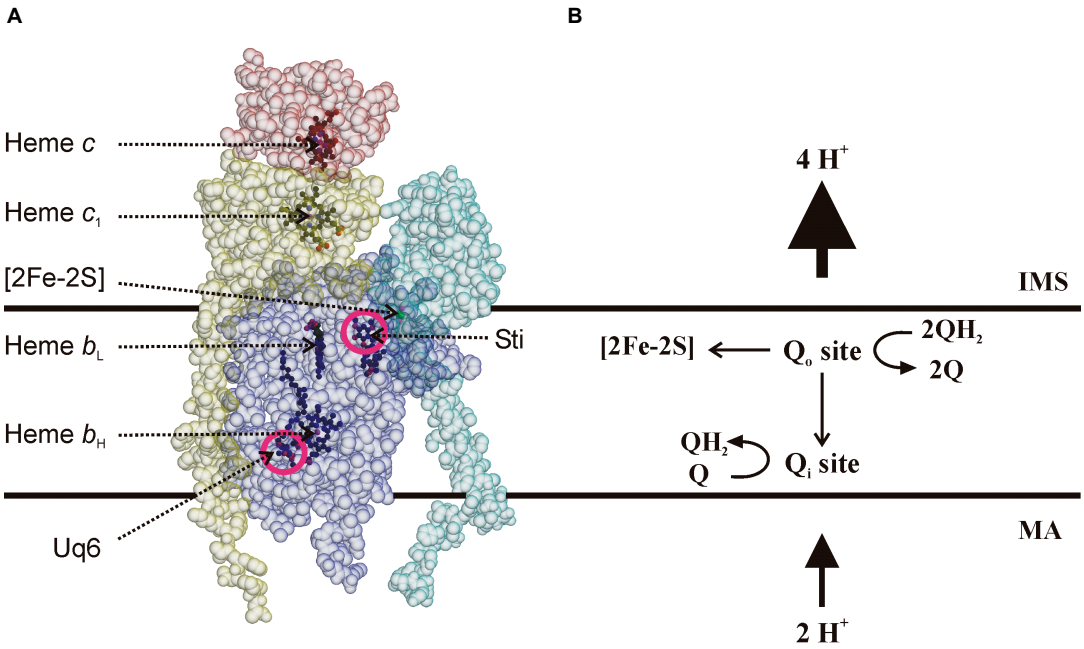

Fig.2 The modified protonmotive Q cycle. A, *the functional unit is shown with the three catalytic subunits: cytochrome b (blue) and cytochrome c_1 (yellow) from one monomer, which interact with Rieske (cyan) from the other monomer. The position of cytochrome c (red) is shown as refined in the X-ray structure of the ternary complex (pdb entry 1KYO). The Q_o site occupied by stigmatellin (Sti) and the Q_i site with ubiquinone (Uq6) bound are encircled (magenta).* ***B****, the protonmotive Q cycle is depicted on the right. Ubiquinol carries protons from the mitochondrial matrix (MA) to the intermembrane space (IMS).*

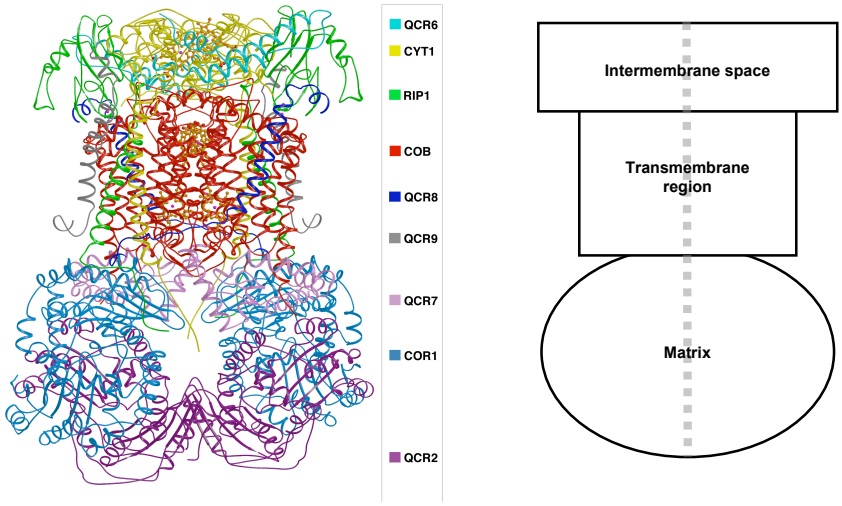

Fig.3 Structural overview of the yeast cytochrome bc_1 complex *(Hunte et al., 2000).*

The 7-8 accessory subunits in the mitochondrial cytochrome bc_1 complexes have proposed roles in regulation, assembly, and stability (di Rago *et al*., 1997; Zara *et al*., 2004) (Table 1). Assembly of the homodimer occurs by congregation of precomplexes, guided by chaperones (Cruciat *et al*., 1999). A precomplex of cytochrome *b*, subunit 8 (Qcr8p) and subunit 7 (Qcr7p) integrates a subcomplex of the two core proteins, Core 1 (Cor1p) and Core 2 (Qcr2p) (Lee *et al*., 2001). The peripheral Cor1p and Qcr2p proteins are homologous to the α and β subunits of the matrix processing peptidases (MPPs), respectively, but have lost MPP activity in yeast. The core proteins appear important for assembly of the complex (Tzagoloff *et al*., 1986; Oudshoorn *et al*., 1987). Qcr7p and Qcr8p deletion mutants are respiratory deficient irrespective of temperature (Schoppink *et al*., 1989; Maarse *et al*., 1988). Yeast deletion mutants have shown that absence of any one of the subunits cytochrome *b*, Qcr7p, or Qcr8p, induces loss of the other two (Zara *et al*., 2004).

A catalytic function of Qcr6p in guiding cytochrome *c* docking on the cytochrome c_1 has been proposed (Kim and King, 1983). Furthermore, in the absence of subunit 6 (Qcr6p), maturation of cytochrome c_1 is blocked (Yang and Trumpower, 1994). Interestingly, deletion of Qcr6p was shown to promote supercomplex formation most likely due to the alleviation of electrostatic repulsion derived from this highly acidic subunit (Pfeiffer *et al*., 2003).

Subunit 9 (Qcr9p) deletion negatively affects assembly and stability of the complex (Phillips *et al*., 1993). Qcr9p is proposed to stabilize the interactions between the 3 catalytic subunits, cytochrome *b*, cytochrome c_1 and Rieske (Saint-Georges *et al*., 2002). Lower turnover numbers and dissociation of Rieske upon purification of the enzyme from a Qcr10p deletion strain points to a role of this subunit in conferring stability to the enzyme (Brandt *et al*., 1994).

1.5 Tight binding of phospholipids to the cytochrome bc_1 complex

The detergent-solubilized cytochrome bc_1 complex forms classical type II crystals (Michel, 1983). The detergent molecules mimic the bilayer and from a cylindrical micelle, that surrounds the transmembrane region of integral membrane proteins. This detergent micelle is typically disordered and therefore not detected by X-ray crystallography (Roth *et al.*, 1989). Nevertheless, already in the first crystal structure of a membrane protein, the bacterial reaction center, a few tightly bound N,N-Dimethyldodecylamine-N-oxide (LDAO) molecules were co-purified and resolved in

the electron density, demonstrating ordered binding to the protein (Deisenhofer *et al*., 1985; Deisenhofer and Michel, 1989). Despite the forced delipidation from exposure to detergent-containing buffers during isolation and crystallization of membrane proteins, data is accumulating that shows tightly bound lipids that are retained and refined in the X-ray structures (see Lee, 2003; Palsdottir and Hunte, *in press*). The extent of specific binding of these molecules, as well as the functional importance of lipid binding to membrane proteins provokes ongoing research.

Cardiolipin is a characteristic phospholipid of the inner mitochondrial membrane (see *S*chlame *et al*., 2000), which is also composed of phosphatidyl ethanolamine (PE), phosphatidyl choline (PC), phosphatidyl inositol (PI), phosphatidyl serine (PS), and phosphatidyl glycerol (PG) (Zinser *et al*., 1991). In addition to the important role of creating a permeability barrier for cellular compartmentalization, as well as sealed integration of integral membrane proteins in the bilayer, phospholipids and their derivatives have assigned roles in a number of physiological processes (see Dowhan, 1997; Carman and Henry, 1989). Anionic lipid headgroups have been proposed to provide proton-conducting pathways at membrane surfaces (Haines, 1983). Furthermore, emerging evidence suggest roles of lipids in protein translocation (de Vrije *et al*., 1988), membrane protein topology (van Klompenburg *et al*., 1997), transporter function (Bogdanov and Dowhan, 1995), membrane protein folding (Bogdanov *et al*., 1998), thermal stability (Fyfe *et al*., 2004), and supercomplex formation (Pfeiffer *et al*., 2003).

The importance of phospholipids for structural and functional integrity of the isolated cytochrome bc_1 complex is best illustrated by decreased enzyme activity as a consequence of increased delipidation of the protein (Yu and Yu, 1980; Schägger *et al*., 1990). Phospholipid digestion reversibly inactivated the isolated enzyme, which regained catalytic activity upon addition of a mixture of cardiolipin and phospholipids (Gomez and Robinson, 1999).

The high resolution X-ray structure of the yeast cytochrome bc_1 complex revealed five tightly bound phospholipid molecules, including a cardiolipin, as well as one detergent molecule per monomer (Lange *et al*., 2001). The tightly bound cardiolipin was suggested to have a role in the proton uptake pathway at the Q_i site, the postulated E/R pathway (Lange *et al*., 2001). One of the 5 identified phospholipids, a phosphatidylinositol, is unusual, because the head group is positioned below the estimated membrane plane (Lange *et al*., 2001). It is referred to

as 'inter-helical' because it is wrapped around the transmembrane helix of the Rieske-protein. The other structurally resolved lipids are thought to represent more faithfully the surrounding annular bilayer.

The combination of X-ray structural analysis, molecular genetics and biochemical studies provides a powerful strategy to address the functional role of these tightly bound phospholipids (Lange *et al*., 2001; Fyfe *et al*., 2004).

1.6 Properties of the catalytic cofactors in the cytochrome bc_1 complex

Early characterization of the cytochromes was based on their redox-specific heme absorbance in the visible spectrum (Keilin, 1925). The *b*-type hemes are stabilized by non-covalent interactions, whereas heme c_1 is a true prosthetic group and covalently linked to cytochrome c_1 with thioether bonds from heme c_1 vinyl groups to conserved cysteines. The midpoint potential (E_m) of heme c_1 is 240 mV in yeast (Sun and Trumpower, 2003). Both *b* type hemes are stabilized between the same transmembrane helices of cytochrome *b*. However, heme b_H is close to the matrix side, whereas heme b_L is closer to the intermembrane space (Fig. 2). Since they experience different electronic environments, they accordingly exhibit different midpoint potentials or 120 mV and -30 mV, respectively (Sun and Trumpower, 2003).

The soluble Rieske domain is connected by a 'linker' region (residues 81–92) to the transmembrane anchor (residues 51–80). A phospholipid molecule has been suggested to have a structural role in stable integration of the transmembrane helix in the cytochrome bc_1 complex (Lange *et al*., 2001). The soluble domain of the Rieske protein (residues 93–215) is formed by layers of antiparallel β sheets, which fold into a compact structure, held by a conserved disulfide bond between residues Cys164 and Cys180, at the tip where the [2Fe-2S] cluster is bound (Iwata *et al*., 1996). Elimination of this disulfide bridge damages the ubiquinol oxidation site (Merbitz-Zahradnik *et al*., 2003).

Several strong and conserved bonds interact with the [2Fe-2S] cluster, which has a high electron midpoint potential ($E_{m,7}$ ~ 285 mV) that is pH dependent. Variants with reduced Rieske midpoint potential exhibit decreased catalytic activity, consistent with ubiquinol oxidation being the rate-limiting step in catalysis (Denke *et al*., 1998; Guergova-Kuras *et al*., 2000). One of the iron atoms of the [2Fe-2S] cluster is coordinated by two histidine ligands, His161 and His181, the latter residue is proposed to be a direct ligand of quinol. Circular dichroism (CD)-monitored redox

titrations (Link *et al*., 1992; Ugulava and Crofts, 1998), protein-film voltammetry (Zu *et al*., 2003) and theoretical calculations (Ullmann *et al*., 2002) agree that when Rieske is oxidized, the lowest pK_a value is ~7.5, or 4 units lower than the pK_a values estimated for the reduced Rieske protein.

The substrate of the yeast cytochrome bc_1 complex, Coenzyme Q_6 (CoQ_6), exhibits nine different chemical states, with the most stable forms being the fully protonated ubiquinol (QH_2) and the oxidized ubiquinone (Q) (see Chambers, 1988). These states are interconvertible through semiquinone (SQ) intermediates (Fig.4).

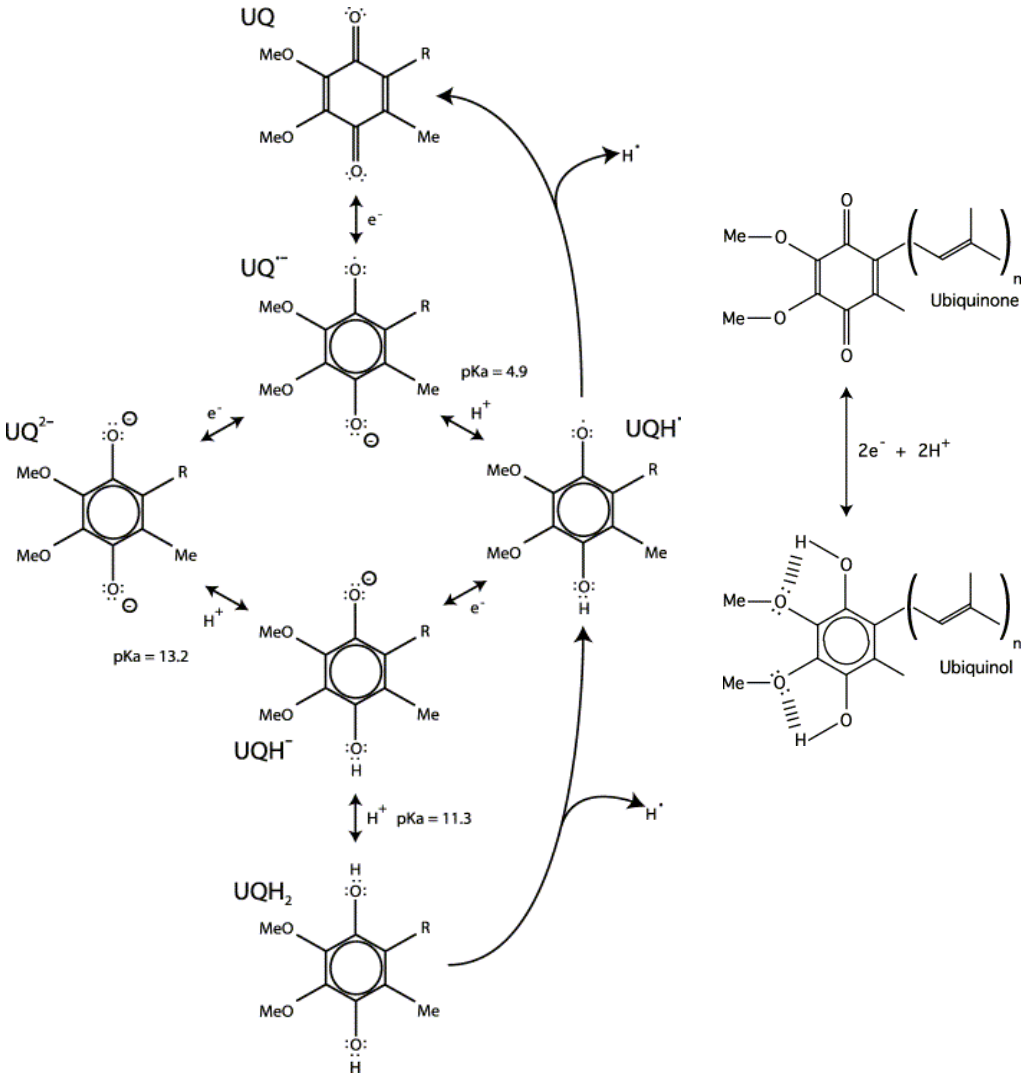

Fig.4 The chemical states of Coenzyme Q. *Interconvertible redox states and protonation reactions. Figure from James et al. (2004).*

The isoprenoid side chain of CoQ is not essential for Q_o site catalysis and can be replaced with an alkyl group, although this substitution is accompanied by decreased turnover rates (Yu *et al*., 1985). Rates of ubiquinol oxidation are found to increase proportionally with the length of the alkyl side chain until a critical length is reached and after which the rates decrease again (Yu *et al*., 1978; Yu *et al*., 1985).

1.7 Inhibitors as tools to study the molecular mechanism

Site-specific inhibitors have provided a bulk of data regarding the enzyme mechanism. Before the X-ray structures were available, kinetic studies on variants with phenotypes of disturbed enzyme mechanism, together with data on inhibitor binding, permitted rough assignment of the active sites in a molecular context (see Brasseur *et al*., 1996). Widely used inhibitors to study the Q_o site include UHDBT (5-n-undecyl-6-hydroxy-4,7-dioxobenzothiazole) and stigmatellin. The bifurcated electron transfer at the Q_o site was first realized when the Q_i site inhibitor antimycin was bound and Q_o site specific inhibitors were observed to terminate the oxidant-induced reduction of heme b_L (Wikström and Berden, 1972).

Unlike the stably bound and structurally resolved Q_i site occupant, X-ray structural analysis has failed in detecting the native Q_o site occupant. Instead, substrate analogs, which serve as competitive inhibitors, are used to analyze the molecular environment at the binding site. Importantly, EPR studies have served as diagnostic tools because the paramagnetic Rieske cluster exhibits characteristic lineshapes with respect to Q_o site occupancy (see Brugna *et al*., 2000; Cooley *et al*., 2004). Recently, pulsed EPR analysis provided the first structural characterization of the interaction of the reduced Rieske [2Fe-2S] cluster with the native occupant at the Q_o site, more specifically with the product of the quinol oxidation reaction (Samoilova *et al*., 2002).

Three types of Q_o site inhibitors can be distinguished; ligands which bind the proximal domain and perturb the spectroscopic properties of heme b_L (Q_o-I, *e.g.* myxothiazol, MOA-stilbene), molecules which bind to the distal domain and affect the Rieske [2Fe-2S] EPR lineshape (Q_o-II, *e.g.* UHDBT), or compounds which exhibit both effects (Q_o-III, *e.g.* stigmatellin) (von Jagow and Link, 1986; Crofts *et al*., 1999a). The binding sites for all three classes of inhibitors overlap with respect to their side chains that tail into a common tunnel, which gradually opens up into the cavity at the dimer interface. The head groups of type I and type II/III inhibitors, on

the other hand, are stabilized in different positions in the bilobal Q_o site, binding proximal and distal to heme b_L, respectively.

Type II/III inhibitors, such as stigmatellin and UHDBT, arrest the [2Fe-2S] cluster in docking position on cytochrome *b* (b-position) at a large enough distance to prevent efficient electron transfer to heme c_1 (Zhang *et al*., 2000). EPR studies have suggested favored interactions of the distal inhibitors, stigmatellin (von Jagow and Ohnishi, 1985), UHDBT (Bowyer *et al*., 1981; Bowyer *et al*., 1982) and UHNQ (Matsuura *et al*., 1983), with the reduced Rieske protein.

Stigmatellin was isolated from the myxobacterium *Stigmatella aurantiaca* (Kunze *et al*., 1984). Its binding to the cytochrome bc_1 complex induces a red shift in the α-band of heme b_{566} and causes a pronounced increase in Rieske midpoint potential from 290 mV to 540 mV (von Jagow and Ohnishi, 1985). Stigmatellin was instrumental for high resolution structure determination of the yeast cytochrome bc_1 complex, where it fixes the mobile Rieske domain in b-position. The stigmatellin carbonyl group was within hydrogen bond distance to the Rieske His181 side chain (Hunte *et al*., 2000). This interaction was recently confirmed by EPR analysis (Samoilova *et al*., 2002). The stigmatellin side chain is important for efficient inhibition, but not essential, as illustrated by alkyl derivatives that still retain inhibitory potency (Thierbach *et al*., 1984). Inhibition with stigmatellin appears to be pH independent (Zhang *et al*., 1999). Stigmatellin is a versatile inhibitor that not only inhibits quinol oxidation in the cytochrome bc_1 complex, but also inhibits quinone reduction in the bacterial reaction center, where it was crystallographically resolved at the Q_B site (Lancaster and Michel, 1997).

The alkyl-4,7-hydroxydioxobenzothiazoles (HDBT) were first synthesized as antimalarial drugs, as described by Friedmann and coworkers (1973). Unlike stigmatellin, undecyl-HDBT (UHDBT) inhibits the complex in a pH dependent manner, with decreasing inhibitory potency at alkaline pH (Zhang *et al*., 1999). Similar to stigmatellin, UHDBT increases the Rieske midpoint potential, although less dramatically, or by 70 mV (Bowyer *et al*., 1982). A pK_a of 6.5 has been determined for the hydroxy group, measured in phosphate buffer containing 1% ethanol, and deprotonation of the 6-hydroxy group was described with a color change from yellow to purple (Trumpower and Haggerty, 1980). Effective inhibition of the complex has been shown for 5-*n*-alkyl-6-hydroxy-4,7-dioxobenzothiazoles containing 7-15 carbon alkyl side-chains (Bowyer *et al*., 1982).

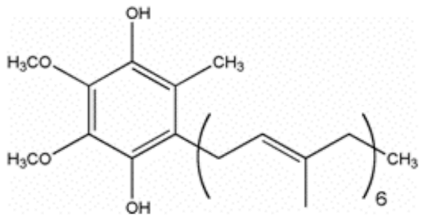

Ubiquinol

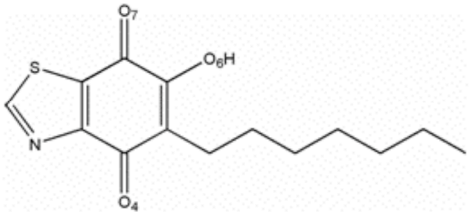

HHDBT

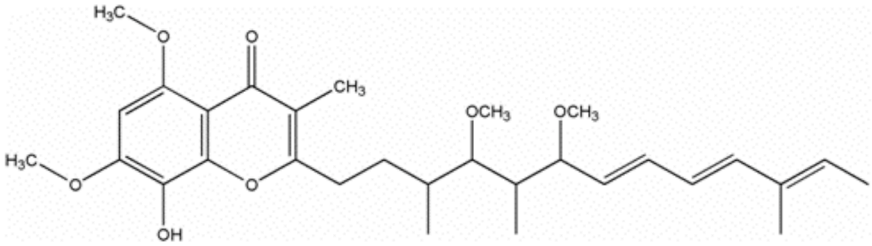

Stigmatellin

1.8 Quinol oxidation reaction

Interpretation of kinetic studies on the cytochrome bc_1 complex is complicated by the fact that duplicates of all reactions and a set of distinct catalytic interfaces have to be considered, including the large scale domain movement of the Rieske from b- to c1-position. The thermodynamically favorable, but energetically wasteful, reduction of Rieske by both electrons of ubiquinol is circumvented by the bifurcated electron flow at the Q_o site, where the second electron enters the lower potential electron transfer chain.

Which are the regulatory mechanisms behind this bifurcated electron transfer? Is a semiquinone transiently stabilized as a reaction intermediate or is ubiquinol oxidation concerted?

Most mechanistic models propose an enzyme-substrate complex with the Rieske cluster ligand His181 and cytochrome *b* residue Glu272 as primary ligands of ubiquinol. The observed pH dependency of quinol oxidation rate in the acidic range (Brandt and Okun, 1997; Covian and Moreno-Sanchez, 2001) suggests that both His181 and Glu272 should be deprotonated to participate in formation of the reaction complex. Also, the probability of forming the reaction complex depends on the correct positioning of the oxidized Rieske soluble domain. Accordingly, changing the

length of the flexible linker region which connects the cluster-containing domain to the transmembrane helix results in loss of ubiquinol oxidation activity (Nett *et al*., 2000; Darrouzet *et al*., 2000). The position of the Rieske extrinsic domain and interactions with the Q_o site occupant affect the midpoint potential (Darrouzet *et al*., 2002; Shinkarev *et al*., 2002; Cooley *et al*., 2004). The observed up-shift in midpoint potential induced by distal inhibitors has been proposed as a gating mechanism to prevent re-reduction of cytochrome c_1 by the semiquinone formed after the initial coupled proton-electron transfer to the Rieske (Link, 1997). Another interpretation is based on conformational gating where the Rieske domain is tied up away from the cytochrome c_1 by interactions with the Q_o site occupant. Kinetic studies suggest that the oxidized Rieske protein has higher mobility than does the reduced (Zhang *et al*., 2000). Redox-regulated movement of the Rieske is an attractive candidate for gating quinol oxidation. It is, however, not clear whether the movement of the Rieske domain is stochastic or a steered molecular motion.

In addition to the large-scale movement of the extrinsic domain from c1- to b-position, smaller movements of the Rieske head domain docked to cytochrome *b* have been proposed (Darrouzet and Daldal, 2002). Studies on variants and observed compensatory mutations suggest that loops at the cytochrome *b* surface construct physical barriers for steering and fine-tuning Rieske movements (Darrouzet and Daldal, 2003; Brasseur *et al*., 2004). Furthermore, movement of the Rieske extrinsic domain was shown to be essential for efficient catalysis, but not required for a single round of oxidation at the Q_o site (Darrouzet and Daldal, 2002).

The complexity of the cytochrome bc_1 complex catalysis is illustrated by the fact that, despite multi-faceted approach spanning several decades, important regulatory elements are still not understood. An ongoing dispute concerns the occupancy of the Q_o site, with models ranging from a single substrate bound (Crofts and Wang, 1989; Snyder *et al*., 1999) to double occupancy (Ding *et al*., 1992; Ding *et al*., 1995b; Brandt, 1996; Brandt, 1998; Bartoschek *et al*., 2001), including a hybrid proposal suggesting a moving semiquinone in the bilobal binding site (Hong *et al*., 1999; Crofts *et al*., 2000).

1.9 X-ray crystallographic and spectroscopic studies of proton transfer pathways

Maintenance of the proton gradient is a prerequisite for energy transduction. How are the protons transferred within the hydrophobic membrane spanning domains?

Nagle and Morowitz proposed in 1978 that proton conduction in membrane proteins takes place through hydrogen bond networks. The available X-ray structures of energy transducing enzymes now permit combined spectroscopic and structural dissection, as well as molecular modeling studies, of proton transfer pathways. Proton conduction by a network of amino acid residues and water molecules has been proposed for bacteriorhodopsin (Le Coutre *et al.*, 1995), the cytochrome *c* oxidase (Riistama *et al.*, 1997; Olkhova *et al.*, 2004), and the photosynthetic reaction center (Baciou and Michel, 1995; Tandori *et al.*, 1999).

In the cytochrome bc_1 complex, ubiquinol carries the protons across the membrane, but defined pathways for proton conduction must exist to and from the active sites. The proton exit pathway at the Q_o site was first proposed by molecular dynamics simulations on the 3 Å X-ray structure of the chicken cytochrome bc_1 complex (Izrailev *et al.*, 1999; Crofts *et al.*, 1999c). Subsequently, the higher resolution structure of the yeast enzyme provided experimental evidence, demonstrating a hydrogen bond network, including the heme b_L propionate and structurally resolved water molecules (Hunte *et al.*, 2000) (Fig. 5).

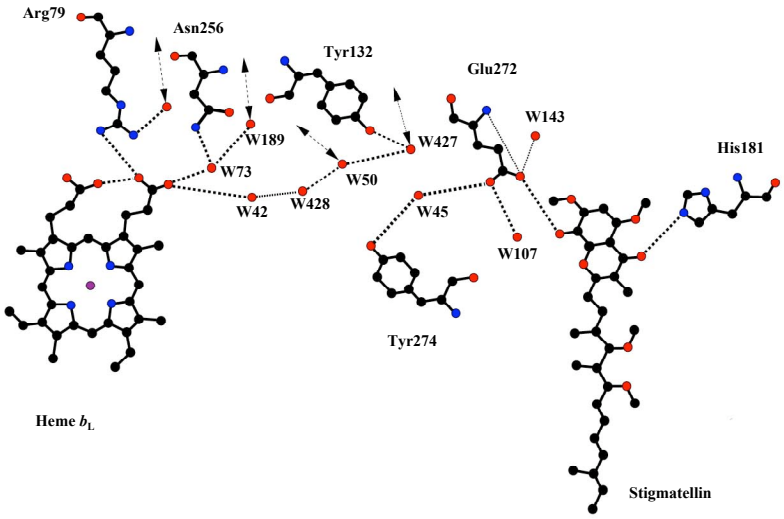

Fig.5 Proposed proton exit pathway from the Q_o site. *X-ray structural analysis revealed a network of hydrogen bonds (stipled lines) which connect cytochrome b residues, structural water molecules and the heme b_L propionate A (from Hunte et al., 2000).*

X-ray crystallography is the most frequently applied technique to obtain atomic models of proteins. However, protons are not resolved at the resolution typically obtained for membrane proteins. Information about redox-dependent protonation states of catalytic residues, therefore, needs to be retrieved by other biophysical techniques. Fourier transform infrared spectroscopy (FTIR) is ideal for this purpose and has been successfully applied, together with structural information from X-ray crystallography, to study a number of photosynthetic and respiratory electron transfer complexes. FTIR permits sensitive measurements of redox-dependent protonation reactions and reliable assignment of bands in the spectra can be carried out when supplemented with structural information, site-directed mutagenesis and isotopically labeled compounds. For instance, ^{13}C-labeling of the heme propionates in cytochrome *c* oxidase was used to study their protonation states with FTIR (Behr *et al*., 1998; Rost *et al*., 1999; Behr *et al*., 2000; Hellwig *et al*., 2002). FTIR studies have been initiated for cytochrome bc_1 complex from *R. capsulatus* (Baymann *et al*., 1999), *P. denitrificans* (Ritter *et al*., 2003), bovine (Iwaki *et al*., 2003), and, recently, *S. cerevisiae* (Ritter *et al*., 2004), as described here.

1.10 Aims of this dissertation

The molecular mechanism and regulatory events in cytochrome bc_1 complex Q_o site catalysis are not clear, including controversial models of Q_o site occupancy and electron transfer reactions. Also, pathways for proton transfer need to be experimentally validated. Here, X-ray crystallography was the method of choice to pursue verification of some of these issues in structural context. Competitive inhibitors and substrate analogs were used to analyze the Q_o site molecular architecture with X-ray crystallography. The structural study presented here was extended by FTIR analysis to monitor the interactions between inhibitors and the enzyme in redox-induced difference spectra. Furthermore, the protein preparation was optimized to increase the lipid content of the isolated enzyme and the binding of phospholipids to the enzyme was structurally characterized.

2. RESULTS

2.1 Preparation of crystallization grade cytochrome bc_1 complex

The purification procedure was scaled-up to accommodate more material and the exposure to detergent-containing buffers was minimized in order to increase the lipid content. The modified preparation yielded more active enzyme that was pure and crystallized readily (Table 2).

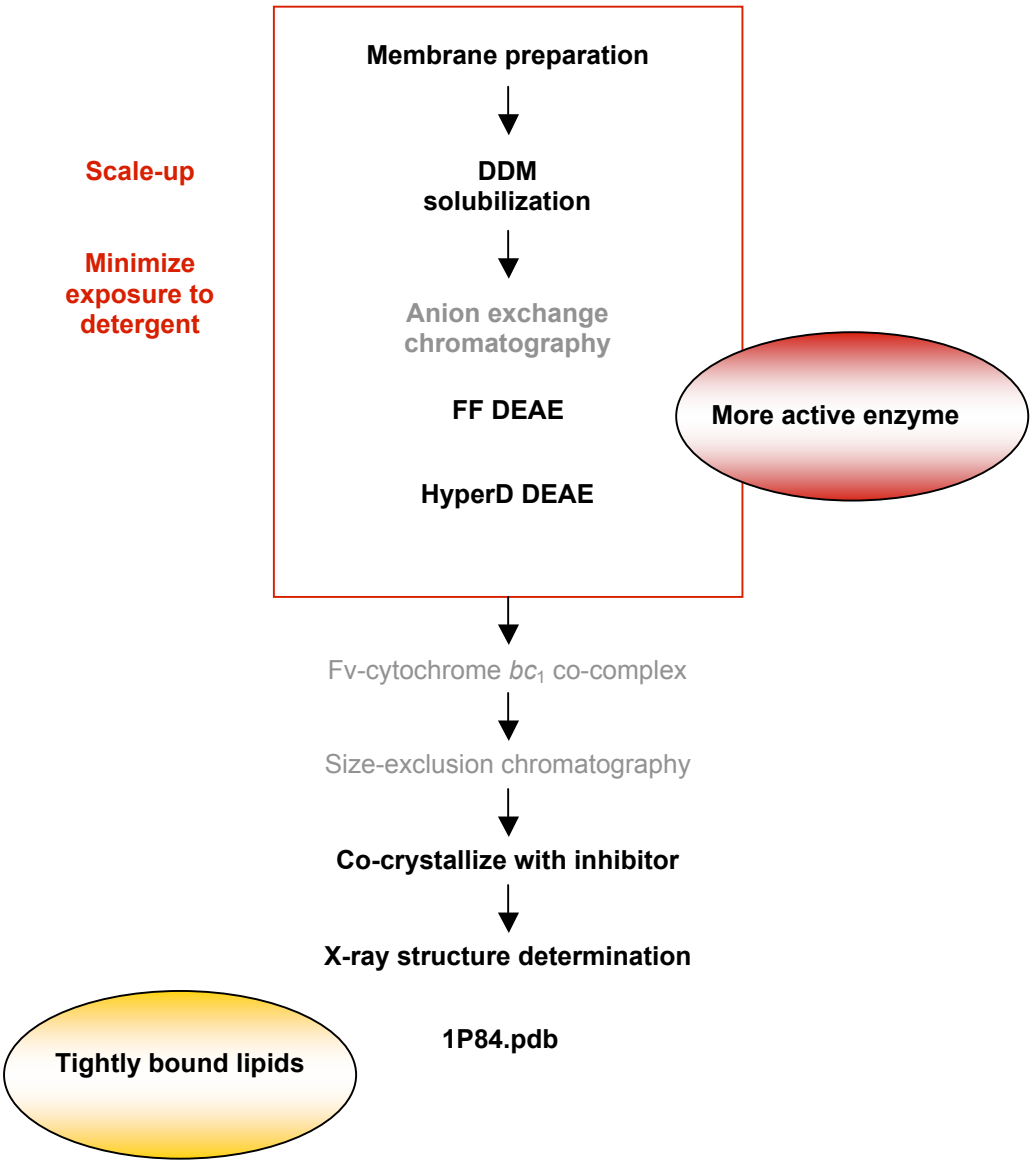

Scheme 1 Flowchart of the preparation of the yeast cytochrome bc_1 complex for X-ray structure determination. *The steps in the purification procedure that were subjected to modifications including scale-up and less exposure to detergents are boxed red.*

2.1.1 Five-fold scale-up of the membrane preparation

The first step in increasing the capacity of the preparation was the physical scale-up of the glass bead mill system used for cell breakage. In this way, more than one kg of yeast cells (wet weight) were processed, instead of the previous limit of 250 g per preparation. A typical yield was ~180 ml membranes from 1300 g cells (wet weight) or roughly 14 ml/100 g cells, which is similar to the original protocol, where ~20 ml of membranes were isolated from 100 g cells (Palsdottir and Hunte, 2003). This slight decrease in membrane yield may be a consequence of less efficient cell breakage when processing larger volumes, or caused by less efficient design of the large glass bead mill system. Increasing the membrane volume from 15 ml to 25 ml in 210 ml extraction buffer resulted in an increase in total protein content from 8.8 mg/ml to 13.5 mg/ml. The observed higher turnover numbers of the cytochrome bc_1 complex in detergent-solubilized membranes (Table 2) may be derived from the higher protein-to-detergent ratio. More than hundred times the critical micelle concentration (c.m.c. ~0.2 mM) of the non-ionic *n*-dodecyl-β-D-maltopyranoside (DDM) detergent was used for solubilization of the protein or a final concentration of ~30 mM. Importantly, the ratio ~1.15 g DDM per 1 g total protein should be kept constant in all preparations to ensure reproducibility.

2.1.2 Less exposure to detergent in the purification procedure

Purification of the enzyme is based on two consecutive chromatographic steps using the weak anion exchange diethylaminoethyl (DEAE) material. This is consistent with moderately acidic isoelectric points of the extramembraneous subunits (Table 1). The crude membrane extract was loaded on a DEAE fast-flow (FF) CL-6B resin and the eluted fractions were applied to a ceramic HyperD DEAE column. Exposure of the protein to detergents was minimized by decreasing the applied buffer volumes in the washing and detergent exchange steps. In the first chromatographic step, washing of the protein when bound to the DEAE sepharose FF column was shortened by 2-fold (Fig. 6A).

For 3-D crystallization of the complex, the detergent DDM had to be replaced with *n*-undecyl-β-D-maltopyranoside (UM) and this was done while the protein was bound to the HyperD DEAE column material. The shorter alkyl chain proved essential for successful crystallization (Hunte *et al.*, 2000). In the original procedure

15 CVs were applied for detergent exchange. The duration of this detergent exchange was reduced with respect to exposure to buffer volumes, or 3 column volumes (CVs) were applied to the scaled-up column that was designed to accommodate twice the previous yield of isolated enzyme. Also, washing of the protein when bound to the HyperD DEAE column (*e.g.* before the detergent exchange), was shortened by a factor of 2 (Fig. 8A). Specific enrichment of the cytochrome bc_1 complex was observed as an increase in heme *b* to heme *c* absorbance in redox difference absorbance spectra (Fig. 6B).

The enzyme was already enriched when it eluted from the FF column (Fig. 6A, *blue arrow*), but silver stained NuPAGE gels revealed contaminating bands (Fig. 7B, *lane 5-6*). The elution profile from the HyperD DEAE chromatography was monitored by comparing the specific heme absorbance at 413 nm with the absorbance at 280 nm, and the pure enzyme eluted at ~35 mS buffer conductivity. The first 10 ml of the peak were of high purity as shown in silver stained gels (Fig. 7B, *lane 8-9*). The fractions eluting as the first peak absorbing at 413 nm in the first gradient of the HyperD elution (Fig. 7B, *lane 8-11*) were selected for co-complex formation with the Fv fragment 18E11 and subjected to preparative size-exclusion chromatography (Hunte *et al*., 2000). The highly pure crystallizable co-complex eluted as a single symmetric peak and exhibited a ratio of AU280nm:AU413nm ~1.1 (Fig. 8B).

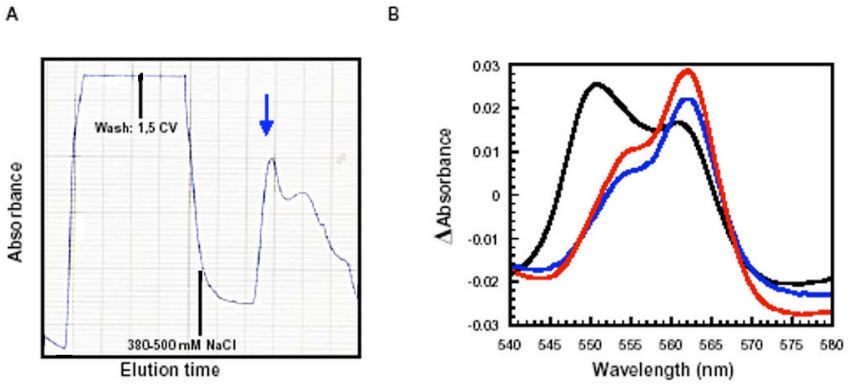

Fig.6 Purification of the cytochrome bc_1 complex. A, *FF-DEAE elution profile drawn from the absorbance at 280 nm. The fraction containing the cytochrome bc_1 complex is marked with a blue arrow.* ***B,*** *difference absorbance spectra of dithionite-reduced minus ferricyanide-oxidized samples; the solubilisate (black), pooled fractions from DEAE-FF (blue), pooled fractions from HyperD DEAE (red).*

2.1.3 Destabilization of the enzyme was observed in the elution profiles

To ensure reproducibility of the preparation for 3-D crystallization, quality control points were constructed based on the chromatographic profiles and enzyme activity. Importantly, the membrane preparation was not stable upon long-term storage, observed as reduced yield of isolated protein and gradual loss of measured enzyme activity. Notably, the yield of the preparation was also highly dependent on the source of yeast cells, demonstrating the importance of optimized growth conditions for specific enrichment of the enzyme. Baker´s yeast (*Wieninger hefe*), yielded half the quantity in mg isolated enzyme per ml membrane compared to the FGY3 strain, that was optimized for aerobic growth under non-fermentable growth conditions (Glycerin-EtOH).

An important quality indicator for the protein preparation was the appearance of a second peak absorbing at 413 nm and eluting in the high salt gradient during HyperD DEAE chromatography (Fig. 9A). The activity of the enzyme eluting at high salt concentrations was less than half of the target peak, which elutes at ~35 mS in the first salt gradient (150-300 mM NaCl) (*Diploma thesis, Christiane Jost*).

Destabilization of the enzyme was also monitored in the size-exclusion chromatography elution profiles, manifest in a greater relative absorbance of a second peak absorbing at 413 nm, in direct continuity of the target peak. The first 80 % of the peak that elutes after 46 minutes or at the retention volume of ~18 ml (~500 kDa) (Fig. 8B and Fig. 9B), contain pure homodimer with bound Fv18E11 and this material is suitable for 3-D crystallization. Other peaks observed in the gel filtration chromatograms eluted at ~22 ml and ~25 ml (Fig. 9B), the latter contained Fv fragment (~28 kDa) alone, which was added in 1.4-fold molar excess prior to the gel filtration run. Gel electrophoretic analysis of the peak that eluted at 22 ml in direct continuity of the main peak, showed that it contains the cytochrome bc_1 complex with bound Fv fragment (*data not shown*), as expected from the observed absorbance at 413 nm. Calibration of the column with molecular mass standards in the form of soluble proteins (see *section 4.8.1*) cannot be transferred directly to membrane protein retention volumes, which have the added complexity of a detergent micelle surrounding the transmembrane regions, thus adding to the apparent molecular mass. Still, calibration of the column demonstrated the resolving power of this chromatographic procedure and the retention volume at 22 ml roughly suggested a

size exclusion limit of half the mass of the prominent peak. The elution profile from the size exclusion chromatography, therefore reflects the quality of the preparation, where the extent of the second peak absorbing at 413 nm, demonstrates the degree of monomerization and/or subunit dissociation, *i.e.* destabilization of the homodimer. Notably, when the enzyme was isolated from cells, which do not synthesize cardiolipin, this second peak was considerably more pronounced compared to wild type preparations, even reaching the same height (*i.e.* measured in absorbance units) as the target peak.

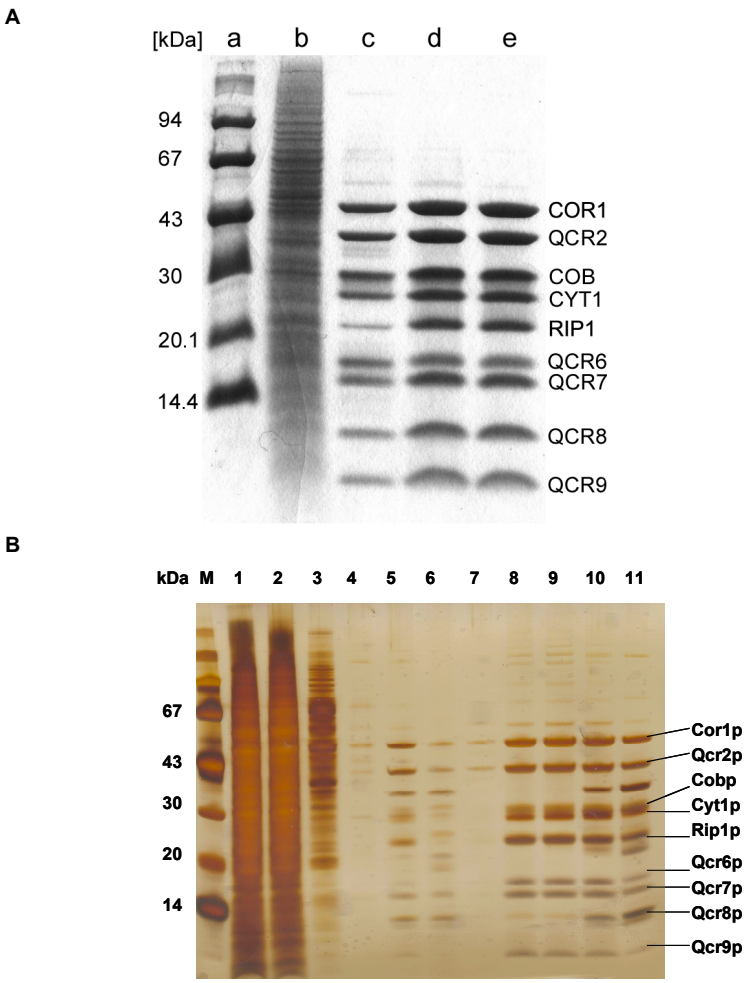

Fig.7 Gel electrophoretic separation of the cytochrome bc_1 complex polypeptides. ***A,*** *the original preparation shown in coomassie-stained Tricine SDS-PAGE using 16.5 % gels:* ***a****, molecular mass standard;* ***b****, solubilized membrane proteins;* ***c****, pooled fractions of DEAE-Sepharose FF;* ***d****, pooled fractions of DEAE-Hyper D;* ***e****, pooled fractions of TSK4000 size exclusion chromatography (from Palsdottir and Hunte, 2003).* ***B****, modified preparation analysed by separation with silver-stained Bis-Tris NuPAGE gels (4-12%):* ***M****, marker;* ***1-2****, solubilisate;* ***3*** *flow through FF DEAE;* ***4****, wash FF DEAE;* ***5-6****, pooled fractions (2x35 ml) as eluted from FF DEAE;* ***7****, wash Hyper D DEAE,* ***8-9****, first four 5 ml fractions of the enzyme eluting from HyperD DEAE.*

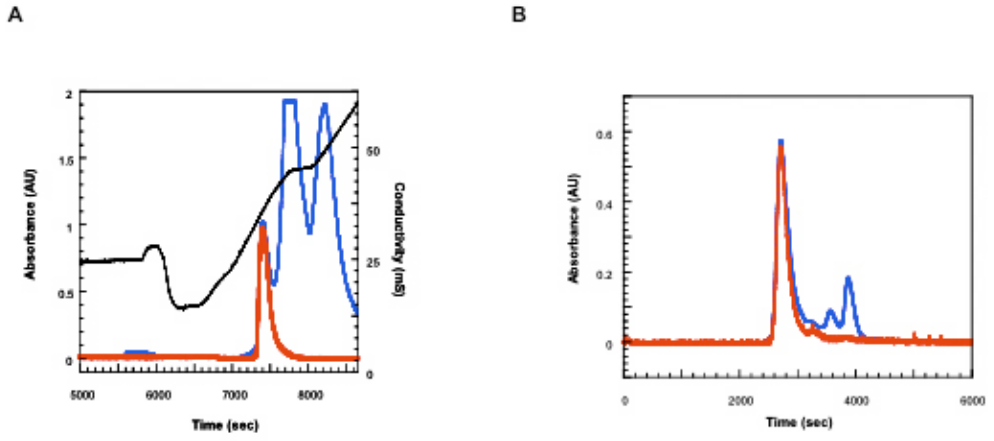

Fig.8 Anion exchange and preparative size-exclusion chromatography of the cytochrome bc_1 complex. ***A****, HyperD DEAE chromatography profile, a two-step salt gradient (conductivity in mS as black line, right axis). The absorbance of the heme groups was monitored by absorbance at 413 nm (red). Also depicted is absorbance at 280 nm (blue). Contaminants are separated from the complex, as they elute at high salt concentration.* ***B****, size exclusion chromatography of cytochrome bc_1 complex with bound Fv fragment. Absolute units for absorbance are shown (AU). These runs were carried out using the Biosys2000 system.*

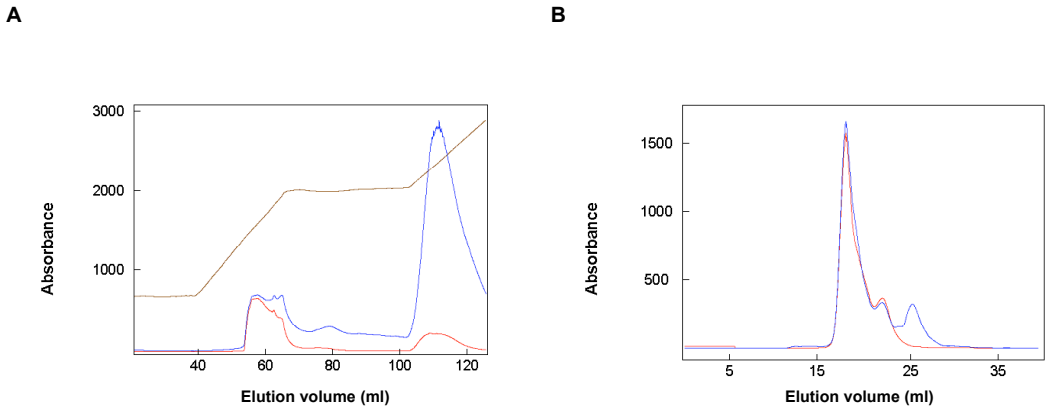

Fig.9 Preparation of the cytochrome bc_1 complex from a membrane preparation of Wieninger yeast stored for 2 years at -80°C. ***A****, the HyperD DEAE elution profile. The conductivity of buffers is drawn as brown lines and illustrates the two step salt gradient. The enzyme elutes in the first and second gradient as shown by absorbance at 413 nm depicted with the red line. For comparison, the absorbance at 280 nm is drawn in blue.* ***B****, the TSK4000 gel filtration chromatogram shows a more pronounced relative intensity of the second peak in direct continuity of the prominent peak when compared to Fig.8B. These chromatographic runs were performed using the ÄKTA chromatographic system.*

2.1.4 Quality checkpoints in the purification procedure

The modified preparation described here permits the purification of a more active crystallization grade enzyme. The main adjustment with respect to the original protocol was less exposure to detergent containing buffers (see *section 4.6*), which presumably increased the lipid content of the preparation, as noticed in the refinement of two new tightly bound phospholipids in the X-ray structures (see *section 2.5*). In addition to the qualitative evaluation of the chromatographic profiles (see *section 2.1.3*), the quality of the preparation was also probed quantitatively by measuring turnover numbers in terms of mol cytochrome *c* reduced per second by mol cytochrome *b*.

The final yield of isolated protein per ml membrane was 0.52 mg/ml or similar to 0.67 mg/ml obtained in the original preparation. The specific enzyme activity increased during the preparation from 0.5 μmol/(min*mg protein) to 24.8 μmol/(min*mg protein), with an enrichment factor of 49.6. The final purified enzyme had a relative heme *b* concentration of 8.2 nmol per mg of protein, and a heme *b* to heme c_1 ratio of 1.9. These data are close to the theoretical values of 8.6 nmol cytochrome *b* per mg of protein and a molar ratio of two heme *b*/heme c_1.

Table 2 Purification table for the cytochrome bc_1 complex preparation.

	Yield protein mg	heme *b* nmol / mg prot.	Cyt bc_1 complex nmol	Turnover s^{-1}	Specific activity μmol / mg * min
Solubilized membranes	2828 [1848 ± 504]	0.2 [0.3 ± 0.1]	336 (2.8%) [272.3 ± 49.6](3.4%)	77 [48.1 ± 20.9]	0.5 [0.4 ± 0.1]
DEAE-Seph. FF	50 [34 ± 7]	3.6 [3.1 ± 0.2]	90 (42%) [52.8 ± 12.3](36%)	137 [52.4 ± 2.3]	14.7 [5.0 ± 0.4]
DEAE-Hyper D	27 [18 ± 2]	5.3 [5.4 ± 0.9]	71 (63%) [49.1 ± 7.6](64%)	111 [63.7 ± 20.9]	16.7 [12.5 ± 5.5]
TSK 4000	13 [10 ± 1]	8.2 [8.1 ± 0.3]	53 (95%) [42.1 ± 5.9] (98%)	101 [48.8 ± 13.1]	24.8 [11.0 ± 3.3]

25 ml membranes from the FGY3-strain (stored at -80ºC for 3-days) were solubilized in 210 ml extraction buffer. The turnover numbers present an average of 5 measurements with the intrinsic error of the assay ±15% (for experimental details see section 4.11). The corresponding values from the original protocol are given below in square brackets and show the average of 3 different preparations from 15 ml membranes solubilized in 210 ml extraction buffer (from Palsdottir and Hunte, 2003). The redox properties of the b type hemes permit specific quantification of cytochrome b content with the extinction coefficient of 28.5 $mM^{-1}cm^{-1}$(562-575 nm). Purity (%) is shown as cyt b (mg) / (yield protein (mg)) x 100 (%). Specific activity was calculated as µmol cytochrome c reduced per minute per mg total protein estimated from the BCAssay (see section 4.9.1).

2.2 Fv fragment-mediated crystallization

The antibody fragment Fv18E11 has a strep-tag on the C-terminus of the heavy chain polypeptide and was purified with streptavidin affinity chromatography, as described by Kleymann *et al*. (1995). A myc-tag was placed on the light chain C-terminus in order to permit immunodetection in Western blot analysis. A streptavidin-coupled alkaline phosphatase served to confirm the presence of the strep-tag. Attempts to modify the standardized purification scheme revealed structural instability of the Fv18E11 fragment.

2.2.1 The unstable assembly of the Fv fragment 18E11

In the original protocol, slow flow CH-Sepharose 4B material was used and typically ~4.5 mg of Fv18E11 were obtained from 120 ml periplasmic extract of *E. coli* cells harvested from 12 L cultures. An effort was made to speed up the purification procedure by coupling streptavidin to a NHS-activated sepharose 4 Fast Flow resin. However, the FF column proved not suitable for Fv18E11 purification, and the Fv fragment eluted in two or more prominent peaks, as judged from the absorbance at 280 nm. In comparison, a single prominent peak was observed to elute from the streptavidin-coupled CH-Sepharose 4B resin, and was followed by a second much smaller or negligible trailing peak (Fig. 14A). Gel electrophoretic and Western blot analysis to detect the presence of the strep- and myc-tags demonstrated that the first peak contained both heavy and light chain polypeptides, whereas the second peak contained only heavy chain. Importantly, this observation demonstrated the instability of the Fv fragment assembly.

2.2.2 Quality control of the Fv fragment

The lack of inter-chain disulfide bonds renders Fv fragments less stably folded than Fab fragments. The observed instability of the Fv fragment assembly (see *section 2.2.1*) required the design of control points to qualitatively monitor its assembly in order to ensure reproducible 3-D crystallization of the cytochrome bc_1 complex. Analytical gel filtration chromatography using Superdex75 column mounted on the SMART system was performed for this purpose (Fig. 10). The peaks in the elution profile were assigned based on calibration of the column by using a set of low molecular mass standards (see *section 4.8.2*). Characterization of the peaks was further confirmed by gel electrophoretic analysis of TCA precipitated fractions. A

high quality Fv18E11 fragment preparation was manifest in a single prominent peak at a retention volume of 1.2 ml (~28 kDa) (Fig. 10A). A split peak at retention volumes in the range 1.6 ml-1.7 ml indicated dissociation of the Fv fragment into heavy and light chain polypeptides and the relative intensity of the peaks in the elution profile served as a reliable criteria to judge if the Fv fragment was stably assembled (Fig. 10). In addition, this procedure permitted an estimation of the degree of aggregation that was monitored by the extent of the peak that eluted in the void volume of the column (marked red in Fig. 10).

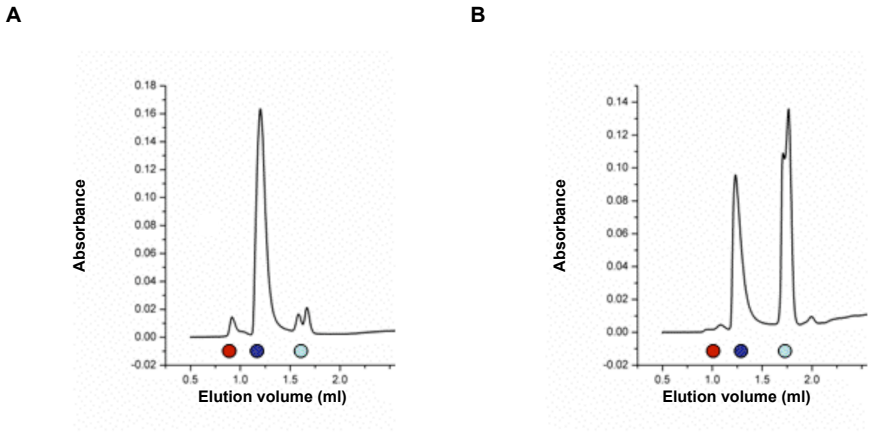

Fig.10. Analytical size-exclusion chromatography of the Fv18E11 fragment. *To monitor the assembly of heavy and light chain polypeptides gel filtration was performed using a Superdex 75 column mounted on the SMART system. The gel filtration chromatographic profiles showed the degree of dissociation of the Fv fragment (blue) into heavy and light chain polypeptides (light blue). The void volume is marked in red.* ***A****, freshly prepared Fv18E11, which was immediately rebuffered and concentrated.* ***B****, Fv18E11 which shows pronounced dissociation. This probe was incubated for more than a week in the dilute DTB buffer as it elutes from the streptavidin column.*

2.2.3 Structural analysis of crystal contacts

In the Fv fragment-mediated 3-D crystallization of the detergent solubilized cytochrome bc_1 complex, important crystal contacts are mediated by the strep-tag, which is located on the heavy chain of Fv18E11 (Hunte *et al*., 2000). Careful analysis of the crystal contacts was carried out in order to explain the pH sensitive crystallization of the preparation, which only produced suitable material for X-ray diffraction experiments in the narrow pH range of 7.5-8.5.

The antibody Fv-fragment and the acidic hinge protein (Qcr6p), which face the intermembrane space, interact in the crystal lattice with the matrix-oriented core

proteins (Cor1p, Qcr2p) of neighboring molecules in the 3-D crystal lattice (Fig. 11). The greatest distance between the strep-tags on either side of the homodimer is ~180 Å, whereas the largest distance from hinge-to-hinge within a homodimer is ~120 Å. Interestingly, despite forming important crystal contacts, the strep-tag is only partially resolved in the experimental electron density. Only the first six amino acids of the strep tag (-SAWRHP-) were resolved and stably refined. A helical extension could be traced in the electron density, starting from Pro127, but did not yield clear residue assignment of the remaining four amino acids (-QFGG).

The strep-tag residue His126 forms crystal contacts to the Core 2 protein (Qcr2p) of a neighboring dimer in the crystal lattice, with 302.7 $Å^2$ buried surface area (*i.e.* interfacial area) of which only 27 % contribute polar interactions, as calculated with Naccess (see *section 4.13.6.3*). The $His126^{strep}$ side chain is within hydrogen bond distance to the carboxylate of $Asp97^{Qcr2p}$. Moreover, a structural water molecule, Wat313, contributes hydrogen bonds to stabilize the interaction. The strep-tag also contacts subunit 7 (Qcr7p) of the symmetry-related second monomer in the neighboring dimer (368.2 $Å^2$: 34 % polar), thus the strep-tag makes crystal contacts to both monomers of a homodimer. More specifically, $Trp124^{strep}$ contributes to crystal contacts with hydrogen bonds from the main chain atoms to the backbone carbonyl and nitrogen of $Glu124^{Qcr7p}$ and $Ser126^{Qcr7p}$, respectively.

The acidic Hinge protein (Qcr6p), makes contacts to the Core1 protein (Cor1p) (560.8 $Å^2$: 35% polar) and the N-terminus of the Rieske protein (Rip1p) (114.2 $Å^2$: 83 % polar). Importantly, the hinge $Glu89^{Qcr6p}$ carboxylate is involved in an ion pair formation with the side chain of the Rieske protein residue $Arg35^{Rip1p}$. Furthermore, $Asn187^{Cor1p}$ is hydrogen bonded to $His96^{Qcr6p}$. The latter is configured in a *plane-to-edge* arrangement (<3.5 Å) with $Tyr65^{Cor1p}$.

To summarize, only a few amino acid residues contribute with relatively small surface area to the crystal contact formation in the 3-D lattice arrangement of this large multisubunit homodimeric membrane protein. The observation that histidines contribute to the crystal contacts may be key to explain the apparent pH dependent crystallization behavior. Histidines typically exhibit pK_a values close to the optimal pH used for crystallization and this may explain the pH sensitive crystallization behavior of the yeast cytochrome bc_1-Fv co-complex (see *section 2.3.2*)

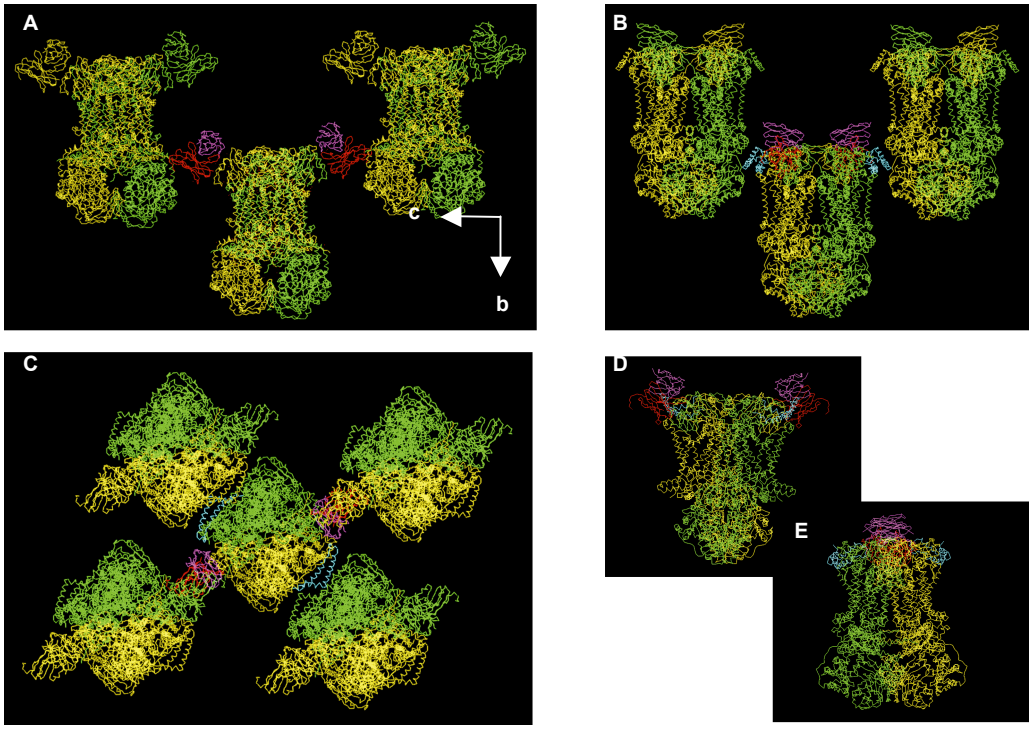

Fig.11 Crystal packing of the cytochrome bc_1 complex. ***A****, the arrangement of homodimers as viewed in plane ((0.5a+c),b) - corresponding to a view from the membrane plane. The different monomers in a homodimer are colored yellow and green, respectively. This view illustrates the crystal contact made from the Fv fragment heavy chain (red) C-terminal strep-tag to the core proteins.* ***B****, rotation around the b-axis (in plane) produces the following view, where crystal contacts mediated by the hinge protein (cyan) on each side of the homodimer are pointed out.* ***C****, a 90 degree rotation around the c-axis and tilting around a-axis generates the following view to show the space occupied per homodimer in the crystal lattice, as viewed from the matrix side.* ***D****, the polar surface area for crystal contacts on the intermembrane side are provided by the Fv fragment (red/magenta), and* ***E****, the hinge proteins (cyan). On the matrix side the peripheral core proteins provide ample opportunities for crystal contact formation.*

2.2.4 Structural analysis of Fv18E11-Rieske interaction

The Rieske residues that are recognized by the Fv fragment 18E11 are not in a linear arrangement, but form a conformational epitope (Hunte *et al*., 2000). Detailed characterization of the atomic interactions at the Fv-epitope interface was carried out (Table 3). This X-ray structural description of the Fv18E11 binding to its epitope combined with a comprehensive sequence alignment of Rieske protein sequences (carried out by O. Anderka) served as the framework for a project where grafting of the yeast epitope onto the Rieske protein from *P. denitrificans* was pursued with the aim to perform Fv-mediated 3-D crystallization of the bacterial enzyme.

Table 3. Characterization of the Fv18E11-Rieske interactions by X-ray structural analysis. *Major interactions are categorized as hydrophobic (hphop) or polar. The latter distinguished as side chain (sc) or main chain (mc) interactions. The single salt bridge is marked in red.*

FvH	Type	Rip1p	FvL	Type	Rip1p
Tyr 111	*hphob*	Gln 127	Ala 56	*hphob*	Pro 123
Arg 98	*sc-mc*	Asn 130	Leu 54	*hphob*	Pro 123
Arg 98	*mc-sc*	Asn 130	His 55	*hphob*	Pro 123
Tyr 102	*sc-sc*	Asn 130	Gly 57	*hphob*	His 124
Glu 100	*sc-sc*	Asn 130	Tyr 49	*hphob*	Ile 126
Tyr 111	*sc-sc*	Ser 131	Ala 56	*hphob*	Gln 127
Tyr 27	*hphob*	Val 132	His 55	*hphob*	Gln 127
Ser 31	*sc-sc*	Asp 133	**Arg 53**	***sc-sc***	**Asp 149**
Ser 28	*mc-sc*	Asp 133	Arg 53	*sc-sc*	Gln 151
Ser 28	*sc-sc*	Asp 133			
Ser 31	*sc-mc*	Met 134			
Ser 31	*hphob*	Thr 142			
Tyr 33	*hphob*	Thr 142			
Tyr 102	*sc-sc*	Asp 143			
Tyr 33	*sc-mc*	Ala 144			
Tyr 102	*hphob*	Val 147			
Ser 103	*sc-mc*	Lys 148			
Val 104	*sc-mc*	Lys 148			
Tyr 102	*hphob*	Pro 150			
Thr 105	*hphob*	Pro 150			

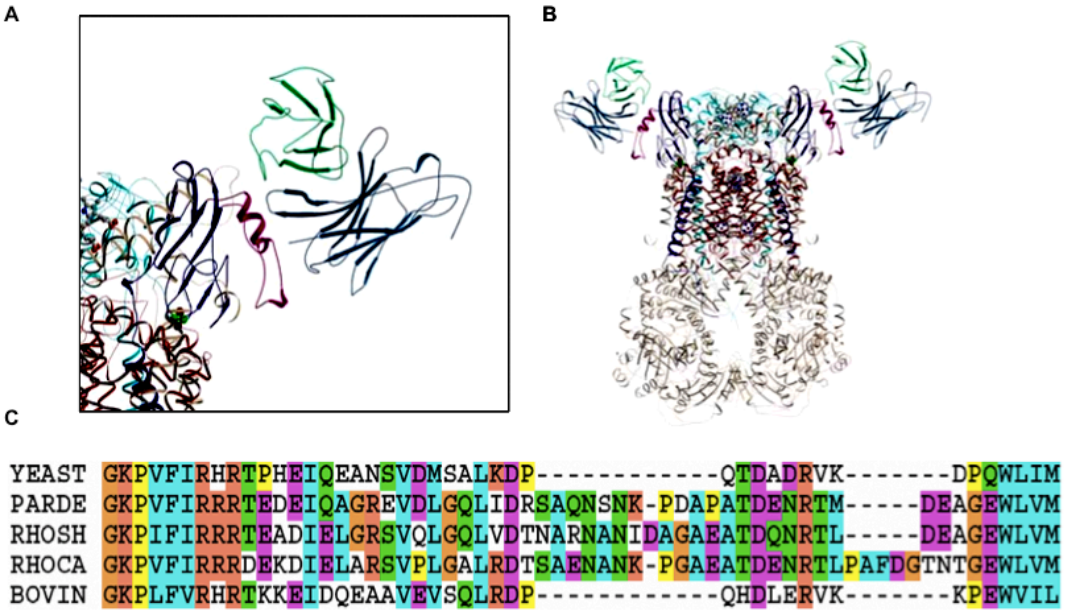

Fig.12 The Fv18E11 binds the extrinsic Rieske domain. ***A****, the position of the epitope (magenta) in the Rieske protein (blue) is shown. FvH (steelblue), covers the majority of contacts compared to FvL (green).* ***B****, the homodimer with bound Fv fragments. Cytochrome* c_1 *and cytochrome b are colored cyan and brown, respectively.* ***C****, an extract from a comprehensive multiple sequence alignment of eukaryotic and prokaryotic Rieske sequences. Shown here are the sequences from yeast (UCRI_YEAST), P. denitrificans (UCRI_PARDE), R. sphaeroides (UCRI_RHOSH), R. capsulatus (UCRI_CAPSU), and bovine (UCRI_BOVIN) (alignment provided by O. Anderka).*

The conformational epitope resides in a non-conserved region (Pro123 to Gln151) (Table 3, Fig. 12C) and is composed of an α-helix and a connecting loop inserted between the more highly conserved β3 and β4 strands of the soluble Rieske protein. Multiple sequence alignment showed that in the non-conserved epitope-containing segment the bacterial Rieske proteins have an inserted span of amino acids (Fig. 12C). Homology-based modeling proposed a helical arrangement of this insertion (Xiao *et al*., 2004).

The majority of contacts is provided by the Fv fragment heavy chain (FvH) (Fig. 12), namely CDR-H1 (residues 27-33) and CDR-H3 (residues 98-111). Interactions with the light chain are confined to CDR-L2 (residues 49-57) and, although not as many as from the heavy chain, include the only salt bridge in this antibody-antigen recognition (Table 3). Calculations using the program Naccess estimated that 38 % of the buried surface area is polar (see *section 4.13.6.3*), with strikingly larger contribution of 12 distinct hydrogen bond pairs, compared to only one salt bridge, *i.e.* $Arg53^{FvL}$ and $Asp149^{Rip1p}$ (Table 3). For comparison, the value reported for the number of hydrogen bond interactions typically observed in antibody-antigen recognition is 8.5 ± 3.5 (Lo Conte *et al*., 1999). Strikingly, structural water molecules were reproducibly identified at the interface in different data sets. The coordinated hydrogen bond network stabilizing these water molecules suggests a contribution of water-mediated hydrogen bonds in antigen recognition by Fv18E11. Water molecule Wat279 is for instance hydrogen bonded to the side chains of $Asp110^{FvH}$ and $Glu100^{FvH}$, as well as it is hydrogen bonded to the $Asn130^{Rip1p}$ side chain. Another example is Wat5, which is stabilized by side chain hydroxyl of $Tyr33^{FvH}$ and main chain nitrogen of $Asp143^{Rip1p}$. Non-polar interactions were mainly mediated by tyrosine residues, which form characteristic clefts and cervices on the Fv fragment surface.

2.2.5 Structural comparison of Fv-fragments bound to membrane proteins

The Fv-mediated 3-D crystallization of the cytochrome *c* oxidase was the pioneer study to demonstrate that Fv fragments can serve as crystallization enhancers of membrane proteins (Ostermeier *et al*., 1995). The second example is the Fv18E11-cytochrome bc_1 complex X-ray structure determination (Hunte *et al*., 2000). A

comparative structural study was carried out to search for common traits in these two successful examples of Fv-mediated crystallization of membrane proteins.

Both Fv fragments form crystal contacts via the strep-tag (see Hunte and Michel, 2002). Also, both Fv7E2 and Fv18E11 recognize discontinuous epitopes, thus are conformation specific, consistent with their applications in X-ray structure determination of the native protein conformation. The strep-tag is only partially resolved in the experimental electron density maps derived from both Fv7E2-cytochrome *c* oxidase and Fv18E11-cytochrome bc_1 complex crystal diffraction, in both cases the disorder starts from the proline. Notably, the strep- and myc-tags were disordered in the 1.28 Å resolution X-ray structure of the Fv7E2 fragment alone (Essen *et al*., 2003).

The antibody-antigen recognition is dominated by hydrogen bonds for both Fv7E2-cytochrome *c* oxidase and Fv18E11-cytochrome bc_1 complex. Indeed, Fv7E2 binds with 16 hydrogen bonds to its antigen and the lack of salt bridges poised the question whether water bridges serve to enforce the binding (see Essen *et al*., 2003). In comparison, the Fv18E11-Rieske protein interaction is composed of 12 hydrogen bond pairs and one salt bridge (see Table 3). Also, structurally resolved water molecules were observed to contribute to the network of hydrogen bond interactions at the Fv18E11-Rieske protein interface.

A noticeable difference between these two reported cases of Fv-mediated crystallization of membrane proteins was uncovered by the extent of buried surface area, where the Fv18E11-Rieske interface is 1521 $Å^2$ or twice the size of the interfacial area covered by Fv7E2 (744 $Å^2$). The mean value for the interfacial area of antibody-antigen complexes was calculated by Lo Conte *et al*. (1999) to be 1680 $Å^2$ (±260). Thus, the Fv18E11-antigen interaction lies within this range, whereas the Fv7E2-antigen recognition presents an unusual exception (Essen *et al*., 2003).

To summarize, except for the unusually small surface area of interaction in the case of Fv7E2, the nature of antigen recognition appears similar to the reported antigen-antibody interactions for soluble proteins, including the distribution of polar and non-polar forces, and the dominant role of hydrogen bond interactions (see Davies and Cohen, 1996).

2.2.6 Magnetic beads pull down assay to probe co-complex formation

Unlike the Fv7E2-cytochrome *c* oxidase co-complex, that was purified by preparative streptavidin affinity chromatography (Ostermeier *et al*., 1995), the cytochrome bc_1-Fv18E11 co-complex could not be purified in large-scale via the strep-tag (*C. Hunte, unpublished*). Analytical pull down assays using streptavidin- and streptactin-coated magnetic beads permitted specific capture of the co-complex, but silver stained gels of the eluted co-complex revealed increased relative intensity, *i.e.* enrichment of the Rieske polypeptide, with respect to the remaining subunits, thus demonstrating unstable integration of the Rieske protein in this type of purification scheme (Fig. 13). As mentioned before, stigmatellin fixes the Rieske extrinsic domain in b-position, but the yield of enzyme eluting from the beads did not change by stigmatellin addition (*data not shown*).

The pull down assay appeared most efficient when the co-complex was formed prior to incubation with the beads. The conditions for antibody-antigen co-complex formation may be less favorable when the antibody fragment is bound to the beads than when both proteins are free to interact in solution. Importantly, the assay with Fv fragment alone confirmed the unstable assembly of heavy and light chain polypeptides that was observed in large-scale streptavidin affinity purification and analytical gel filtration chromatography (see *section 2.2.1* and *2.2.2*). Extensive washing of the Fv fragment when bound to the beads increased the relative amount of Fv heavy chain (FvH) to Fv light chain (FvL), as detected in silver stained gels of the eluted fractions. Even complete absence of FvL was noticed after overnight washing, meaning it was in effect 'washed off' the heavy chain. This was shown by gel electrophoretic analysis and the lack of immunodetection of the myc-tag in Western blots (*data not shown*).

Importantly, the magnetic beads pull down assay demonstrated the species-specific binding of Fv18E11 that was predicted, because the epitope resides in a non-conserved region of the Rieske protein (see Fig. 12C). This lack of cross-reactivity was observed in inefficient pull down of the homologous enzymes from *P. denitrificans* (Fig. 13), bovine heart mitochondria, and *R. sphaeroides* (*data not shown*). Candidates responsible for the observed lack of cross-species reactivity were exposed in multiple sequence alignment, *i.e.* residues were identified, which are expected to introduce electrostatic and/or steric disturbance at the binding site (Fig. 12C). For instance, $Asn130^{Rip1p}$ is replaced with Arg in the bacterial Rieske

sequences, which is clearly electrostatically incompatible with $Arg98^{FvH}$ (Table 3). Furthermore, Ala144, Val147, and Lys148, from the yeast epitope, are replaced with Arg, Asp and Glu, respectively, which confers further incompatibility. In contrast, interactions could, theoretically, still be mediated by $Asp133^{Rip1p}$ that is conserved in *P. denitrificans*. Also, the $Gln151^{Rip1p}$ side chain that interacts with the side chain of $Arg53^{FvL}$ is replaced with a Glu in the bacterial sequence, which could participate in an ion pair interaction provided that the tertiary structure is conserved. This, however, is unlikely because the fold of this region in the bacterial Rieske protein is expected to be different, due to the inserted extra loop, as well as the absence of 3 prolines, which are present in the segment containing the yeast epitope. It was therefore not surprising to find that the bacterial enzyme was not efficiently captured by Fv18E11 in the magnetic beads pull down assay (Fig. 13).

An attempt was made to graft the complete epitope-containing segment, *i.e.* Pro123 to Gln151 (see Table 3), into the enzyme from *P. denitrificans* (by O. Anderka). This construct was not stably assembled. Therefore, chimeras were constructed, which contained the complete soluble domain of the Rieske protein, with and without the yeast linker region that connects the soluble domain to the transmembrane helix. The chimeras were named *Chimera(sc)* and *Chimera(pd)*, respectively. The chimera Rieske proteins were recognized by the Fv fragment in the pull down assay (*T. Kleinschroth, Diploma thesis*) (see Fig. 13). A stable co-complex of *Chimera(sc)* with Fv18E11 was formed and isolated by analytical size-exclusion chromatography and addition of 1,2-Dioleoyl-*sn*-Glycero-3-Phosphocholine (DOPC) to the preparation stabilized the integration of the engineered Rieske protein in the complex (*T. Kleinschroth and H. Palsdottir, unpublished*).

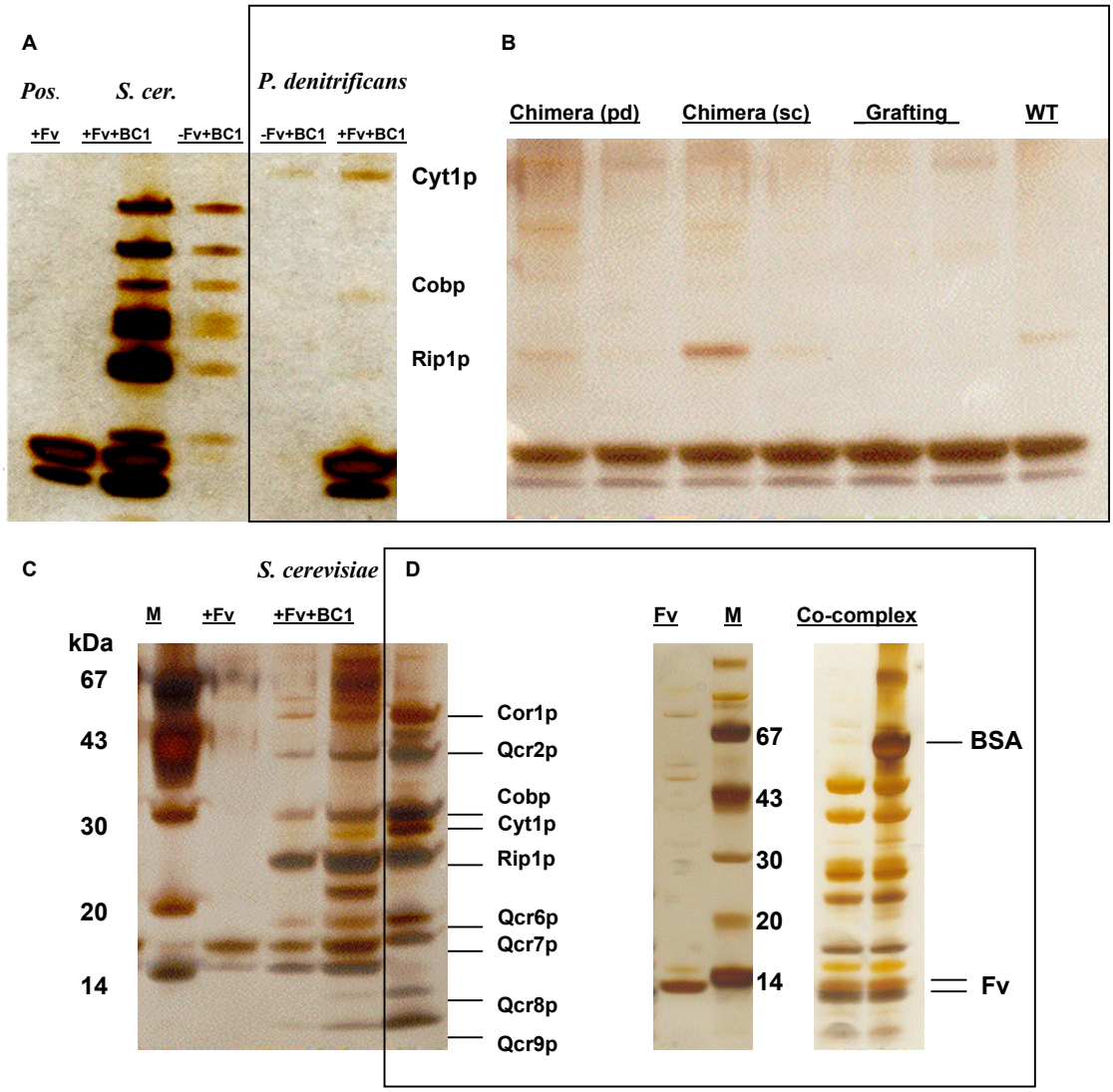

Fig.13 Magnetic beads pull down assay to probe co-complex formation. *Silver stained NuPAGE (4-12%) gel electrophoretic analysis of elution from beads.* ***A****, the positive control (Pos.) shows pull down of Fv fragment alone. In the pulldown of yeast cytochrome bc_1 complex (BC1) enrichment in the relative intensity of the Rieske polypeptide (Rip1p) with respect to the remaining polypeptides demonstrates the structural instability of the enzyme in this type of purification scheme. Insignificant pull-down of the enzyme from P. denitrificans illustrates the specificity of the Fv18E11 fragment for the yeast epitope.* ***B****, the two chimeras have the soluble domain of the bacterial Rieske protein replaced by the yeast domain. The two lanes show undiluted and five fold dilution of eluted fraction from the beads to confirm comparative intensity of bands. Eluate from Fv18E11 pull down is shown for of chimera (pd) with the bacterial linker, chimera (sc) with yeast linker, "grafting" refers to insertion of the epitope containing segment into the bacterial Rieske domain, and wildtype (WT) is shown for comparison.* ***C****, pulldown of yeast cytochrome bc_1 complex. The assay was optimized to reduce unspecific binding. Addition of the 67 kDa bovine serum albumine did not interfere with detection of the enzyme polypeptides. Lanes marked with M contain marker.* ***D****, the probes before the assay are shown for comparison of the relative intensity of cytochrome bc_1 complex and Fv fragment polypeptides before and after pull down.*

2.2.7 Fluorescent labeling of the Fv18E11 was hindered by its unstable assembly

Superimposition of the yeast enzyme with the X-ray structures where Rieske is found in different positions, showed that the Fv fragment light chain C-terminus was also rotationally displaced upon the movement from b- to c1-position. Thus, fluorescent labeling of the Fv fragment was pursued in order to estimate the Fv fragment affinity for the antigen by Fluorescence Correlation Spectroscopy. For this purpose an Fv fragment with a Cys engineered at the light chain C-terminus, was labeled with tetramethylrhodamine-5-maleimide (TMR5M). The yield of the modified Fv fragment from the streptavidin affinity purification was dramatically reduced compared to the wild type Fv18E11 preparation, or 5-fold less, *i.e.* ~800 µg from 12 L cultures of *E.coli*. Furthermore, destabilization of the engineered fragment was illustrated in the elution profile from streptavidin affinity chromatography. The second peak, marked with arrow in Fig 14B, was shown by Western blot analysis to contain only heavy chain (*data not shown*).

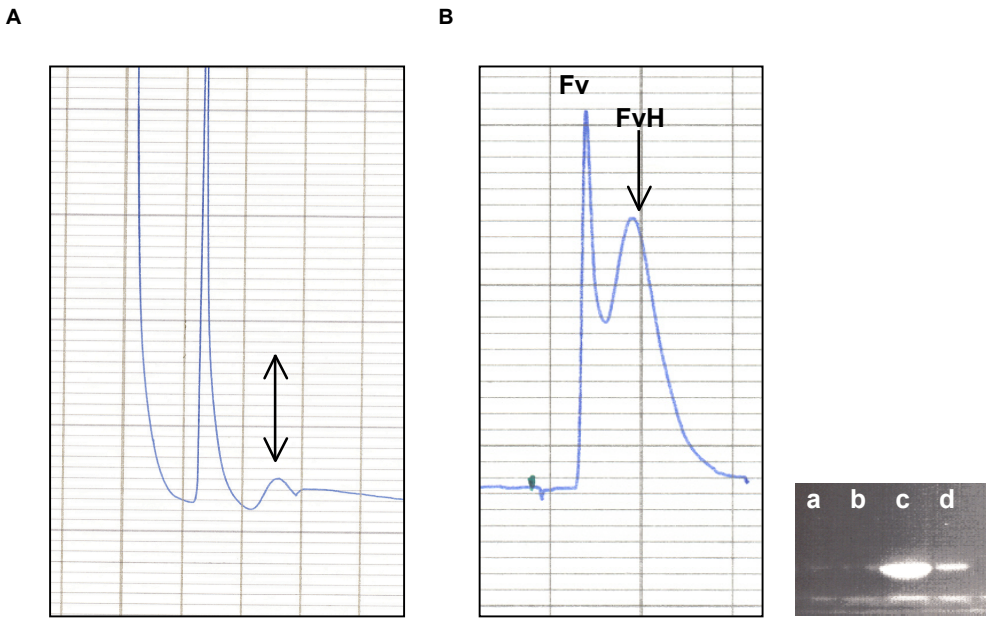

Fig.14 Streptavidin affinity chromatography of Fv18E11 and the variant. ***A****, the elution profile of WT Fv18E11 as monitored by absorbance at 280 nm. The second peak in the elution profile is much smaller (arrow).* ***B****, elution profile of the Fv fragment variant with a cysteine introduced at the light chain C-terminus, before the myc-tag. The relative intensity of the second peak (arrow) is greater compared to A. This peak was shown to contain the heavy chain alone. The insert on the right shows gel electrophoretic analysis to probe labeling by UV-irradiation in gels:* ***a****, negative control, WT Fv18E11;* ***b****, 5 times dilution of a;* ***c****, Fv-TMR5M;* ***d****, 5 times dilution of c.*

2.2.7.1 Assignment of surface accessible free thiols in the cytochrome bc_1 complex

Since instability of the Fv fragment hindered its fluorescent labeling, structural analysis was performed to evaluate the accessibility of free cysteines in the detergent solubilized or reconstituted enzyme. The aim of this analysis was to identify targets within the enzyme for fluorescence or spin labeling to study to the enzyme mechanism. The majority of cysteines were observed to be buried, involved in disulfide bond formation or other atomic interactions ($SH^{\cdots}O$) and therefore not accessible for labeling. However, a few putative candidates for labeling were identified. $Cys188^{Cyt1p}$ was appointed as the most feasible residue for labeling on the intermembrane space side (Fig. 15). $Cys188^{Cyt1p}$ is located close to the Q_o site, above the estimated bilayer. On the matrix side, $Cys312^{Cor1p}$, $Cys137^{Cor2p}$ and $Cys25^{Qcrp7p}$, appeared surface accessible and free.

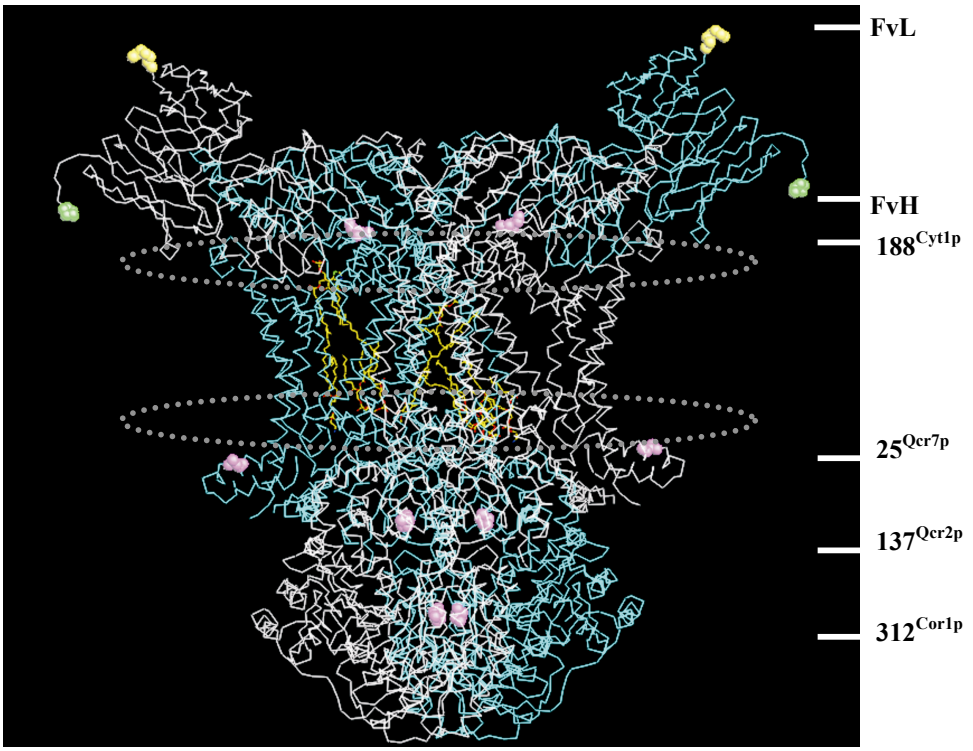

Fig.15. Identification of free and surface accessible cysteines in the X-ray structure. *A structural overview of potential targets for labeling. Solvent exposed and free cysteines are depicted as magenta spheres. The C-terminus of Fv-fragment light chain (i.e. myc-tag) is marked with yellow spheres and C-terminus of heavy chain (i.e. strep-tag) in green. Refined lipids (yellow ball-and-stick) permit positioning of the enzyme in the bilayer and the lipid-aqueous interface is marked with gray stipled ellipsoids.*

2.3 Crystallographic analysis of the binding mode of HHDBT at the Q_o site

The inhibitor 5-*n*-heptyl-6-hydroxy-4,7-dioxobenzothiazole (HHDBT) is structurally similar to ubiquinone, the substrate of the cytochrome bc_1 complex. The similarity is accomplished by a carbonyl and a hydroxy group on opposite sides on the benzothiazole ring (see Fig. 17). To analyze whether hydroxydioxobenzothiazoles compete with the substrate at the Q_o site, determination of the apparent K_m of the yeast cytochrome bc_1 complex for decyl-ubiquinol in the presence and absence of HHDBT were performed by Dr. C. G. Lojero in the laboratory of Prof. B. Trumpower. From *Lineweaver-Burk* plot it was concluded that HHDBT is a competitive inhibitor, which is consistent with the assumption that it is a substrate analogue. Ubiquinone has not been detected by X-ray crystallography at the Q_o site. The binding mode of competitive inhibitors is instead assumed to provide a reliable molecular description of the substrate binding site.

2.3.1 Crystallization with a negatively charged inhibitor bound at the Q_o site

A color change from yellow to purple was observed when HHDBT (20 mM stock in DMSO) was diluted in the buffer used for crystallization (pH ~8 at 4ºC). This color change is indicative of ionization of the 6-hydroxy group that was shown by Trumpower and colleagues to have a pK_a of 6.1 in detergent micelles. The inhibitor was crystallized at a $pH_{cryst} > pK_a$ and ca. 98 % of the inhibitor were calculated from the Henderson-Hasselbach equation to be ionized in the crystallization mixture.

The absorbance maxima of the protonated inhibitor HHDBT at 241 nm, 287 nm and 445 nm have extinction coefficients of 10.6, 12.2 and 0.77, respectively (in MeOH, acetic acid) (von Jagow and Link, 1986). Difference spectra of the yeast cytochrome bc_1 complex with bound inhibitor *versus* the enzyme alone at pH 6.0, were recorded by C.G. Lojero. When the inhibitor was added in molar excess the absorbance maximum shifted to longer wavelengths, whereas when added in substoichiometric amounts the spectra appeared similar to the spectra of inhibitor alone at pH 8.7. It was therefore concluded that the inhibitor is ionized when bound to the enzyme. These data refute previous reports that the ionized inhibitor cannot bind at the Q_o site (Zhang *et al*., 1999). Instead, the observed pH dependency of inhibition is attributed to a dissociable group within the complex, namely the catalytic residue His181 of the Rieske protein, as will be discussed in more detail below.

2.3.2 X-ray structure determination of HHDBT bound at the Q_o site

Because previous attempts to obtain high-resolution structures of the cytochrome bc_1 complex with undecyl-HDBT (UHDBT) bound at the Q_o site were not successful, the inhibitor with shorter alkyl chain, namely heptyl-HDBT (HHDBT), was selected for the X-ray structural studies presented here. The only difference between HHDBT and UHDBT is the shortening of the flexible side chain from 11 to 7 C atoms, thus the head group moiety, *i.e.* the functional groups which specifically bind to the enzyme, are the same. The inhibitor efficacy of UHDBT was shown to depend on the oxidation-reduction poise of the catalytic subunits, demonstrated by enhanced binding when the Rieske protein is reduced (Bowyer *et al*., 1982). The purified cytochrome bc_1 complex used in this study has a partially reduced Rieske (*F. McMillan, unpublished*) and was fully inhibited by the applied amount of HHDBT. The crystals with HHDBT bound diffracted to 2.5 Å resolution and a model of the enzyme was submitted to the PDB databank (PDB entry 1P84: Palsdottir *et al*., 2003) (Table 4). The experimental procedures for obtaining the crystals and subsequent structure determination are described in *section 4.13*.

Successful 3-D crystallization of the co-complex was restricted to the narrow pH_{cryst} range of 7.5-8.5 (4ºC). Crystal growth was monitored at different pH {6, 6.5, 7, 7.5, 8, 8.5}. Bis-tris-propane was used instead of Tris to buffer the precipitation solution below pH 7.5 (RT). Lowering the pH caused a shower of minute crystals to appear, which pointed to defect crystal contacts. Pre-formed crystals grown under feasible conditions (pH 7.5-8, 4ºC) cracked when they were soaked to acidic pH. It was therefore not possible to soak the crystals of the HHDBT inhibited enzymes below $pH_{cryst} < pK_a$. The crystal lattice is fragile and held together by few polar contacts of small surface area (see *section 2.2.3*). Importantly, structural analysis showed that a number of histidines participate in crystal contact formation, perhaps explaining this pH sensitive behavior in crystal formation. It is important to point out that at the given conditions, crystallization of the enzyme without inhibitor bound at the Q_o site was not possible (*C. Hunte, unpublished observations*). Although important crystal contacts are mediated by the strep-tagged Fv18E11, it is not sufficient to support crystallization. Without Q_o site inhibitor bound, the Rieske protein may not be fixed in b-position and this lack of stabilizing interaction is presumably the reason why the enzyme only crystallizes in the presence of inhibitor.

2.3.3 Binding of HHDBT at the Q_o site

The difference electron density map (F_o-F_c) calculated prior to inclusion of HHDBT in the model clearly showed specific binding at the Q_o site (Fig. 16). The asymmetric form of the difference density for the head group moiety permitted unambiguous orientation of the hydroxy-dioxobenzothiazole ring.

The Q_o site is formed by the C-terminus of cytochrome *b* transmembrane (TM) helix $C^{111\text{-}134}$, N-terminus of TM helix $D^{173\text{-}204}$, the intervening *cd* loop$^{135\text{-}173}$ including two small non-transmembrane a-helices *cd*1$^{138\text{-}153}$ and *cd*2$^{158\text{-}166}$, the *ef* loop$^{246\text{-}288}$ with a-helices *ef*1$^{254\text{-}257}$ and *ef*2$^{274\text{-}283}$ and the N-terminus of TM helix $F^{288\text{-}307}$ (Fig. 17). The *ef* and *cd* loops serve as 'lids' from the intermembrane side and provide a narrow opening for the Rieske cluster containing domain to access the substrate. Residues which interact with HHDBT are confined to the *cd*1 helix and the *ef* loop (Table 5).

Table 4 Crystallographic table. *Statistics for two datasets obtained from the modified preparation (described in section 2.1) with stigmatellin and HHDBT bound at the Q_o site.*

	Stigmatellin	**HHDBT**
PDB entry	n.s.	1P84
	Space group C2	
a, b, c [Å]	214.6, 164.1, 147.7	215.0, 165.1, 147.5
β [°]	117.6	117.3
atoms	18115	18069
amino acid residues	2168	2168
Non-protein molecules	13	13
solvent molecules	321	326
	Data collection	
Resolution range (OS) [Å]	30.0-2.5 (2.59-2.50)	25.0-2.50 (2.56-2.50)
Measured reflections	445,775 (42,078)	372,220 (20,853)
Redundancy	2.9 (2.8)	2.5 (2.3)
Unique reflections	153,177 (15,221)	149,103 (9,128)
Completeness [%]	98.3 (98.5)	92.4 (84.6)
Rmerge [%] ξ	6.8 (56.2)	6.6 (37.4)
I/s(I) < 1	20.3 (2.3)	13.4 (1.2)
	Refinement	
Resolution range (OS) [Å]	25.0-2.50 (2.52-2.50)	25.0-2.50 (2.52-2.50)
R factor [%]*	21.4 (34.6)	22.5 (40.9)
Rfree [%]#	24.1 (34.2)	25.3 (38.4)
Root mean square deviations from ideal values		
Bond lengths [Å]	0.007	0.008
Bond angles [°]	1.269	1.305
	Structure validation	
Most favored regions [%]	88.0	86.8
Additional allowed [%]	11.3	12.5
Generously allowed [%]	0.5	0.5
Disallowed [%]	0.3	0.2

*n.s.=not submitted. OS=outer shell. Diffraction data collected at ESRF, ID14-EH3 at 4°C, l 0.9299 Å, ξRmerge=ShSi|Ii(h)-<I(h)>|/ShSII(h), Ii(h): intensity of ith measurement, <I(h)>: average intensity of a reflection, *R factor=Sh||F(h)obs|-|F(h)calc||/Sh|F(h)|, #Rfree calculated for 2.5% of reflections.*

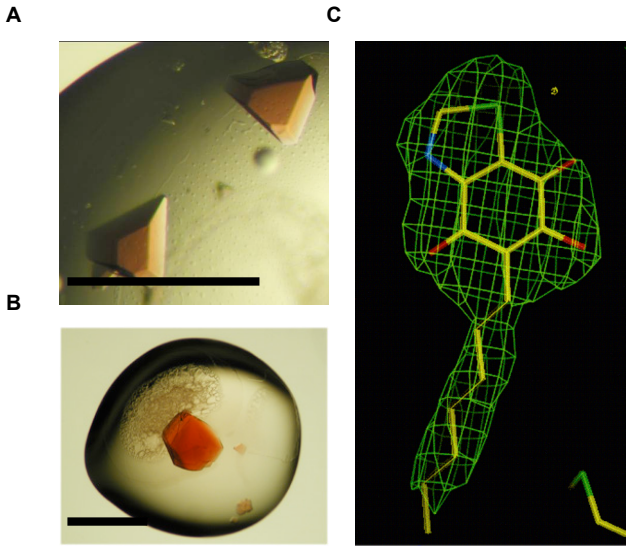

Fig.16 Crystallization of the HHDBT-Fv18E11-cytochrome bc$_1$ co-complex. A, *crystals grown with HHDBT bound were smaller and had a purple shade compared to the B, intensely red crystals with stigmatellin bound. The black bar measures 1 mm.* ***C****, asymmetric difference electron density of HHDBT at the Q_o site allows unambiguous modeling of ligand orientation.*

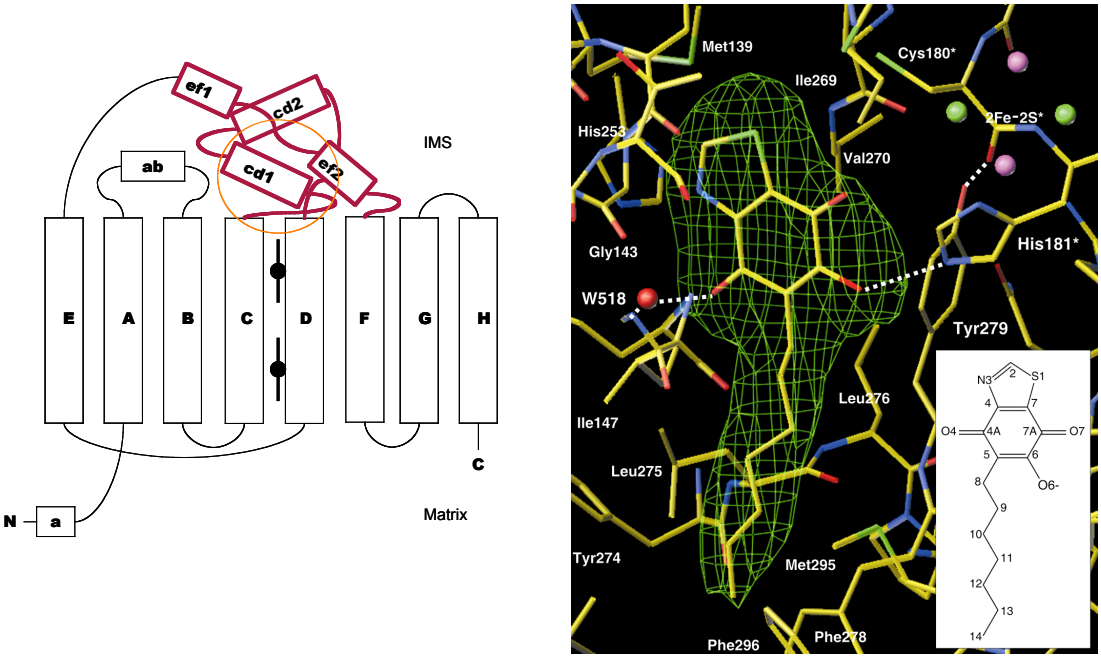

Fig.17 A structural overview of the Q_o site. A*,the topological arrangement of a-helices in cytochrome b. The regions which construct the Q_o site are marked in red. The orange circle points out the site.* ***B****, the binding mode of HHDBT at the Q_o site (from Palsdottir et al., 2003)*

2.3.4 Comparison of HHDBT and stigmatellin binding at the Q_o site

The X-ray structures of the enzyme with stigmatellin (PDB entry 1KB9: Hunte *et al*., 2000) and HHDBT (PDB entry 1P84: Palsdottir *et al*., 2003) were superimposed by structural alignment using LSQMAN. Differences between the structures were estimated by the root mean square deviation criteria (RMSD) in terms of atomic positions after superimposition of the Cα atoms (see *section 4.13.6.4)*. The resulting values for the catalytic subunits were RMSD(all atoms)/RMSD(Cα atoms) of 0.369 Å (3089 atoms)/0.235 Å (385 atoms), 0.272 Å (1941 atoms)/0.214 Å (246 atoms), and 0.270 Å (1411 atoms)/0.238 Å (185 atoms), for cytochrome *b*, cytochrome c_1 and Rieske protein, respectively.

The inhibitors, stigmatellin and HHDBT, overlap with their head groups positioned in the tight binding pocket carved by cytochrome *b* residues and enclosed by the Rieske protein, which is in b-position, and contributes a hydrogen bond via the cluster ligand $His181^{Rip1p}$ to the carbonyl and hydroxyl group of stigmatellin and HHDBT, respectively. The larger surface area of stigmatellin, its rigid side chain, as well as an additional hydrogen bond provided by cytochrome *b* residue $Glu272^{Cobp}$ confer stronger binding than for HHDBT, observed in greater inhibitor potency of stigmatellin (Zhang *et al*., 1999). The side chain of HHDBT coincides and ends where the stigmatellin side chain bends. Both inhibitor side chains extend into the gradually opening hydrophobic cavity at the dimer interface.

The flexible alkyl chain of HHDBT was defined to full length in the experimental difference density, demonstrating tight and specific binding. The short heptyl side chain of HHDBT is stabilized by *van der Waals* interactions with cytochrome *b* residues: Ile147, Leu275, Met295 and Phe278. The following residues contribute to the binding site, but are not in close contact to HHDBT (> 3.9 Å) and therefore not listed in table 5: Ile125 (4.0 Å), Phe129 (6.0 Å), Tyr132 (5.5 Å), Leu150 (5.5 Å), Thr265 (6.0 Å), Glu272 (5.0 Å), Leu275 (4.0 Å), Leu282 (4.0 Å), Met295 (4.0 Å), and Phe296 (5.3 Å). The largest surface area at the binding site is provided by residues: Tyr279, Met295, Val146, Ile147, and Leu275, in decreasing order of contribution.

Stigmatellin makes *van der Waals* contacts with a larger number of cytochrome *b* residues, of which nine are not involved in contacts to HHDBT: Thr122, Ala126, Leu130, Thr148, Phe151, Leu165, Phe179, Leu182 and Val270. The

largest surface contact area to stigmatellin is provided by Tyr279, Met295, Ile147, Phe129 and Leu275, listed with decreasing contribution.

The conserved and catalytically important *cd* loop residue Trp142 (see Brasseur *et al.*, 1996), discriminates between HHDBT and stigmatellin by only contacting HHDBT. Phe129^{Cobp}, a side chain stabilizing ligand of stigmatellin was observed in alternate conformations when HHDBT is bound. The short tail of HHDBT does not extend far enough to stabilize this residue (0.3 Å^2 contact area) compared to the greater or 45.1 Å^2 surface contact area to the stigmatellin side chain. Variants at this position exhibit impaired ubiquinol oxidation (see Brasseur *et al.*, 1996), which suggests a role of this residue in stabilization of the quinone side chain, or at least its importance for maintaining proper molecular structure at the site. Mutagenesis studies in *R. sphaeroides* showed that when Phe129^{Cobp} was replaced with a positively charged residue quinol oxidation was abolished. Furthermore, EPR spectral properties of the Phe129Arg variant, suggested ion pair formation with an anionic ubiquinone (Ding *et al.*, 1995a).

The aromatic rings of stigmatellin and HHDBT are *in plane* and both positioned at 90 degree angle to the side chain of Tyr279^{Cobp} (Fig. 19). The distances between the O6 atom of HHDBT and the Tyr279^{Cobp} side chain atoms, Cδ1 and Cε1, respectively, are below the sum of their *van der Waals* radii ($d_{C_\delta 1\text{-}O6}$=3.2 Å and $d_{C_\varepsilon 1\text{-}O6}$=3.3 Å), indicating a weak hydrogen bond (C-H···O) with the aromatic C-H groups as donors. Hydrogen bond angles and bending angles at the acceptor atom ($\theta_{C_\delta 1\text{-}H\text{-}O6}$ =125 °, $\theta_{C_\varepsilon 1\text{-}H\text{-}O6}$ =113 °, $\phi_{H_\delta 1\text{-}O6\text{-}C6}$ =107 °, $\phi_{H_\varepsilon 1\text{-}O6\text{-}C6}$ =94 °) are only slightly lower than the optimal range for non-conventional hydrogen bonds (Desiraju and Steiner, 1999). The bifurcation is not fully symmetrical as conditions for the bond involving Cd1 are more favorable. The acidity of the aromatic C-H groups is increased, because the hydroxy group of Tyr279^{Cobp} donates a hydrogen bond to the backbone oxygen of the disulfide bridged Cys180^{Rip1p} (dOH-O= 2.7 Å; φCz-OH-O = 112°). Cys180^{Rip1p} contributes to the fold of the cluster containing tip of Rieske.

B factor analysis indicates a tight binding of stigmatellin with average B factors of 37.4 Å^2 and 35.6 Å^2 for the inhibitor and cytochrome *b,* respectively. HHDBT appears less tightly bound with average B factor of 50.9 Å^2 compared to 40.2 Å^2 for cytochrome *b*. Kinetic studies agree that stigmatellin is more tightly bound than UHDBT, as it is a more potent inhibitor (Zhang *et al.*, 1999).

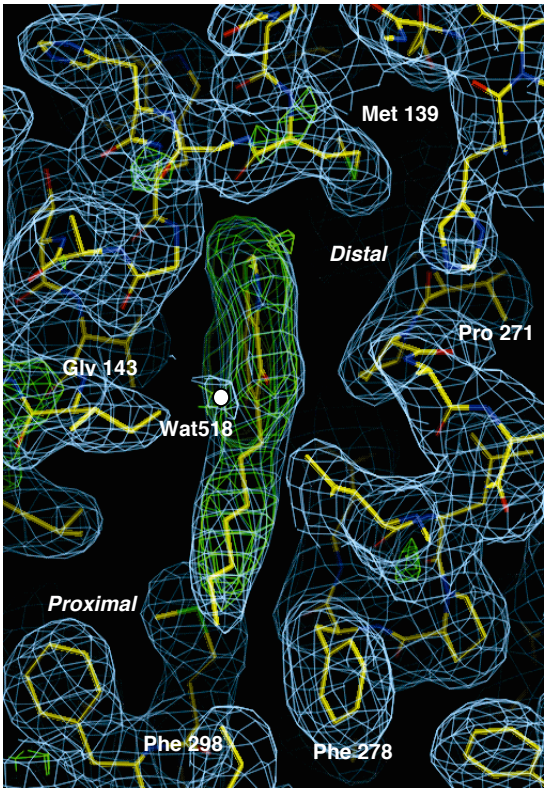

Fig.18 Electron density map and structural model of the Q_o site viewed from heme b_L. *A structural water molecule (Wat518) was refined at the active site and is involved in hydrogen bond stabilization of the ligand. The Q_o site is divided into two domains, referred to as proximal and distal to heme b_L.*

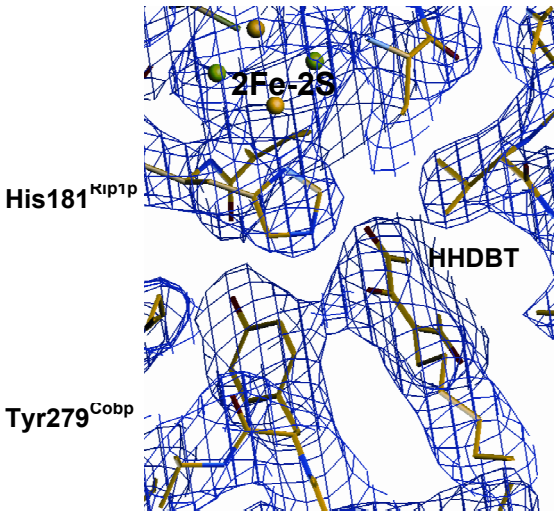

Fig.19 Electron density and model of the Q_o site viewed from the intermembrane space. *$2F_o$-F_c electron density map illustrated the tight interaction of the inhibitor with the Tyr279 side chain.*

2.3.5 The ionized HHDBT hydroxy group binds the protonated His181^{Rip1p}

Stigmatellin and HHDBT head group moieties are stabilized by a network of weak and strong hydrogen bonds and numerous *van der Waals* interactions. Importantly, the oxygen atom of the ionized 6-hydroxy group (O6) of the hydroxy-dioxobenzothiazole head is in close contact with the nitrogen atom Nε2 of His181^{Rip1p}, of which the second imidazole nitrogen coordinates the [2Fe-2S] cluster of the Rieske protein. The distance and geometry of the interaction ($d_{N_\varepsilon 2\text{-}O6}$= 2.8 Å; θ = 148°) are in good agreement with a conventional hydrogen bond. Likewise, the carbonyl (O8) of stigmatellin forms a hydrogen bond to His181^{Rip1p}. When superimposed both functional groups occupy exactly the same position (Fig. 20). Crystallographic analysis of stigmatellin binding suggested that Nε2 is protonated at pH 8.5, as the fixation of Rieske protein in b-position is stabilized by a hydrogen bond between this atom and the carbonyl group of stigmatellin (Hunte *et al*., 2000). For crystallization of the cytochrome bc_1 complex in the presence of HHDBT the pH was lowered by half a unit, and Nε2 is expected to be protonated under these conditions. With both donor and acceptor of the hydrogen bond ionized, this type of a polarized hydrogen bond provides a strong stabilizing interaction. On the other side the carbonyl group O4 is oriented towards heme b_L and forms a hydrogen bond to a structural water molecule (Wat518) that is also stabilized by a hydrogen bond to the backbone nitrogen atom of Glu272^{Cobp} (Fig. 22). The Glu272^{Cobp} side chain, which was observed to form a hydrogen bond to the hydroxy group of stigmatellin (Hunte *et al*., 2000), re-orients when HHDBT is bound and points out of the binding site.

Table 5 The binding mode of HHDBT at the Q_o site.

Cobp	**Å**	**Q_o**	**Cobp**	**Å**	**Q_o**	**Cobp**	**Å**	**Q_o**	**Rip1p**	**Å**	**Q_o**
M139(O)	3.6	C2	V146(Cγ1)	3.6	O7	P271(Cβ)	3.4	O4	C180(Cβ)	3.8	O7
W142(C)	3.9	C2		3.7	C7		3.7	C4	H181(Cε1)	3.4	O7
	3.9	S1		3.6	O6	P271(Cγ)	3.6	C4		3.6	O6
W142(Cβ)	3.8	S1		3.7	C6		3.7	O4	H181(Cδ)	3.9	O6
W142(O)	3.9	S1	V146(Cγ2)	3.2	O7		3.8	C5	H181(Nε)	2.8	O6
G143(N)	3.4	C2		3.7	C7	F278(Cβ)	3.9	C12		3.5	O7
	3.8	N3	I147 (Cδ1)	3.4	C9	Y279(Cδ)	3.2	O6			
G143(Cα)	3.5	N3	I269 (Cδ1)	3.7	S1		3.7	C6	**Water**	**Å**	**Q_o**
	3.6	C2		3.6	C7A	Y279(Cε1)	3.3	O6	Wat 518	2.9	O4
V146(Cβ)	3.8	O7		3.8	C7		3.7	C6			
	3.9	C7		3.9	O7	I299(Cδ1)	3.9	C14			

A few polar and several non-polar interactions stabilize the hydroxy-dioxobenzothiazole. Residues within interatomic distances of less than 3.9 Å from inhibitor are listed (from Palsdottir et al., 2003).

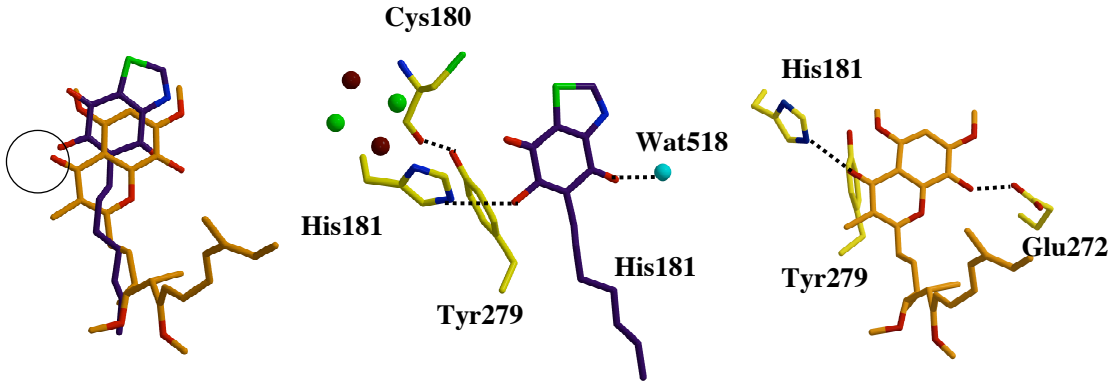

***Fig.20 Comparison of stigmatellin and HHDBT binding at the Q_o site. Left**, when the X-ray structures of the stigmatellin (orange) and HHDBT (purple) inhibited enzymes were superimposed the inhibitors were found to be in plane, with the functional groups at the same position (encircled). **Middle**, HHDBT is stabilized by a hydrogen bond from the ionized hydroxy group to protonated His181 and from the carbonyl group on the other side to Wat518. **Right**, Glu272 side chain rotates into the binding site to form a hydrogen bond to the stigmatellin hydroxyl group and on the other side the carbonyl group of stigmatellin forms a hydrogen bond to His181. Please note that the polar interactions from Tyr279 side chain to the backbone carbonyl of Cys180 as well as the [2Fe-2S] cluster are not depicted in C, although present at the same position as shown in B.*

2.3.6 Conformational flexibility at the Q_o site

Superposition of the X-ray structures of the enzyme with stigmatellin and HHDBT bound, revealed that major conformational changes were confined to cytochrome *b* residues, which form the Q_o site (Fig. 21). Conformational changes illustrated Q_o site occupancy induced plasticity of the enzyme. RMSD comparison of the two structures revealed a short span of main chain displacement and a few side chain rearrangements. Comparison of residue accessibility did not expose large differences between the two data sets (*data not shown*). Upon HHDBT binding, an expansion of the binding pocket was noticed in a local displacement of the *ef* segment Cα trace, including residues Ala267, Ser268, Ile269 and Val270, located just before the catalytic PEWY loop (Pro271-Tyr274). The greatest Cα trace displacement was at Ser268 (1.7 Å) (see also *Appendix A4*). The most pronounced side chain displacements were observed for His253 and Glu272 (Fig. 21).

Based on the binding mode of stigmatellin, Glu272 is proposed to be a direct ligand of ubiquinol and a primary proton acceptor in quinol oxidation (Crofts *et al.*, 1999; Hunte *et al.*, 2000). A hydrogen-bond network established by cytochrome *b* residues Arg79, Tyr132, Asn256, Glu272, Tyr274, the heme b_L propionate A, and

structural water molecules, was identified in the crystal structure of the yeast enzyme with stigmatellin bound at the Q_o site (see Fig. 5). In the X-ray structure of the cytochrome bc_1 complex with HHDBT bound at the Q_o site, the side chain of Glu272 is rotated out of the Q_o site, and forms a hydrogen bond to a structural water molecule (Wat42) that is further stabilized by heme propionate A (L1O2A) (Fig. 22). The side chain atoms of Glu272 occupy the previous position of two structural water molecules (Wat428 and Wat50) that were refined in the structure of the stigmatellin inhibited enzyme. Upon rotational displacement of the Glu272 side chain, a water molecule Wat518 is positioned at the previous location of the carboxylate and forms a hydrogen bond with backbone nitrogen of Glu272 and the carbonyl O4 atom of HHDBT (Fig. 22). The reorientation of Glu272 is accompanied by subsequent rearrangements in the hydrogen bond network. His253 is rotationally displaced and forms a hydrogen bond to the Glu272 side chain. Tyr274 remains in position and stabilizes the rotationally displaced Glu272. Arg79 is hydrogen bonded to the heme propionate and provides a possible proton escape route by connecting to the bulk solvent (see Fig. 22).

Charged residues are not abundant in the membrane spanning part of integral membrane proteins. Most of the membrane immersed titratable residues have a functional role, for instance in stabilization of cofactors (*i.e.* histidines ligating hemes), binding of substrate at the active sites (Q_o and Q_i site), in proton transfer pathways, or interact with lipid phosphodiester groups. From above it is clear that structural analysis of titratable residues close to the quinol oxidation site has been useful in proposing possible proton escape routes from the Q_o site. To summarize, in the 8 transmembrane helix protein cytochrome *b*, 11.4 % of the total amino acid residues are titratable, 3.4 % can carry a negative charge (8 Asp, 2 %; 5 Glu 1.3 %) and the remaining 8 % (13 His, 3.4 %; 7 Lys, 1.8 %; 11 Arg, 2.9 %) can be positively charged. Protonatable residues in the vicinity of the Q_o site that were identified by structural analysis include: Glu66, Arg70, Arg79, His253, Asp255, Glu272, Arg283, and Lys288. Functional characterization of these residues relies on other techniques and Fourier-Transform infrared spectroscopy can for instance provide information about redox-induced protonation behavior of amino acid residues, as will be described in the next section.

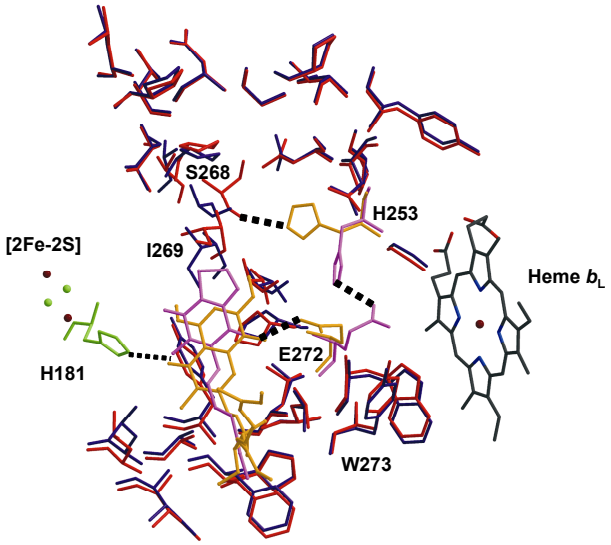

Fig.21 Q_o site occupancy induced conformational changes. *Structural alignment with stigmatellin (orange, red) and HHDBT (purple, blue) bound at the Q_o site revealed that the most pronounced main and side chain displacements, as response to binding of different ligands at the active site in the X-ray structures of the yeast enzyme, are confined to cytochrome b residues 245-274 from the catalytic ef loop. Also shown here are heme b_L and His181 of the Rieske protein that occupy the same position in these two structures.*

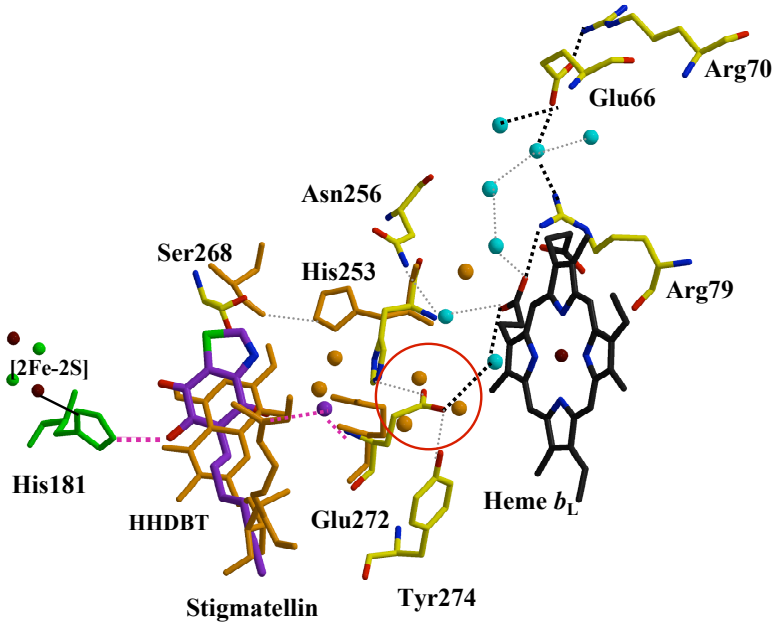

Fig. 22 The proton exit pathway from the Q_o site. *X-ray structural analysis of hydrogen bonds pointed out a putative proton escape route. The reorientation of Glu272 side chain is encircled. Possible proton exit via hydrogen bonds is marked with stipled lines (black). The coordinates shown are from PDB entry 1P84, except for the position of His253, Ser268, Glu272 and stigmatellin that are from PDB entry 1KB9 and are depicted in orange.*

2.4 Stigmatellin and HHDBT binding probed by FTIR analysis

Based on the structural study presented here, an electrochemical and spectroscopic study was carried out, in collaboration with Dr. P. Hellwig and Dr. M. Ritter. The aim of this study was to address redox-dependent alterations in the protonation state of titratable amino acids close to the Q_o site in order to identify catalytically important residues.

The binding of diverse inhibitors, including: HHDBT, Stigmatellin, Undecyl stigmatellin (UST), ^{13}C-UST, Methoxyiminoacetamide (MIA), ^{13}C-MIA, UK2A and antimycin, to the yeast cytochrome bc_1 complex, was monitored by electrochemically induced FTIR difference spectroscopy. The oxidized-minus-reduced FTIR difference spectra revealed redox-induced conformational and/or protonation changes within the enzyme. In the spectra, positive bands show signals associated with the oxidized state of the protein, and negative signals represent the reduced state. An important outcome of this study was that stigmatellin itself appeared to be redox-active (Ritter *et al*., 2004). The effect of stigmatellin binding on the electrochemically induced FTIR difference spectra of the enzyme is presented in Fig. 23. Compared to the native enzyme, clear variations were observed upon binding of substoichiometric amounts of stigmatellin to the enzyme (Fig. 23B). Even more dramatic was the spectral change when 10-fold increase of stigmatellin was added (Fig. 23C), but this revealed an increase in amplitude of several signals that were derived from stigmatellin itself. In order to discriminate protein-specific variations from signals derived from the redox active inhibitor, model compound studies in solvent with a stigmatellin derivative (UST), having the conjugated trienes replaced by an aliphatic tail, were performed. The carbonyl group shown in crystal structures to interact with His181^{Rip1p} was specifically ^{13}C-labeled. The studies with labeled (4-^{13}C=O) UST led to a more detailed understanding of the electrochemically induced FTIR difference spectra (Ritter *et al*., 2004).

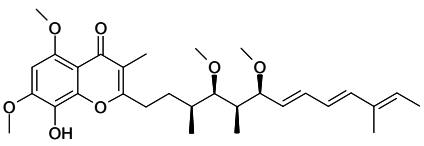

Stigmatellin

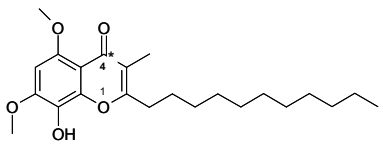

UST

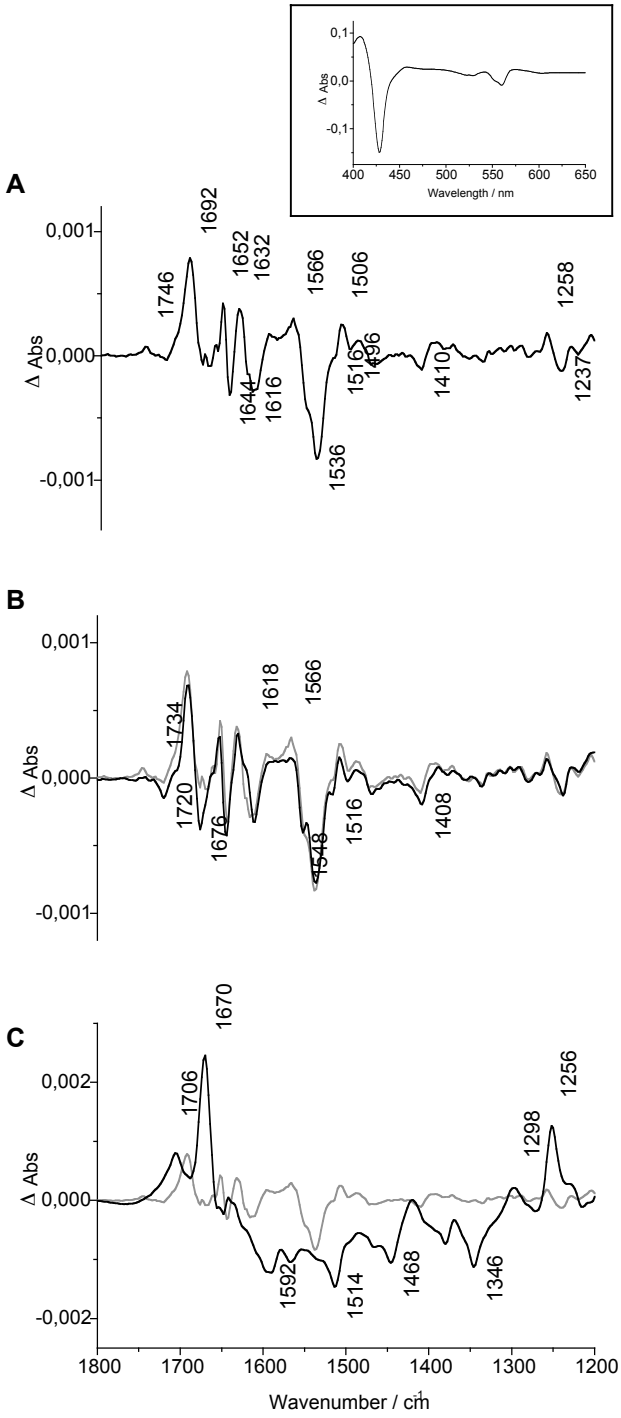

Fig.23 Oxidized-minus-reduced FTIR difference spectra. A, *yeast cytochrome* bc_1 *complex with* ***B****, 1 µM or substoichiometric amount of natural stigmatellin A (black, full line) and* ***C****, 10 µM of the inhibitor (black, full line), shown overlayed with A (gray line,* ***B*** *and* ***C****) for a potential step from –0.292 to 0.708 V (vs SHE'). The insert above shows the oxidized-minus-reduced visible difference spectra as typically monitored to control the full reaction if the enzyme (from Ritter et al., 2004).*

Absence of quinone characteristic signals in the spectra suggested that the Q_o site is empty in the protein preparation from yeast. This interpretation is based on the assignment of Q_o site quinone signals in the cytochrome bc_1 complex preparation from *P. denitrificans* (Ritter *et al*., 2003).

To address mechanistic aspects of proton transfer and catalysis, the spectral region above 1710 cm^{-1}, which is characteristic for protonated aspartic or glutamic acids, is of interest. Comparison of the spectral region for protonated carboxylates in the native enzyme (*i.e.* empty Q_o site) with the spectra when stigmatellin and HHDBT are bound at the Q_o site, is shown in Fig. 24. In the absence of inhibitor, a prominent positive peak is present at 1746 cm^{-1}, which points to the presence of protonated carboxylate groups in the oxidized enzyme. Interestingly, the signal at 1746 cm^{-1} is decreased when stigmatellin is bound. This spectral change is accompanied by an increase in signal at 1732 cm^{-1} (see Fig. 24). In order to interpret the spectral changes that occur upon stigmatellin binding, two different scenarios can be considered. One explanation could be that the binding of inhibitor causes an environmental change of a protonated residue, leading to weaker hydrogen bonding and inducing the downshift of the ν(C=O) vibrational mode. Alternatively, the decrease in signal at 1746 cm^{-1} could be explained by the deprotonation of an acidic residue, whereas the emerging signal at 1732 cm^{-1} would be derived from protonation of another residue. It is most likely that Glu272 is deprotonated when rotated into the binding site as it binds the hydroxyl group of stigmatellin. Therefore, an additional residue should be considered to be perturbed upon binding. In Fig. 25 titratable carboxylates (*i.e.* Glu66, Asp255, and Glu272) identified by structural analysis of the Q_o site are pointed out.

Importantly, this FTIR spectroscopic study demonstrated that changes in protonation state and/or conformational change of protonated carboxylates are linked to the events, which occur upon binding of inhibitors to the Q_o site of cytochrome bc_1 complex from *S. cerevisiae*. Exact assignment of these signals in the FTIR difference spectra needs support from site-directed mutagenesis.

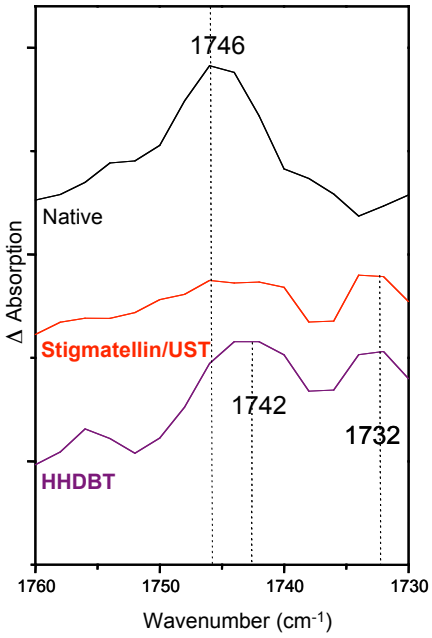

Fig.24 Comparison of the spectral region for protonated carboxylates. *Difference spectra recorded in the presence of the inhibitors stigmatellin/UST and HHDBT were compared with native enzyme. The difference in absorption, i.e. distance between ticks on y-axis, equal 0.00005 absorbance units. Lack of Q_o site specific quinone signals suggests that the native preparation has an empty Q_o site.*

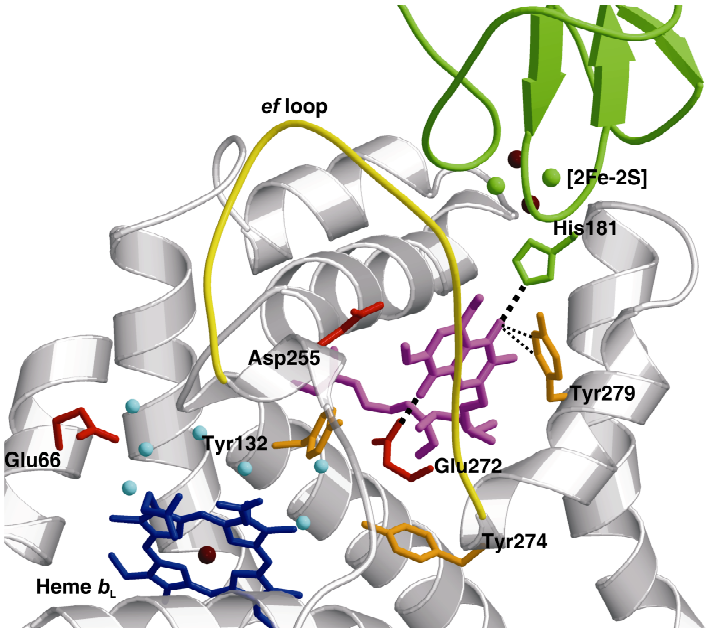

Fig.25 The Q_o site viewed from the intermembrane space. *Cytochrome b (gray) forms the crater into which the [2Fe-2S] cluster bearing tip of the Rieske (green) docks. Stigmatellin binding is stabilized by hydrogen bonds (dotted lines) to $His181^{Rip1p}$ and $Glu272^{Cobp}$. Acidic residues and tyrosines at the Q_o site are depicted in red and orange, respectively. The flexible ef loop is depicted in yellow.*

2.5 Specific binding of phospholipids to the yeast cytochrome bc_1 complex

The transmembrane helices of cytochrome *b* bundle up to shape the internal cavity at the dimer interface, where the majority of tightly bound phospholipids and the refined detergent molecule are identified in the structure of the yeast enzyme with stigmatellin at the Q_o site (Lange *et al.*, 2001). Notably, all active site occupants tail into this cavity at the dimer interface. This is best illustrated by the side chain of stigmatellin, which extends into the lipophilic cavity to meet the end of the isoprenoid terminus of endogenous CoQ_6, which is bound at the Q_i site of the other monomer (see Fig. 26 A). Preferential side chain stabilization of ligands at the Q_o site is demonstrated where the full length flexible alkyl chain of HHDBT coincides with the side chain of stigmatellin (see *section 2.3.4*), despite no obvious steric preferences in the spacious distal domain of the Q_o site. Another interesting observation is that close to the end of the HHDBT heptyl chain, unresolved lipid-like density is observed to extend and tail towards the Q_i site occupant. The position of this unresolved compound coincides with the position of the stigmatellin side chain. Obvious polar ligands are not available and partial density does not permit identification of this molecule. Importantly, this passage that leads to the lipid filled cavity at the dimer interface, may serve as the substrate entrance channel to the Q_o site.

The modified preparation presented here (see *section 2.1*) was optimized for less delipidation. Consistent with increased lipid content of the preparation, the protein preparation exhibited higher enzyme activity (Table 2). Furthermore, two new phospholipids were identified in the X-ray structures derived from this preparation (Table 4), in addition to the detergent molecule and five previously identified phospholipids (Lange *et al.*, 2001). The distribution of average B factors for the refined lipids compared to their ligating protein subunits, demonstrates their tight binding to the complex (Table 6). The reproducibility of assigned lipid binding sites was noteworthy and pointed to high specificity of binding, including selective stabilization of the acyl chains. Even structural features, such as kinked side chains, were remarkably conserved. In Fig. 26A the refined lipids are shown as they appear in the structural context of a homodimer. Common features in stabilizing interactions with the identified phospholipids, include stabilization of the negatively charged head group moiety by positively charged residues (Fig. 26B), as well as aromatic residues, such as Trp and Tyr were frequently observed to contact both acyl chains and head groups (Fig. 26C) (see also Table A5, *Appendix A5*).

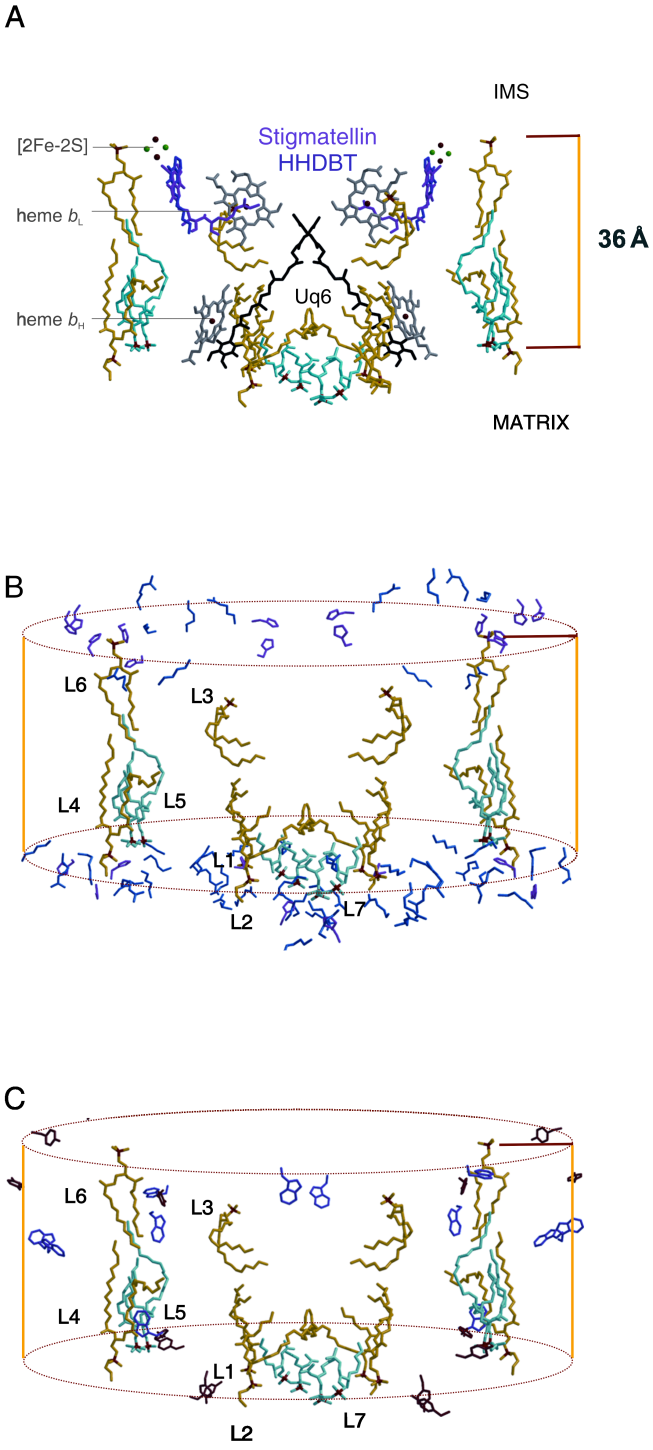

***Fig.26 Arrangement of tightly bound phospholipids in the structure of the homodimer. A**, lipids (yellow, cyan), b-type hemes (gray), Q_i site CoQ_6 (black), HHDBT (purple) and stigmatellin (red). The thickness of the bilayer was estimated from the distance between the phosphate moieties of matrix leaflet lipid L4 and intermembrane space leaflet lipid L6. The atoms P, Fe and S are marked in red, brown and green, respectively. **B**, surface accessible positively charged residues, which are positioned in the lipid head group region, are depicted, with His (magenta) and Lys/Arg (blue) (see text). **C**, surface exposed Tyr (brown) and Trp (blue) (From Palsdottir and Hunte, in press).*

Notably, all of the identified lipids made contacts to cytochrome *b* (Table 6). In Fig. 26B a cut-off criteria of > 50 Å^2 accessible surface area and 5 Å distance from estimated polar region of the membrane plane clearly demonstrates how '*the positive-inside rule'* takes effect for the mitochondrial encoded 8 TM helix cytochrome *b*, with enrichment of positively charged residues at the negative side of the membrane, or the matrix side (von Heijne, 1986; von Heijne and Gavel, 1988). This is also where the majority of refined lipid head groups is stabilized.

The distribution of the selected 41 basic residues is shown in Fig. 26B (12His/14Lys/15 Arg): Cor1p (1/1/4), cytochrome *b* (4/3/4), cytochrome c_1 (3/3/1), Rieske (0/1/1), Qcr7p (2/0/0), Qcr8p (1/2/4) and Qcr9p (1/4/1).

Tyr (brown) and Trp (purple) have a proposed role of positioning the complex by 'anchoring' the transmembrane region in the lipid bilayer. The applied cut-off criteria for displaying residues in Fig. 26C is surface accessibility of more than 50 Å^2 within the bilayer embedded regions. In this way 8 Tyr and 6 Trp were selected for each monomer, or more specifically (Tyr/Trp): cytochrome *b* (3/3), cytochrome c_1 (1/0), Rieske (1/0), Qcr8p (3/2) and Qcr9p (0/1)

Table 6 Contacts between phospholipids and cytochrome bc$_1$ complex subunits.

Subunits			**Cor1**	**Qcr2**	**Rip1**	**Cob**	**Cyt1**	**Qcr6**	**Qcr7**	**Qcr8**
		B factors	*76-79*	*91-94*	*60-66*	*37-40*	*55-59*	*78-81*	*54-56*	*75-78*
Lipid	*B factors*	Chain length								
L1	*67-70*	5-15 ; 13	X			X				
L2	*64-68*	16-18 ; 7				X/X*				
L3	*54-56*	14 ; 12			X	X	X			
L4	*62-63*	14 ; 16-18				X			X	X
L5	*74*	11 ; 10 ; 18; 9				X	X		X	
L6	*78-93*	9-10 ; 11				X	X			
L7	*86-88*	2 ; 2 ; 2 ; 7	X			X				

Style of lipid designation is taken from Lange et al., 2001: ***L1-L5****.* ***L6*** *(Palsdottir et al., 2003) and* ***L7*** *were identified in crystal structures from the modified preparation described here. The acyl chain lengths show number of carbon atoms counting from the carboxy-ester bond. The side chains were truncated according to visibility in the experimental electron density and are therefore presented as the interval of length as refined in 3 different datasets. Likewise, the average B factors (Å^2) calculated for subunits and ligands in the analyzed datasets are shown. Chain length gives an indication of the extent of tight binding of acyl chains, but does not necessarily reflect the real length of the respective side chains (from Palsdottir and Hunte, in press).*

2.5.1 Phospholipid that marks the intermembrane space leaflet at the Q_o site

A tightly bound phospholipid (L6) was identified at the surface of the Q_o site (Palsdottir *et al*., 2003). Importantly, L6 marks the intermembrane space leaflet of the membrane (Fig. 26A). It is bound at the interface of cytochrome *b* (Cobp) and cytochrome c_1 (Cyt1p). A highly conserved residues, $His185^{Cyt1p}$, was observed to stabilize the phosphodiester moiety, whereas the acyl chains interact with cytochrome *b* residues. Continuous density from the phosphodiester moiety pointed to a bulky head group, which led to the tentative assignment of a phosphatidylcholine.

The acyl chains of L6 were clearly resolved in all examined data sets and extended to within *van der Waals* distance of the oppositely oriented acyl chains of a phosphatidyl ethanolamine (L4) and cardiolipin (L5) from the matrix leaflet. The distance between the phosphodiester groups of L6 and the oppositely oriented L4 and L5 is 36 Å (Fig. 27). This is in good agreement with the experimentally determined thickness of pure phosphatidylcholine bilayers with 18:1 acyl chains, where 38 Å were measured between the phosphodiester groups and 27 Å for the hydrophobic core (Lewis and Engelman, 1983). Accordingly, using L6 as reference and assuming HHDBT and stigmatellin bind similarly to substrate, the position of quinol oxidation within the membrane spanning part could be estimated. The functional groups of Q_o site occupants, such as stigmatellin and HHDBT, were observed at 6 Å below the polar zone of the head group region.

The largest contribution made by a single residue to stabilize L6, is provided by the highly conserved residue $Trp273^{Cobp}$. Other residues that add to the hydrophobic stabilization or create the *van der Waals* surface area to which the lipid adheres include $Pro219^{Cyt1p}$ and a number of cytochrome *b* residues: Met91, Phe94, Thr250, Leu251, Gly252, Val270, Leu276, Pro277, Phe333, Val334, and Ala341. Cytochrome c_1 residue His185 is a direct ligand of the phosphate head group.

Also, $His67^{Cyt1p}$ and $Arg184^{Cyt1p}$ together with $His253^{Cobp}$, $Gln338^{Cobp}$ and $His343^{Cobp}$ contribute in the immediate neighborhood to generate feasible electrostatic environment for stabilization of the negatively charged phosphate. Strikingly, polar contacts are made to $Ser268^{Cobp}$, which is the residue of major main chain displacement (see *section 2.3.6*). The observation that the lipid interacts with the displaced loop region (Ala^{267}–Val^{270}) shows that the conformational rearrangement of the protein takes place in the membrane spanning region.

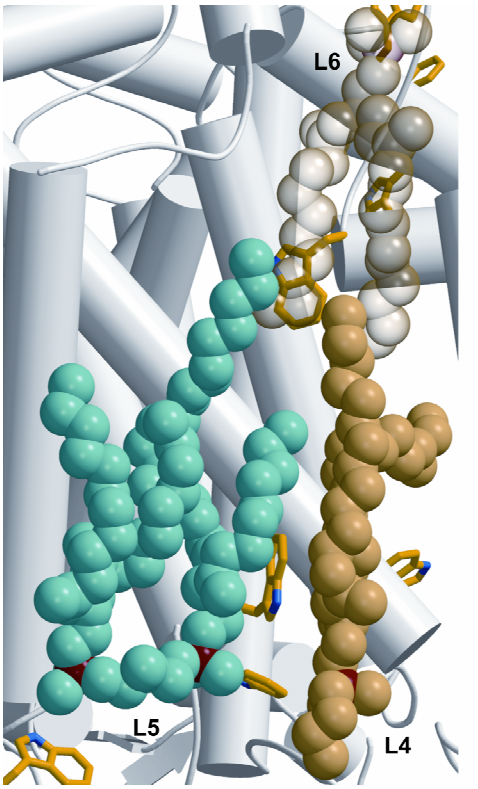

Fig.27 Lamellar oriented tryptophan residues structure the protein surface for lipid binding. *Phospholipids L4, L5 and L6, mark the transmembrane region. The helices are shown as white cylinders and Trp residues are painted yellow with the nitrogen depicted in blue. L6 is for made transparent to show Trp273, a residue in the conserved catalytic PEWY loop, which provides the largest surface area for the acyl chain stabilization at the Q_o site surface (from Palsdottir and Hunte, in press).*

2.5.2 A cardiolipin identified in the cavity at the dimer interface

The dianionic head group of a cardiolipin (L7), was unambiguously identified in F_o-F_c difference density maps. L7 adheres to the protein surface in the frontal cleft at the homodimer interface. The head group is stabilized on the matrix side via several polar and non-polar interactions with C-terminal domain of core 1 (Cor1p) and the N-terminal region of cytochrome *b* (Cobp) from the same monomer (Fig. 28). Lys349^{Cor1p} is the primary ligand of phosphodiester group A (P_A) and phosphodiester group B (P_B) is stabilised by polar interaction with Arg4^{Cobp}. Also, backbone nitrogens of Phe3^{Cobp} and Arg4^{Cobp} are within hydrogen bond distance to P_B-O12 and the backbone nitrogen atom of Met455^{Cor1p} is within hydrogen bond distance to P_A-O4′. The position of L7 at the interface of different subunits suggests a role in structural integrity or assembly. Interestingly, the primary ligands of the polar head group are confined to the termini of the respective polypeptides, *i.e.* C-terminus of cytochrome *b* and N-terminus of Cor1p. The head group stabilizing ligands are

involved in hydrogen bond networks at the Core 1 and cytochrome *b* interface. For instance, Arg4^{Cobp} interacts with Asp19^{Cobp} which binds Arg447^{Cor1p}. Also, a structural water molecule Wat60 forms a hydrogen bonded bridge between Asp341^{Cor1p}, Asp342^{Cor1p} and Arg4^{Cobp}. The ligand, Arg4^{Cobp}, is well conserved among metazoan cytochrome *b* sequences where it is present as an XRK motif and X is a hydrophobic residue (see *Appendix A1*).

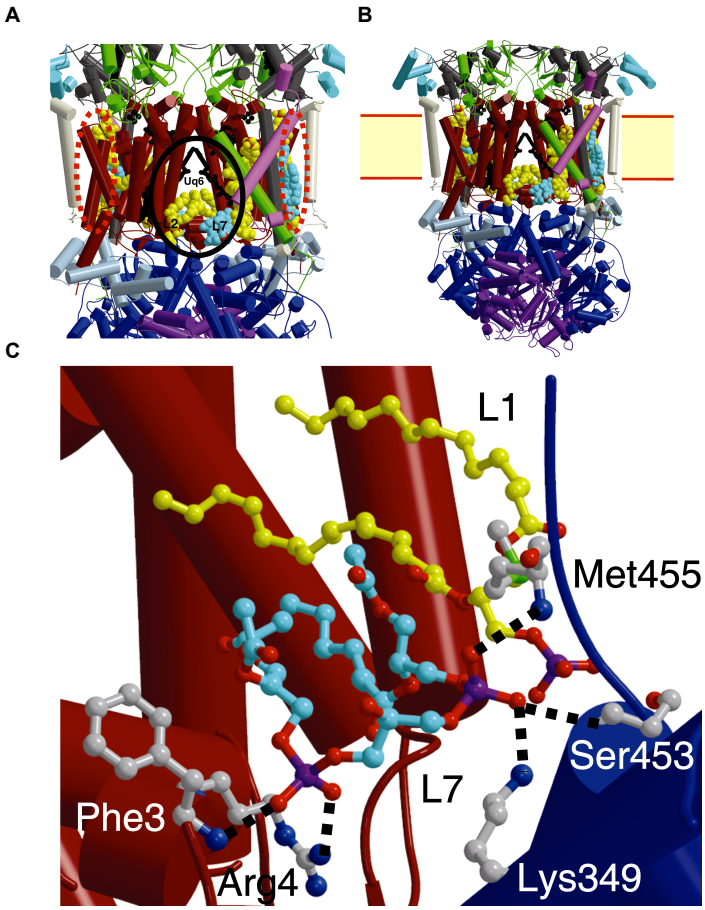

Fig.28 The lipid filled cavity at the dimer interface. ***A,*** *majority of identified lipids are confined to the matrix leaflet of the bilayer. Lipids are shown in space-fill representation and colored yellow, with the exception of the two cardiolipin molecules (cyan). Cofactors and Q_i site occupant (ubiquinone, Uq6) are shown as black ball-and-stick models. Helices are depicted as cylinders and colored according to subunits: Cytochrome b (brown), cytochrome c_1 (darkgray), Rieske (green), Qcr6p (cyan), Qcr7p (midgray), Qcr8p (white), Qcr9p (magenta), Cor1p (blue), and Qcr2p (purple). The two lipid-filled cavities are encircled, the frontal cavity (black) and at each side of homodimer (brown, dotted line).* ***B****, the identified lipid molecules define the vertical positioning of the complex in the membrane.* ***C,*** *the binding site of cardiolipin, L7 (cyan), at the subunit interface of cytochrome b (brown) and Cor1p (blue). Hydrogen bonds to direct ligands (lightgray) of the phosphodiester moieties are depicted and the neighboring lipid, L1, is shown in yellow. P, O and N atoms, are marked in purple, red and blue, respectively (from Palsdottir and Hunte, in press).*

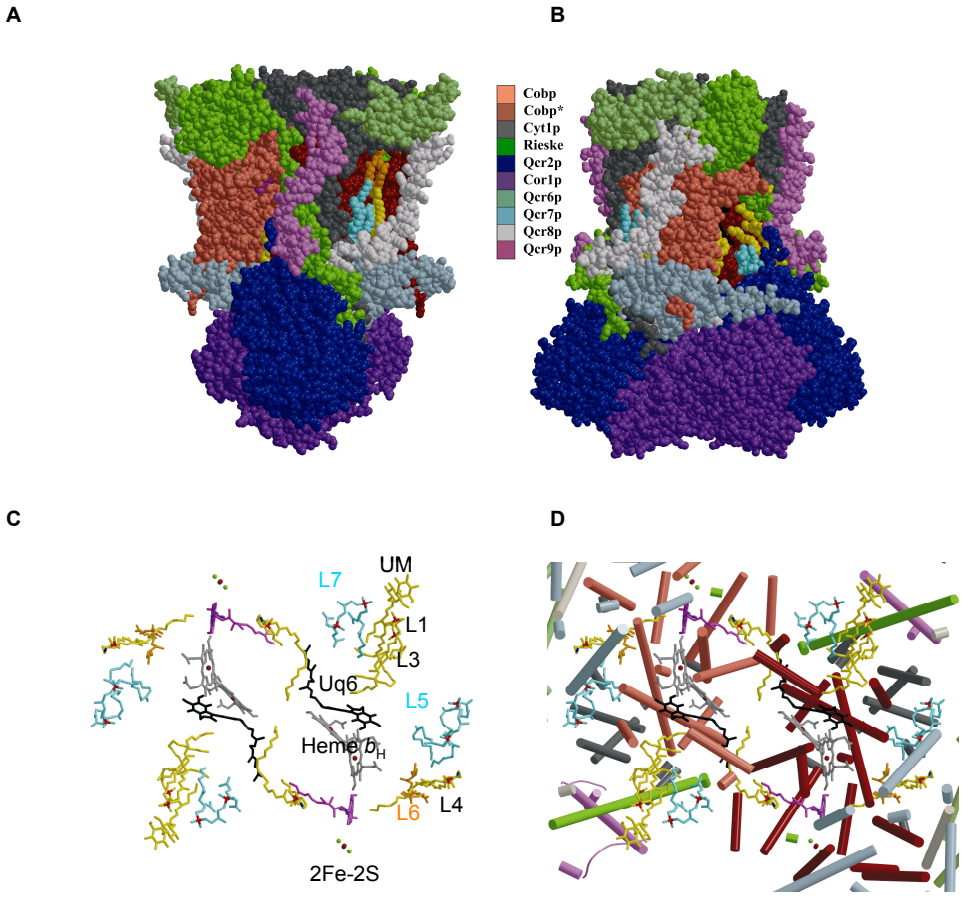

Fig. 29 The homodimer and tightly bound lipids displayed as van der Waals spheres. A, *the intermembrane leaflet lipid L6 depicted in orange. Previously identified phosphatidyl ethanolamine (L4, yellow) and cardiolipin (L5, cyan) that represent the matrix leaflet of the bilayer are shown. Proposed site for supercomplex formation with COX.* ***B,*** *90 degrees clockwise rotation reveals how the second identifed cardiolipin (L7, cyan) positioned at the interface of Cor1p and cytochrome b, contributes to the lipophilic cavity which presumably promotes access to the active site, as demonstrated by the isoprenoid tail of the bound substrate UQ6, at the Q_i site (black). This cavity could serve as a docking site for supercomplex formation with SQR.* ***C****, the arrangement of cofactors, active site occupants, lipids and detergents as viewed from the matrix side.* ***D****, same as C but with added TM helices. Color coding as in A, B.*

Stabilization of several phospholipids and detergent molecules in the cavity at the dimer interface uncovers an intricate network of polar and non-polar interactions where the lipophilic molecules are frequently observed to share ligands. For example, a ligating residue of L7, $Phe3^{Cobp}$, forms a hydrophobic contact to the lipid L2, which is tightly bound by cytochrome *b* residues from both monomers at the dimer interface (Cobp-Cobp*). Also, $Met454^{Cor1p}$ forms a hydrophobic contact to L7 in addition to a polar contact to the head group of a stably refined undecyl maltopyranoside (UM) detergent molecule, which is tightly bound by Cor1p, Rip1p and Qcr9p. Furthermore,

Met455^{Cor1p} forms hydrophobic contact to UM, whereas its backbone nitrogen is hydrogen bonded to the phosphodiester group of L7. His222^{Cobp}, the phosphodiester ligand of L1, an immediate neighbor of UM, contributes to hydrophobic stabilization of L7. These molecules (L1, L2, L7, UM) are in proximity or directly contributing to the entrance to the Q_i site (Fig. 29B).

2.5.3 Conserved lipid binding sites

The current resolution of the structure of the yeast protein does not permit assignment of unsaturated side chains. It is still valid to make the observation that some of the refined phospholipids possess highly curved (*i.e.* kinked) side chains, which suggest double bond character as supported by mass spectrometric analysis of the lipid content in the 3-D crystals used for structure determination (*C. Lange and C. Hunte, manuscript in preparation*). The acyl chain of L4 in the yeast cytochrome bc_1 complex is reproducibly refined in several datasets to bend at a ~90° angle and extend into a narrow and highly hydrophobic dent coated by cytochrome *b* residues, including side chains of Phe94, Leu101, Ile330, and Phe278 (see Palsdottir and Hunte, *in press*).

Lipid-detergent exchangeability was observed when comparing the structures of the yeast and chicken enzymes (see *C. Lange, PhD thesis*). Structural alignment of the yeast and chicken cytochrome bc_1 complexes showed that a detergent molecule, octyl glucoside is assigned to the position where the interhelical phosphatidyl inositol (PI) (L3) is stably refined in the yeast enzyme and likewise a lipid binding site in the structure of the chicken enzyme is occupied by a detergent, undecyl maltoside, in the yeast enzyme.

Structural alignment with the recently determined X-ray structures from the homologous protein, the cytochrome b_6f complex (Plastohydroquinone : Plastocyanin Oxidoreductase), showed conserved lipid-filled cavities. 3 endogenous tightly bound lipid molecules were identified in the X-ray structure of the cytochrome b_6f complex from alga *Chlamydomonas reinhardtii* (Stroebel *et al*., 2003: PDB entry 1Q90). At the matrix side one sulfolipid (SL) was identified (Fig. 30). Notably, it is stabilized by three catalytic subunits, subunit IV, cytochrome *f* and Rieske of the cytochrome b_6f complex. The head group is stabilized by polar and non-polar interactions with Trp32 side chain of subunit IV (corresponds to C-terminus of cytochrome *b*). The negatively charged sulfate is mainly stabilized by electrostatic interactions with positively

charged residue Lys272 from cytochrome *f*, which is implicated in biogenesis of the enzyme (Stroebel *et al*., 2003).

On the intermembrane side, two *1,2-distearoyl-monogalactosyl-diglycerides (DMG)* were identified in a similar position like the intermembrane space lipid in yeast (see *section 2.5.1*). Importantly, one of the DMGs is stabilized by subunit IV residue Trp79, which is homologous to Trp273 (PEWY loop) (see *Appendix A1*). Interestingly, Trp273 contributes the largest surface area for stabilization of the intermembrane space lipid (L6) observed in the yeast structure (Fig. 27). Furthermore, polar contacts with the head group are made by subunit IV residues Glu74 and Thr148, homologous to Ser268 and Val344 in cytochrome *b*. The former is also a stabilizing ligand of L6 (see *section 2.5.1*) and the residue where most pronounced main chain displacement takes place, when comparing the structures with stigmatellin and HHDBT bound at the Q_o site (see *section 2.3.6*).

In the cyanobacterial cytochrome b_6f complex 2 exogenous lipids were crystallographically resolved (Kurisu *et al*., 2003). Like the endogenous SL from alga, both of the exogenous lipids were identified in the lipid enriched frontal cavity at the dimer interface (Fig. 30). In the cyanobacterial enzyme, the intermembrane space leaflet lipid occupies unusual position below the membrane plane similar to the interhelical lipid (L3: Lange *et al*., 2001). Both exogenous lipids make contacts with the catalytic subunit Rieske, as well as cytochrome b_6 from both monomers, underlining their importance in promoting structural stability of the complex, as demonstrated by Zhang *et al*. (2003). Lipid-mediated stabilization of this preparation was a prerequisite for successful structure determination (Kurisu *et al*., 2003).

Notably, in the X-ray structures of the homologous enzymes from yeast, chicken, alga and cyanobacteria, tightly bound lipids were identified in the cavity at the dimer interface. Furthermore, the acyl chains of L7 and the algal SL, provide only fragmental density, although the head groups are well resolved. This points to conformational flexibility of these side chains, which presumably extend into the lipid bilayer, *e.g.* in structural context into the surrounding layer of detergent side chains, rather than being fixed by tight interactions on the protein surface. The observed mobility of these acyl chains suggests that they may participate in forming a feasible environment to promote substrate diffusion. Structural and/or functional relevance of the L7 binding site has to be explored by site-directed mutagenesis.

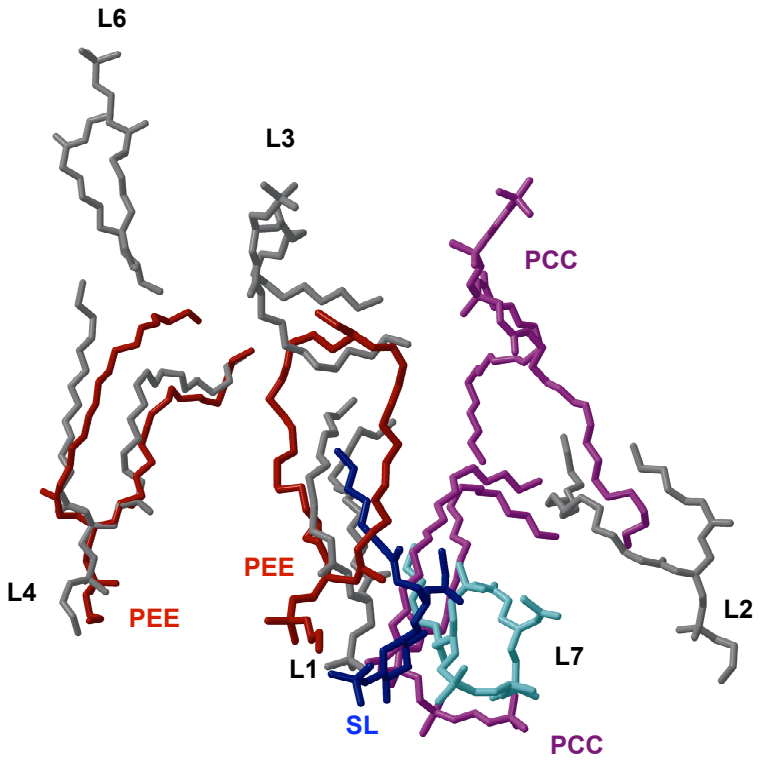

Fig. 30 Conserved lipid binding sites in the cytochrome bc_1 complex and related enzymes. *Superposition of tightly bound lipids refined in the X-ray structures of the cytochrome bc_1 complex from yeast (L1-L7, gray/cyan) and chicken (PEE, red), as well as the photosynthetic cytochrome b_6f complex from alga (SL, blue) and cyanobacteria (PCC, magenta). Note that structurally resolved lipids are enriched at the dimer interface in all species.*

3. DISCUSSION

3.1 Fv-mediated crystallization of a less delipidated and more active protein

The purification of the yeast cytochrome bc_1 complex presented here was modified in favor of increased lipid content by decreasing the extent of detergent exposure. This resulted in isolation of crystallization grade enzyme with higher turnover numbers than previously reported (Palsdottir and Hunte, 2003).

The multi-factorial procedure behind Fv-mediated crystallization and structure determination of this enzyme is complicated because of destabilization of this homodimeric multisubunit membrane protein (see *section 2.1.3*) and unstable assembly of the Fv fragment (see *section 2.2.1*). To ensure reproducible crystallization behavior checkpoints were designed for quality control of both the enzyme and Fv fragment preparation. The presence of individual subunits and purity of the preparation was analyzed by denaturing sodium dodecyl sulfate polyacrylamide gel electrophoresis (SDS-PAGE). Furthermore, the chromatographic profiles demonstrated the degree of monomerization and/or subunit dissociation. Also, the enzyme activity was inspected by monitoring the reduction of cytochrome *c*. The turnover numbers of yeast cytochrome bc_1 complex can approach 200 s^{-1} (Ljungdahl *et al*., 1987), but are typically lower for detergent solubilized and isolated complexes (Sidhu and Beattie, 1982; Siedow *et al*., 1978; Snyder and Trumpower, 1999) (see Table 2). The specific enzyme activity of 24.8 µmol/(min*mg protein) shown here is comparable to the 17.1 µmol/(min*mg protein) reported for the Triton X-100 solubilized yeast enzyme, which was purified by ammonium sulfate precipitation and size exclusion chromatography (Sidhu and Beattie, 1982).

In both successful examples of Fv-mediated crystallization of membrane proteins, the strep-tag mediates important crystal contacts and the antibody fragments are conformation-specific (see *section 2.2.5*). In contrast to the strep-tag affinity purification of the Fv7E2 cytochrome *c* oxidase co-complex (Kleymann *et al*., 1995; Ostermeier *et al*., 1995), preparative streptavidin affinity chromatography proved incompatible for purification of the Fv18E11-cytochrome bc_1 co-complex (C. Hunte, *unpublished*). Here, specific capture of the co-complex was, however, accomplished in an analytical streptavidin-coated magnetic beads pull down assay (see *section 2.2.6*) (Fig. 13). This assay underlined the unstable assembly of the Fv fragment

18E11. A quality control point was therefore designed and the stability of the Fv fragment preparation was routinely investigated by analytical gel filtration (see *section 2.2.1*).

Detailed structural characterization of the binding of Fv18E11 to the cytochrome bc_1 complex was carried out (see Table 3). Water-mediated hydrogen bonds and aromatic residues are postulated to contribute to antibody-antigen interactions (see Davies and Cohen, 1996; Essen *et al.*, 2003). Here, structural water molecules were reproducibly identified and stabilized by hydrogen bond bridges between the epitope and the antibody fragment. Also, a number of tyrosine residues were observed to create a characteristic fold at the Fv fragment interface.

The epitope (Pro123-Gln151) resides in a non-conserved region of Rieske (see Fig. 12), thus explaining the apparently yeast specific binding of Fv18E11. Based on structural characterization of the antibody-antigen interaction, site-directed mutagenesis approach was carried out to create (*i.e.* to graft) the yeast epitope on the soluble domain of the Rieske protein from *P. denitrificans*, in order to pursue Fv18E11-fragment mediated crystallization of the bacterial cytochrome bc_1 complex (see *Diploma thesis, T. Kleinschroth*). Disappointingly, even the introduction of the entire yeast sequence, which contained the non-linear segments encoding the conformational Rieske epitope, did not permit efficient recognition by the antibody fragment. The reasons for this may be two-fold. First, the engineered Rieske protein was not stably integrated into the bacterial enzyme. Second, incompatible folding of this non-conserved part of the Rieske protein may not permit correct tertiary structure. In an attempt to overcome these obstacles, chimeras were constructed with the complete extrinsic domain of the yeast Rieske protein engineered in the bacterial enzyme. Two types of chimeras were constructed, both contained the soluble Rieske domain from yeast, and one also included the flexible linker region from yeast. Interestingly, the chimera domains appeared to fold properly, as judged from successful recognition by the Fv18E11 in streptavidin-magnetic beads pull down assays (Fig. 13). Subsequently, analytical gel filtration showed that the Fv-chimera co-complex eluted as a single symmetric peak and structural integrity of the preparation was enhanced by the addition of phospholipids (*i.e.* DOPC) (*T. Kleinschroth and H. Palsdottir, unpublished*). Fv-fragment mediated crystallization of this construct will be pursued.

Recently, the inserted extra fragment in the bacterial Rieske sequence, that breaks up the epitope-containing region in yeast (see Fig. 12), was shown to be important for structural stability of the enzyme from *R. sphaeroides* (Xiao *et al*., 2004). Likewise, mutagenesis studies showed that Rieske deletion mutants Δ122-135 and Δ138-153 were not efficiently assembled into the cytochrome bc_1 complex, despite being properly processed and imported to mitochondria. Thus, the Fv18E11 recognizes a part of the yeast Rieske protein that appears important for biogenesis of the enzyme (Gatti *et al*., 1989; Obungu *et al*., 1998; Beattie *et al*., 1999).

3.2 Structural insight into the enzyme mechanism

Water-mediated hydrogen bond interactions are prominent at the Rieske-cytochrome *b* interface (see *Appendix A3*), and also observed in ligand stabilization at the Q_o site (see *section 2.3.3*). Additive weak forces in transient molecular interactions are energetically more feasible than strong atomic interactions, especially in enzyme catalysis, where the substrate should be specifically, but still reversibly bound (see Jiang and Lai, 2002; Sarkhel and Desiraju, 2004). Likewise, the interaction between the catalytic interface of Rieske and cytochrome *b* should permit proper positioning of Rieske to enclose the quinol oxidation site, but also allow the release and rotational displacement of the Rieske domain. The position of the Rieske extrinsic domain has been proposed to dictate the midpoint potential of the [2Fe2S] cluster (Darrouzet *et al*, 2002). It is however clear that not only position, but also other factors, must contribute to this effect (see Cooley *et al*., 2004). For instance, stigmatellin binding raises the midpoint potential (E_m) of the Rieske protein by 250 mV (von Jagow and Ohnishi, 1985), whereas UHDBT binding causes less increase in E_m (~70 mV), as was shown for the bovine (Bowyer *et al*., 1982) and the yeast enzyme (T. Merbitz-Zahradnik and B. Trumpower, *unpublished*). This difference in Q_o site inhibitor induced increase of the midpoint potential is not likely to be caused by the position of the Rieske soluble domain alone, because the molecular interactions at the cytochrome *b*-Rieske interface were observed by X-ray structural analysis to be almost identical when stigmatellin and HHDBT are bound, at least in the yeast enzyme (see *Appendix A3*).

Structural comparison of the quinone/quinol (CoQ) binding sites shows that water-mediated hydrogen bonds are frequently involved in ligand head group

stabilization. This is observed in stabilization of stigmatellin (Hunte *et al*., 2000), HHDBT (Palsdottir *et al*., 2003), famoxadone (Gao *et al*., 2002), and NQNO (Gao *et al*., 2003) at the Q_o site, and also by the binding mode of native occupant at the Q_i site (Hunte *et al*., 2000). A common feature in stabilization of the head group of CoQ and derivatives are polar interactions of the functional groups with titratable residues, frequently histidines, which serve as primary ligands and proton acceptors. In the structures of the bacterial reaction center, a menaquinone is hydrogen bonded to $His217^M$, and the non-heme iron ligand $His190^L$ is hydrogen bonded to the carbonyl group of a truncated quinone at the Q_B site (Deisenhofer *et al*., 1988). The latter binding mode was reproduced for stigmatellin (Lancaster and Michel, 1997). Link (1997) transferred this information of coinciding substrate and stigmatellin binding sites to the Q_o site of the cytochrome bc_1 complex and suggested that the complex between stigmatellin and Rieske mimics the reaction complex between protonated semiquinone and the reduced Rieske protein.

The observed binding mode and orientation of stigmatellin and HHDBT at the Q_o site provide an important foundation for modeling the substrate in the active site. In agreement with EPR studies and kinetic characterization of variants, X-ray structural analysis revealed that HHDBT and stigmatellin binding sites coincide. Furthermore, superimposition of the X-ray structures showed that the inhibitor ring systems are *in plane* (Fig. 20). Interestingly, the inhibitors are oriented with their functional groups at the same distance and geometry to the Rieske [2Fe-2S] cluster ligand His181. More specifically, the oxygen atom O6 of the ionized hydroxy group of HHDBT is at the same position as the carbonyl oxygen atom O8 of stigmatellin, allowing in both cases for a hydrogen bond to the Nε2 atom of a protonated His181. Importantly, the residues involved in binding of the hydroxy-dioxobenzothiazole and stigmatellin head groups are highly conserved (see Degli-Esposti *et al*., 1993). Kinetic characterization of variants has shown that the following residues, which interact with the head groups: Trp142, Gly143, Ile269, Pro271, and Tyr279, have phenotypes of disturbed ubiquinol occupancy and/or oxidation (see Brasseur *et al*., 1996; Crofts *et al*., 2000), suggesting that the inhibitors bind at the substrate binding site. Based on these data and structural resemblance to the substrate, the competitive inhibitors, HHDBT and stigmatellin, are here regarded as substrate analogs and their binding mode will be discussed as resembling the binding of CoQ. Recent EPR studies

support this assumption. Samoilova *et al*. (2002) detected the product of Q_o site catalysis and reported similar interactions with the reduced Rieske cluster, as in the case when stigmatellin was bound. The X-ray crystallographic analysis of stigmatellin binding suggests single occupancy with ubiquinol hydrogen bonded to $His181^{Rip1p}$ and $Glu272^{Cobp}$ side chains (Hunte *et al*., 2000). In this way, the Enzyme-Substrate (ES) complex was created by docking ubiquinol into the X-ray structure of the yeast enzyme. The substrate was modeled *in plane* with stigmatellin and HHDBT, with the functional groups coinciding accordingly (Hunte *et al*., 2003). After energy minimization the quinol hydroxyl groups were at a distance of ~2.1 Å and ~2.4 Å to the putative primary proton acceptors, the imidazole nitrogen of $His181^{Rip1p}$ and carboxylate of Glu272, respectively (Fig. 31).

Single occupancy models comprise either simultaneous or sequential electron transfer at the Q_o site. For the latter, a proton-gated affinity change mechanism claims the presence of a relatively stable semiquinone intermediate with the rate-limiting step at the second electron transfer (Link, 1997). Since a semiquinone radical has not been detected at the Q_o site, this has been explained away by an EPR silent anti-ferromagnetically coupled semiquinone-$[2Fe\text{-}2S]^{reduced}$ pair (Link, 1997; Jünemann *et al*., 1998). Based on kinetic considerations, another explanation for the undetectable semiquinone is provided by Crofts and colleagues, who suggest rapid dissociation of the product after the first electron transfer and movement of the semiquinone within the bilobal Q_o binding pocket to allow fast reduction of heme b_L (Hong *et al*., 1999). A third reaction mechanism suggests a concerted reaction and is based on the kinetic interpretation that the midpoint potentials of the *b* type hemes control the rate of cytochrome c_1 reduction (Snyder *et al*., 1999; Snyder *et al*., 2000). In such a mechanism the concentration of semiquinone is so low as to be almost non-existent. Still, the structural study presented here clearly illustrates the possibility of stabilizing a negatively charged ligand at the Q_o site.

The identification of a backwards operating cytochrome bc_1 complex in the acidophilic chemolithotrophic organism *Acidithiobacillus ferrooxidans* was a topical finding (Elbehti *et al.*, 1999; Brasseur *et al.*, 2002). This observation formed the basis for reaction schemes that stress the reversibility of the enzyme mechanism (Osyczka *et al*., 2004). Based on kinetic characterization of cofactor knockouts, the reversibility of electron transfer in quinol oxidation is suggested to be key in eliminating short-

circuits. The bypass reactions, that have to be avoided to prevent short-circuits in quinol oxidation, comprise the oxidation of ubiquinol by sequential electron transfer to the Rieske and oxidation of heme b_L by the unstable Q_o site semiquinone. The O_2 respiring mitochondria are the main location for production of reactive oxygen species (see Crofts, 2004). If a semiquinone is formed at the Q_o site, the necessity to stabilize it is illustrated by these two potentially harmful events, which would promote damaging superoxide production: 1. Escape of the semiquinone from the Q_o site and 2. Reduction of O_2 by an unstable semiquinone. Experimental conditions aimed to accumulate semiquinone at the Q_o site cause enhanced superoxide production, whereas Q_o site inhibitors block superoxide production either partially or completely depending on their inhibitory characteristics (Müller *et al*., 2003; Sun and Trumpower, 2003).

The reversible reaction scheme, proposed by Osyczka *et al*. (2004), fails to discriminate between concerted and sequential reactions. The latest mechanistic model proposed by P. Rich (2004) suggests that, the coupling of the protonation state of primary proton acceptors to the redox state of the cofactors is the crucial event in Q_o site catalysis. FTIR analysis may be the most suitable technique to address redox-dependent protonation behavior of catalytic residues.

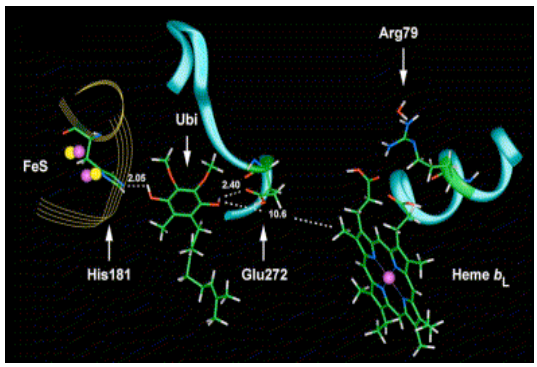

Fig.31 The enzyme-substrate complex at the Q_o site. *Ubiquinol truncated to the first two isoprenoid repeats was modeled into the active site according to the observed binding mode for stigmatellin. The distances to the proposed primary proton acceptors $His181^{Rip1p}$ and $Glu272^{Cobp}$ after energy minimization are depicted (from Hunte et al., 2003).*

The double occupancy model suggests synergistic interaction between two substrate molecules, which occupy the Q_o site simultaneously (Ding *et al*., 1992; Ding *et al*., 1995a; Brandt *et al*., 1996; Bartoschek *et al*., 2001). Interpretation of EPR lineshapes even suggested different affinities of these two occupants, with a strong and weak CoQ binding site (Ding *et al*., 1992). All reports on double occupancy are, however, based on indirect observations. Although the Q_o site is divided into two spacious domains, X-ray structural analysis has shown that the binding sites of bulky Q_o site inhibitors overlap and the substances compete with each other and substrate in kinetic studies. Moreover, the proposed tightly bound CoQ has not been detected by other methods than interpretation of EPR lineshapes. Modeling of two CoQ at the site requires considerable structural distortion. Furthermore, energetic considerations speak in favor of single-occupancy models (see Crofts, 2004). In addition, reports on crystallographic analysis of a truncated quinone, CoQ_2, partially resolved at the Q_o site, does neither reveal strong binding, nor two molecules at the site (Gao *et al*., 2003). So far, the latter is true for all crystallographically resolved Q_o site inhibitors.

The observation that UHDBT did not inhibit the cytochrome bc_1 complex efficiently at alkaline pH was explained by restricted access of an ionized compound to the Q_o site (Zhang *et al*., 1999). The study shown here presents contrasting evidence to this assumption and a dissociable group within the complex, namely $His181^{Rip1p}$, is instead suggested to cause the observed pH dependency of UHDBT inhibition. The apparent pK_a of 7.5 for inhibitor efficacy is more alkaline than the pK_a of alkyl-HDBT (~6.1), whereas it closely matches the pK_a ~7.5 suggested for the imidazole nitrogen (Nε) of His181 of the oxidized Rieske protein (Link *et al*., 1992). Spectroscopic evidence and the crystal structure of the enzyme with HHDBT bound at pH > pK_a demonstrate that this alkyl-hydroxyquinone derivative is bound in the ionized form and is proposed to be stabilized by a polarized hydrogen bond to the protonated $His181^{Rip1p}$ (Palsdottir *et al*., 2003). This is consistent with the observation that $His181^{Rip1p}$ donates a hydrogen bond to the carbonyl group of stigmatellin at pH ~8.5 or half a pH unit above that used for HHDBT crystallization.

Considering the possibility that at least a transiently stable, anti-ferromagnetically coupled semiquinone is formed (Link, 1997; Jünemann, 1999), stigmatellin binding would mimic the binding of a protonated semiquinone, whereas HHDBT resembles the deprotonated form, *i.e.* the semiquinone anion.

Based on the structural considerations presented here, snapshots of the reaction mechanism can be discussed (Fig. 32). Reversible gating would permit sequential electron transfer through a semiquinone and prevent short circuits only if the [2Fe-2S] cluster and the heme b_L have the same redox state (Osyczka *et al*., 2004; Rich, 2004). If both cofactors are oxidized, $His181^{Rip1p}$ and $Glu272^{Cobp}$ should be deprotonated. When ubiquinol enters the binding site, the deprotonated Glu272 side chain re-orients to ligate the hydroxyl group on one side and the oxidized Rieske is captured in a hydrogen bond between $His181^{Rip1p}$ and the other hydroxyl group (Fig. 32: Panel 2-3). The weak hydrogen bond interactions from the $Tyr279^{Cobp}$ side chain position the hydroxyl group of ubiquinol for optimal interaction with $His181^{Rip1p}$ and thus efficient electron-proton transfer to the Rieske. Reduction of the oxidized [2Fe-2S] cluster occurs as a first step after formation of the ES-complex, and involves coupled electron-proton transfer to the Rieske similar to when stigmatellin is bound (Fig. 32: Panel 4). After coupled electron-proton transfer to the Rieske, Glu272 accepts a proton from the singly protonated semiquinone and re-orients towards heme b_L and the resulting negative charge is stabilized as in the case of HHDBT (Fig. 32: Panel 5). Conformational gating is accounted for in that the reduced Rieske protein is firmly held in b-position by interactions with the reaction intermediate in a polarized hydrogen bond. After the second electron reduces heme b_L the destabilized product leaves the binding site and allows for increased mobility of the highly conserved Tyr279 side chain. Kinetic characterization of Tyr279 variants supports its importance in the catalytic cycle (see *section 3.4.1*). Tyr279 responds to Q_o site occupancy by rotating into the binding site in the absence of ligand, as shown in the structures of the enzyme with empty Q_o site (Crofts *et al*., 1999a) (Fig. 32: Panel 6). When the substrate leaves the active site, the soluble domain of the Rieske protein is released from docking position on cytochrome *b* because the hydrogen bond to Q_o site occupant and the hydrogen bond from $Tyr279^{Cobp}$ to $Cys180^{Rip1p}$ is broken.

If reversibility of quinol oxidation is taken into account, a feasible mechanistic coupling to prevent short circuits would be the redox-governed protonation state of the primary ligands, namely His181 and Glu272 (Osyczka *et al*., 2004; Rich, 2004). Thus, substrate binding should only occur when the enzyme is redox poised to accept electrons from both sides. The redox dependent protonation behavior of $His181^{Rip1p}$ is accounted for in a bulk of experimental and theoretical studies that assume coupled electron-proton transfer to the Rieske and pK_a values estimated for the reduced Rieske

cluster are much higher than for the oxidized Rieske (Link *et al*., 1992; Ullmann *et al*., 2002; Zu *et al*., 2003). Still, the question whether protonation state of Glu272 is coupled to heme b_L redox state remains to be addressed.

Fourier transform infrared (FTIR) spectroscopy is a feasible technique to address this question. The initial findings from the redox-induced FTIR study presented here (see *section 2.4* and *PhD thesis, M. Ritter*). Differences in redox induced spectra were observed when the enzyme with empty Q_o site was compared to the enzyme with HHDBT and stigmatellin bound. The study of the binding of ^{13}C-labeled stigmatellin, demonstrated that changes in conformation and/or protonation state of acidic residues, such as Glu or Asp, take place when the inhibitors bind to the Q_o site of cytochrome bc_1 complex from *S. cerevisiae* (Ritter *et al*., 2004). Ongoing studies, especially the spectral characterization of variants, are needed for exact band assignment.

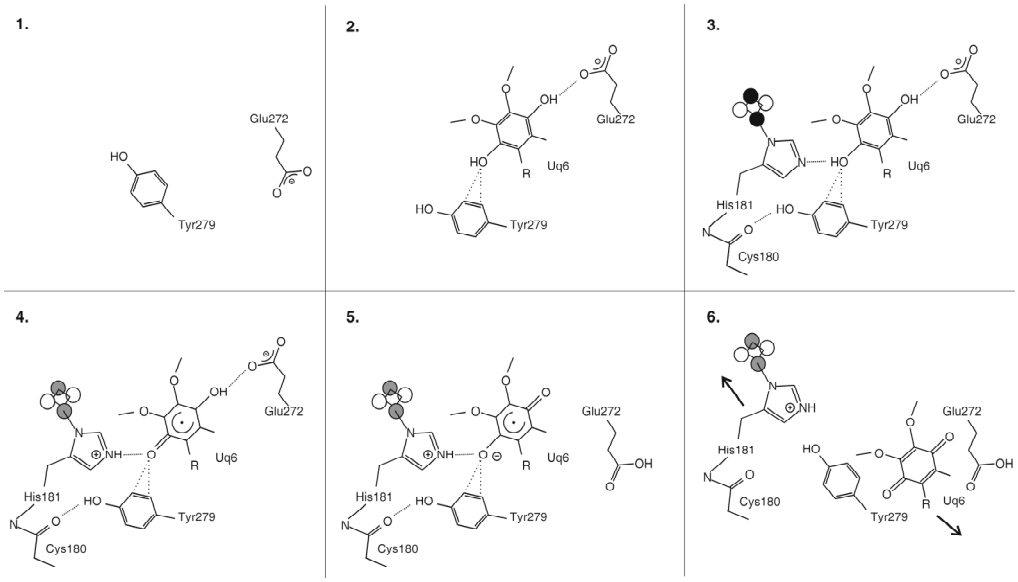

Fig.32 Structure-based snapshots of the reaction mechanism. *The oxidized [2Fe-2S] is indicated with black circles, the reduced in grey. Hydrogen bonds stabilizing the enzyme-substrate complex are indicated with dotted lines.* ***1.*** *Empty Q_o site with Glu272 oriented out of the binding pocket.* ***2***. *Initial stabilization of ubiquinol by cytochrome b residues.* ***3***. *The enzyme-substrate complex with the Rieske protein docked in the b-position.* ***4***. *Coupled electron-proton transfer to the Rieske protein.* ***5***. *Stabilization of the anti-ferromagnetically coupled ubisemiquinone anion and rotational displacement of protonated Glu272.* ***6***. *Release of the reduced and protonated Rieske protein and of the oxidized ubiquinone accompanied by rotational displacement of Tyr279 into the binding site (from Palsdottir et al., 2003).*

3.3 Proton transfer pathways

Molecular dynamics simulation studies using the 3 Å X-ray structures of the cytochrome bc_1 complex from chicken were first to propose a proton exit pathway from the Q_o site via the Glu272 carboxylate and heme b_L propionate (Izrailev *et al*., 1999; Crofts *et al*., 1999c). The first experimental support for this proposed pathway emerged with improved resolution, which permitted the refinement of structural water molecules at 2.3 Å resolution in the yeast enzyme (Hunte *et al*., 2000). In the X-ray structure of the HHDBT inhibited enzyme, the hydrogen bond network revealed that a single water molecule connects the reoriented Glu272 carboxylate to the heme b_L propionate A (Fig. 22). The protein-stabilized hydrogen bond network from heme b_L propionate to outside was shown in the structure, including crystallographic water molecules and cytochrome *b* residues: Arg79, Asn256, Glu66 and Arg70. Arg79, Glu272, and Tyr274 are highly conserved in mitochondrial cytochrome *b* supporting their importance for the catalytic mechanism (Degli-Esposti *et al*., 1993).

The functional importance of Glu272 is shown in a number of mutagenesis and kinetic studies (Brasseur *et al*., 1996; Covian and Moreno, 2001). Mutation to Asp or Gly causes decreased rates of quinol oxidation, whereas exchange with a Gln renders the enzyme inactive. The shorter side chain of Asp could still fulfill the role in proton transfer, although not as efficiently due to non-optimal hydrogen bond geometry and in the case of a small side chain, such as Gly, it is conceivable that a water molecule migrates to the site to mediate hydrogen bonds to outside.

In addition to the main pathway proposed for proton conduction, alternative and less effective proton exit pathways may exist in the cytochrome bc_1 complex. This is suggested by the functional analysis of Glu272 variants, where smaller side chains are tolerated. Furthermore, rearrangements in hydrogen bond networks have been shown to accommodate for loss of catalytic residues in other energy transducing enzymes. For instance, formation of an alternative proton transfer pathway was demonstrated in variants of the bacterial reaction center, where inhibited proton uptake at the Q_B site in Asp213Asn^L variant was restored by second site revertants (Xu *et al*., 2004).

Interestingly, in some microorganisms, such as the chemolithotrophic acidophilic bacteria *Acidithiobacillus ferrooxidans,* Glu272 is replaced with a Pro (PPWY) (Brasseur *et al*., 2002). Brasseur and colleagues found that Pro was also present in the cytochrome bc_1 complex of the hyperthermophilic aerobic craenarchae

Aeropyrum pernix and acidophilic obligate aerobic *Sulfolobus acidocaldarius.* Another deviation from the conserved PEWY loop is replacement with Val observed for instance in the neutrophilic chemolithotrophic bacteria *Nitrosomonas europea*. However, these organisms have an inserted span of amino acids in this region of the enzyme and an upstream acidic residues may therefore be repositioned within the binding site and provide the necessary ligand and proton acceptor to compensate for the missing function of Glu272. Also, in the X-ray structures of the cytochrome b_6f complex, the complement of non-homologous small subunits changes the molecular architecture at the site. In this case, structural analysis suggests different proton exit pathway than that proposed for the cytochrome bc_1 complex, such as a hydrogen bonded water chain, which was structurally resolved in cytochrome *f* (see Ponamarev and Cramer, 1998; Stroebel *et al*., 2003).

The conformational changes described for the side chains of Glu272 and His253 (Fig. 33) invite the following speculations: Does the rotational displacement of the Glu272 side chain induce rotational displacement of the His253 side chain, which in turn releases Ser268 and subsequently causes relaxation of the span of residues within the *ef* loop which are observed to be displaced? Is the observed conformational change of functional importance? Does it present an event in relaying a signal to the surface which senses Q_o site occupancy?

The observed conformational changes can be put into mechanistic context. Once ubiquinol binds, rotational displacement of the Glu272 side chain to bind the substrate may release the His253 side chain to rotate away from the binding site and form a hydrogen bond to the main chain atom of Ser268 (Fig. 33). This cycle is repeated when the substrate is oxidized and Glu272 rotates away from the binding site. In this way a domino-like cascade of hydrogen bond rearrangements and subtle conformational changes may serve to sense Q_o site occupancy and perhaps relay signals to the surface, which capture or release the Rieske protein.

The observed rotational displacement of His253 and the contact it makes to the head group of the intermembrane space lipid (L6) (see *section 2.5.1*) may as well provide an alternative proton exit pathway? Although His253 is not a completely conserved residue it must not be excluded that it has at least secondary roles in proton escape pathways from the site, and it should be pointed out that it is partially conserved, at least in fungi, parasites and some bacteria *R. sphaeroides* and *P. denitrificans* (see *Appendix A1*).

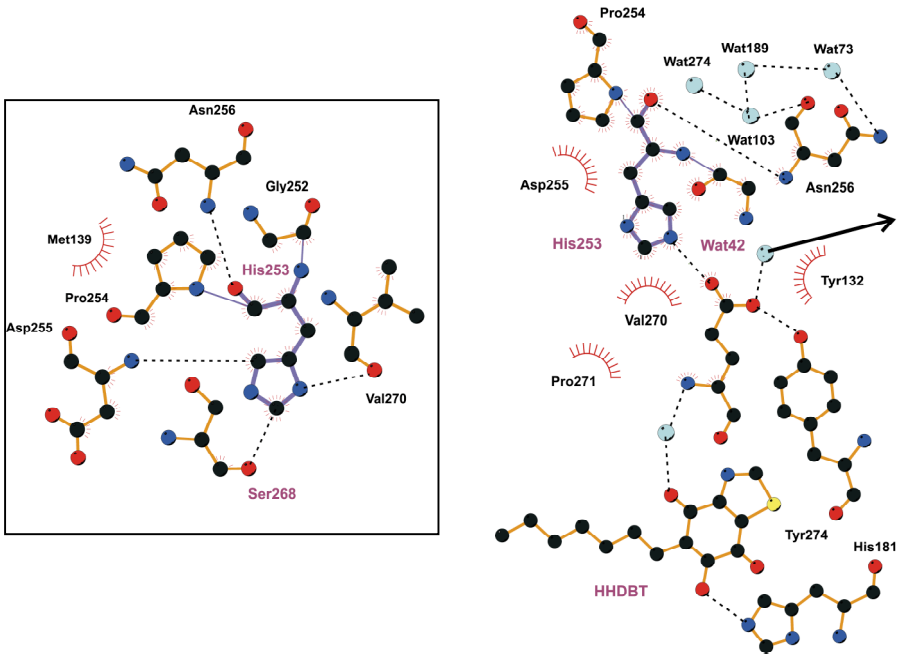

Fig.33 Q_o site occupancy dependent conformational switch? *When stigmatellin is bound at the Q_o site (left) Glu272 carboxylate is hydrogen bonded to the hydroxyl group of stigmatellin. When HHDBT is bound (right) His253 rotates to form a hydrogen bond to Glu272.*

3.4 Structural analysis assists functional interpretation of mutagenesis data

The prokaryotic origin of mitochondria presumes that much of the information retrieved from massive efforts by mutagenesis studies on the bacterial cytochrome *b*, may be transferred to eukaryotes. However, although highly conserved, the enzymes are not fully conserved and careful inspection of sequence similarities is required when interpreting functional aspects in structural context . Recent technical advances based on biolistic transformation allow genetic manipulation of mitochondrial DNA (mtDNA) and subsequently data is accumulating about functional effects in yeast (Fisher and Meunier, 2001; Kessl *et al.*, 2003; Kessl *et al.*, 2004). In general, nonsense and frameshift mutations are observed to affect assembly, conformation and stability of the enzyme. Missense mutations are more difficult to interpret. The molecular structures provide a necessary fundament to discuss the molecular reasons for the observed phenotypes. The Q_o site and heme surroundings are highly susceptible to amino acid replacements. Variations in the *van der Waals* surface area and changes in electrostatic properties are typically not tolerated and frequently even conservative substitutions may cause inhibitor resistance and/or impaired quinol

oxidation reaction (Bruel *et al*., 1995; Saribas *et al*., 1995; Saribas *et al*., 1997; Fisher *et al*., 2004a). Cytochrome *b* residues described as susceptible to variation with respect to Q_o site occupancy and catalysis are clustered mainly on the *cd* or *ef* segment of cytochrome *b* including residues: F129, Gly131, Gly137, Met139, Trp142, Thr145, Thr148, Asn256, Ile269, Pro271, Glu272, Trp273, Tyr274, Leu282, Lys288, Gly291, and Val292 (summarized by Brasseur *et al*., 1996).

Temperature sensitive yeast mutants with $Thr85^{Rip1p}$ replaced by an Ile showed hypersensitivity to UHDBT in addition to slower rates of ubiquinol oxidation (Ljungdahl *et al*., 1989). Before the structural data was available original interpretation for this effect was a proposed enrichment of hydrophobicity at the site leading to stronger binding of UHDBT. Another explanation was based on a model with $Thr85^{Rip1p}$ involved in catalysis. However, structural analysis renders these previous interpretations obsolete and inspection of the structure reveals more likely reasons for this phenotype. $Thr85^{Rip1p}$ is located in the flexible linker region of the Rieske (see Table A3). Several studies have shown that the length of the linker region is important for quinol oxidation. Insertion or deletion of amino acids in the linker region disturbs catalysis and changes sensitivity to inhibitors presumably because of improper positioning of the Rieske soluble domain on the catalytic interface of cytochrome *b* (Tian *et al*., 1998; Tian *et al*., 1999; Darrouzet *et al*., 1999; Obungu *et al*., 2000; Nett *et al*., 2000). Furthermore, $Thr85^{Rip1p}$ side chain and main chain atoms are hydrogen bonded to $Asp87^{Rip1p}$ side chain and $Val88^{Rip1p}$ main chain, respectively. $Thr85^{Rip1p}$ therefore also contributes indirectly to intersubunit interactions, where $Asp87^{Rip1p}$ is observed to stabilize a structural water molecule Wat104, which is hydrogen bonded to cytochrome c_1 residues $Ser152^{cyt1p}$ and $Arg113^{cyt1p}$. Accordingly, in addition to hypersensitivity to UHDBT, the T85I variant exhibits reduced thermostability possibly derived from destabilized subunit association. The functional importance of the network of interactions at the cytochrome *b* and Rieske interface in proper positioning of Rieske soluble domain for Q_o site catalysis is further illustrated in recent mutagenesis studies. Functionally impaired mutants in the Rieske linker region were rescued by suppressor mutations in cytochrome *b* (*cd* and *ef* loops) and *vice versa* (Darrouzet and Daldal, 2003; Brasseur *et al*., 2004).

3.4.1 Human diseases derived from defect Q_o site and impaired catalysis

The yeast *S. cerevisiae* has been used as a model system to study diseases derived from Q_o site deficiency in humans (Fisher and Meunier 2001; Fisher *et al.*, 2004b; Brasseur *et al.*, 2004).

The deletion of cytochrome *b* residues 252-259 (Δ252-259) causes myopathy and the mutation inserted in yeast inactivates the enzyme. In the same segment another disease in man, histiocytoid cardiomyopathy, corresponds to point mutation $G252D^{Cobp}$. Interestingly, when introduced in yeast it does not display immediate pathogenic effects (Fisher *et al.*, 2004b). Meunier and Brasseur reported that purification of this variant yielded highly unstable and less active enzyme (*unpublished observation*). They proposed that introduction of Asp at position 252 interferes with the binding of the structural lipid close to Q_o site (see Fig. 34 and *section 2.5.1*). Although the G252D variant showed wild type behavior in yeast under standard conditions it was found to exhibit disturbed respiratory function when cells were grown at 36°C and biogenesis was negatively affected observed as reduced levels of Qcr9p. Furthermore, Qcr9p was found to be essential for enzyme activity at 28°C for this mutant. A compensating mutation $P174T^{Cobp}$ was identified which alleviated this effect (Saint-Georges *et al.*, 2002). It was concluded that Qcr9p contributes to thermal stability of the enzyme. Phospholipids are highly sensitive to temperature, therefore the phenotype may also be a result of enhanced delipidation at the protein surface due to electrostatic repulsion of the lipid. It is here important to point out that the next neighbor to this point mutation is not conserved when comparing mammals (Asp 253) and fungi (His 253) (see *Appendix A1*). This may indeed explain why the human phenotype is more dramatic than in yeast. In yeast, the presence of His253 may partially compensate for the introduction of a negative charge at position 252, whereas in man Asp253 would repulse negative charge at position 252. Hence, the human G252D variant could prevent binding of the anionic phospholipid, but also overall conformational changes at this site may be expected. Clearly, this case study underlines how subtle differences in genotype may have dramatic effects on phenotype.

The mutation Y279C is found in human diseases such as exercise intolerance and multiple system disorder. Introduction of this mutation in yeast yielded a less active enzyme (Fisher *et al.*, 2004b). Structural analysis showed direct interactions of

Tyr279 with Cys180^{Rip1p} that contribute to Rieske stabilization in b-position. The functional importance of this residue in positioning Q_o site ligand was proposed (Palsdottir *et al*., 2003, see Fig. 34). EPR spectra showed an altered signal, indicative of lower occupancy of the Q_o site. To further analyze substitutions at position 279, Ala and Trp were introduced. The latter completely inactivated the complex. When substituted with Cys or Ala, the Rieske protein was integrated and the phenotype was judged from EPR to be derived from impaired Q_o site occupancy, which in the case of Y279A caused more than 4-fold reduction of enzyme activity. Together with lower K_m values this indicated lower quinol on-rate. These studies supports the role of Tyr279 for proper positioning of substrate in the active site (see Fig. 34), as observed in the weak hydrogen bond interactions with stigmatellin and HHDBT. Functional importance of this highly conserved residues is also supported by mutagenesis in bacteria (*R. sphaeroides*) where mutation of the homologous residue Tyr302 caused 3-, 40- and 50-fold reduced rates of quinol oxidation when replaced with a Leu, Gly, and Gln, respectively (Crofts *et al*., 2000).

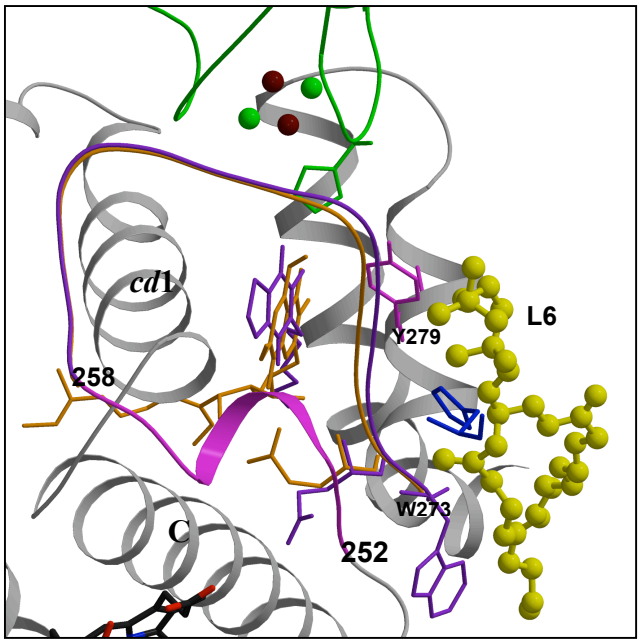

Fig.34 Residues at the Q_o site implicated in human diseases. *G252D (cardiomyopathy), Δ252-259 (myopathy) and Y279C (multiple system disorder) are depicted in magenta. Also shown is the intermembrane space lipid L6 (yellow) and the stabilizing ligand His185 from cytochrome c_1 (blue). The Rieske (green) is in b-position and His181 interacts with stigmatellin (orange) and HHDBT (purple).*

3.5 Modeling of atovaquone binding to the Q_o site

The Q_o site is a target of many compounds of agricultural or pharmaceutical importance. These compounds utilize subtle molecular differences at the active sites to bind target in a species-specific manner. Atovaquone is a substituted 2-hydroxynaphthoquinone that is used therapeutically to treat malaria, pneumonia, and toxoplasmosis and targets the Q_o site of the corresponding pathogens, the parasites *Plasmodium* and *Toxoplasma* and the opportunistic fungi *Pneumocystis*. Atovaquone (AtQ) has structural similarity to both HDBT and stigmatellin. Based on this analogy AtQ was modeled into the Q_o site of the structure of yeast cytochrome bc_1 complex (Kessl *et al.*, 2003). Sequence comparison and structural analysis suggested the reasons for differential efficacy of AtQ inhibition in the pathogens and mammalian enzymes. The molecular reasons for selectivity of the drug are exposed by the emergence of resistant strains. Pathogens frequently become desensitized to drugs which bind cytochrome *b* due to the inherently higher mutation rates in mtDNA compared to nucleus. AtQ resistant strains have been cultivated *in vitro*, generated in mice as well as isolated from human hosts. Importantly, natural selection propagates viable and drug resistant variants, thus the pathogen has to compromise the need for rejecting the drug, but still allow binding of substrate and effective catalysis at the Q_o site. Studies of AtQ binding have therefore functional perspectives, in addition to the important medical impact.

AtQ was shown to inhibit the yeast cytochrome bc_1 complex (Kessl *et al.*, 2003). EPR lineshapes were consistent with distal occupancy of the Q_o site and similar to when HHDBT is bound, AtQ binding raised the midpoint potential of the Rieske iron-sulfur protein from 285 to 385mV. The interaction of AtQ with cytochrome bc_1 complex from *S. cerevisiae* was simulated by modeling this substance into the active site based on the binding mode observed for HHDBT. The AtQ head group, including the position of the hydroxyl group, was presumed to be oriented like in the case of HHDBT (Kessl *et al*., 2003). The observed rotational displacement of Glu272 when HHDBT is bound was used in the modeling studies by relaxing the constraints on the Glu272 side chain and a water molecule was modeled into the site. Also the conformational flexibility of the *ef* loop provided important basis for the molecular dynamics studies, because constraints were introduced that allowed relaxation of this region. The results from the molecular dynamics simulations

revealed a very similar binding mode as observed for HHDBT, including a water-mediated hydrogen bond to Glu272.

The computed energy-minimized structure suggested that the Phe at position 275 of cytochrome *b* in the bovine enzyme, instead of Leu at the equivalent position in the yeast and parasite enzyme, is responsible for decreased sensitivity of the bovine cytochrome bc_1 complex. The L275F mutation was introduced into the yeast cytochrome *b*, and accordingly AtQ sensitivity decreased drastically. Seven of the mutations from AtQ-resistant fungi *P. jirovecii* were introduced in the cytochrome *b* gene from yeast (Kessl *et al*., 2004). Three (I147V, L150F, and L275F) are expected to interact directly with AtQ. Other two, T148I and S152A, are in the *cd*1 helix. Turnover rates were not affected in the T148I and L275 variants, whereas the I147V, L150F, S152A and P266L, displayed disturbed quinol oxidation.

The important role of Tyr279 in stabilizing ligands at the Q_o site is demonstrated by the mutation Y279S that is the most frequent cause of *in vivo* treatment failure, because the parasites that carry this mutation are resistant. This observation underlines the importance of Tyr279 in stabilizing the drug at the binding site. Resistant *P. yoelii* lines generated upon drug exposure in infected mice included a substitution of Y279 with Cys, which caused nearly 2000 fold increase in AtQ IC50 (Srivastava *et al*., 1999). Also, L282V and I269M, and the non-conserved positions 278 and 283 were mutated. AtQ resistant lines of *P. falciparum* generated *in vitro,* exhibit similarly variants at positions 139, 283, 286, 291, 279, 291 and 295 (Korsinczky *et al*., 2000; Fivelman *et al*., 2002, Gil *et al*., 2003). Interestingly, initial mutation in the *cd* loop of the conserved Met139 exhibited low resistance, which was enhanced by additional mutations in the *ef* region from 283 to 290. Similarly, three mutations in *Plasmodium berghei* lines associated with resistance to AtQ, were identified as M139I, L150S and the non-conserved position 295 (Syafruddin *et al*., 1999). Mutations conferring AtQ resistance typically result in loss-of-fitness in terms of impaired respiratory growth (Kessl *et al*., 2004). Based on structural and functional analysis tailor-made drug development is now feasible. Consistent with conservation of the mechanism for active site catalysis, the homologous mammalian cytochrome *b* protein differs from that of the malaria parasite only in a few of the amino acids at Q_o site. To summarize, the highly conserved residues, which affect AtQ binding include F129, G137, M139, I147, T148, L150, I269, Y279, L282, and G291.

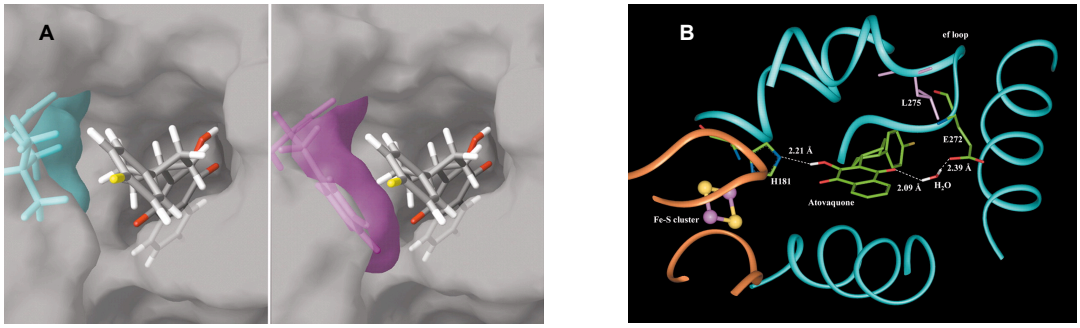

***Fig.35 Energy-minimized structure of atovaquone modelled at the Q_o site. A**, AtQ binding site viewed from the lipid filled cavity. The steric hindrance to atovaquone binding that results from the amino acid replacement is illustrated by the van der Waals surfaces for Leu275 (blue) and Phe275 (magenta). The chloride atom on the atovaquone side chain is colored in yellow. **B**, the structure viewed from the intermembrane side. Cytochrome b is shown in cyan, and Rieske cluster containing tip in orange. Leu275 and Glu272 in the ef loop of cytochrome b are also shown. AtQ is hydrogen-bonded to His181 of the Rieske protein and to a water molecule that forms a hydrogen bond bridge to the Glu272 side chain (from Kessl et al., 2003).*

The *ef* segment exhibits more pronounced sequence differences than the *cd* loop and non-conserved positions are observed to mutate in resistant strains, especially at position 283 and 295. Furthermore, the L275F mutation in AtQ resistant fungi *P. jiroveci*, was pointed out as position for drug selectivity (Kessl *et al*., 2004). However, in *Plasmodium* strains position 275 is a Phe like in humans. The drug selectivity in parasites must therefore be derived from another loci. Based on sequence and structural comparison a putative candidate could be at position 283. Arg283 is highly conserved in mammalian enzymes, whereas in the *Plasmodium* strains this residue is replaced with a Lys. In *P. jiroveci* a Trp occupies this position (see *Appendix A1*). Structural analysis shows that Arg283 interacts with the functionally relevant Tyr279. Furthermore, Arg283 is within *van der Waals* sphere of cytochrome *b* residues Ile269, Ala280, Pro286, Gly340, His343, Val344, Tyr348 and Val349 and makes close contacts to Leu282, Ser284, Ile285 and Cys342. When the Q_o site is empty and Rieske is in c-position Tyr279 is rotated into the binding site and the interatomic contacts made to Arg283 change accordingly, with 4.6 Å separating the Tyr279 hydroxyl group and the sidechain NH1 atom of Arg283 instead of 3.2 Å observed when Rieske is in b-position. Similar to the L275F mutation in fungi, the resistant K283R mutant presents another example for pathogen mimicking the host genotype to alleviate drug effects. Better understanding of the binding mode of atovaquone to the Q_o site is expected to aid in strategies for drug design to overcome the emerging resistance to this compound.

3.6 Tightly bound lipids in the X-ray structure of cytochrome bc_1 complex

Increased lipid content of the protein preparation was illustrated in two new structurally resolved tightly bound phospholipids, which were included in the model and refined. The relative orientation of integral membrane proteins with respect to the bilayer can be roughly estimated from hydropathy plots and structural features, such as the arrangement of transmembrane α-helices, distribution of refined water molecules and configuration of aromatic residues. The bilayer must have regional differences in thickness depending on its protein complement, as demonstrated by variable thicknesses shown for transmembrane regions of different integral membrane proteins (see Lee, 2003). The membrane spanning part dictates bilayer morphology and the bilayer exerts lateral pressure which presumably affects structural integrity of membrane proteins. These interactions between lipids and the highly structured protein surface support a sealed integration of the protein in the bilayer. The observed destabilization upon detergent solubilization, may be derived from decreased lateral pressure accompanied by increased conformational freedom of the protein. Importantly, lipids refined in membrane protein structures may aid in assigning the annular bilayer. A phospholipid stabilized at the Q_o site surface gave first reliable estimation of the intermembrane space (IMS) leaflet of the bilayer and together with previously identified lipids from the matrix side allowed vertical positioning of the complex in the membrane (Fig. 26 and Fig. 28). Based on the position of the IMS leaflet lipid the observed main chain displacement of the *ef* loop at the Q_o site surface was shown to extend into the lipid phase.

Cardiolipin (L5) binding on both sides of the complex, together with the neighboring phosphatidyl ethanolamine (L4) are proposed to provide a feasible docking site for supercomplex formation with cyt *c* oxidase (Pfeiffer *et al*., 2003). The recently assigned intermembrane space lipid (L6), contributes to this lipid filled cavity on each side of the homodimer (Fig. 27).

Interestingly, in the cavity at the dimer interface (Fig. 28), the isoprenoid tail of native Q_i site occupant refined in the X-ray structures extends to meet the stigmatellin side chain that is bound at the Q_o site of the other monomer of the homodimer (Fig. 26). This observation triggers ideas based on intermonomer cross-talk, as suggested by models based on alternating half-of-the-sites mechanism and observed anti-cooperativity of inhibitor binding (Gutierrez-Cirlos *et al*., 2002; Covian *et al*., 2004), suggesting that regulatory mechanisms may be related to active site

occupancy. This cavity is discussed as substrate entry point where substrate may diffuse from the membrane into the active sites. Also, the product from Q_o site may turn in the lipophilic cavity at the dimer interface to find its way into the Q_i site without leaving the complex, as an internal substrate tunneling event. It is also conceivable that this lipid rich interface provides a docking site for supercomplex formation, where substrate tunneling from for instance, succinate dehydrogenase (succinate:quinone oxidoreductase) and cytochrome bc_1 complex, could occur.

The majority of tightly bound lipids with strongly stabilized head groups is bound on the electronegative side of the membrane (*n* side), *i.e.* the mitochondrial matrix side. This is consistent with the asymmetric charge distribution on the membrane protein surface, where the mitochondrial encoded 8 TM helix of cytochrome *b* is noticed to have enrichment of positive charges at the *n* side, consistent with the 'positive-inside rule' (von Heijne, 1986; Gavel and von Heijne, 1988). Importantly, all identified phospholipids in the X-ray crystal structure make contacts to cytochrome *b* (table 6), which is the host of both active sites of cytochrome bc_1 complex. The assigned phospholipids are positioned at subunit interfaces, pointing to a structural role in assembly and/or stability of this multisubunit complex. In the structure, arginine and lysine residues are prevalent at the level of the phosphodiester groups on the matrix side, whereas the ratio is shifted to histidine residues on the side of the intermembrane space (Fig. 26B). Aromatic residues are frequently observed in lipid binding, including stabilization of acyl chain and interacting with the head group region. Tyrosines are observed with their side chains at the level of the phosphodiester groups at both sides of the membrane domain surface (Fig. 26C).

To summarize, lipid phosphodiester groups are often stabilized by two or more residues, with non-linear motifs typically combining a positively charged and polar ligands (see Table A5). Also, head group ligands were frequently observed to be from different subunits, further illustrating that structure-based and not sequence-based searches are required to identify lipid binding sites *in silico*. The majority of identified lipids in membrane protein structures are endogenous and reproducibly co-purified with the protein despite exhaustive purification procedures based on detergent extraction of the proteins. Interestingly, endogenous lipids have been reproducibly refined in conserved positions in both detergent solubilized protein crystallization and under conditions of lipidic cubic phase crystallization, as observed for

bacteriorhodopsin (see Cartailler and Luecke, 2003) and the bacterial reaction center (Katona *et al*., 2003), demonstrating specific stabilization of certain lipid species despite different purification and crystallization conditions.

Ordered and reproducible binding of the described lipids is demonstrated in their average B-factors, which are similar to the values obtained for the membrane spanning region of the protein (table 6). In comparison, an average B-factor of 27 $Å^2$ of the protein model in contrast to 57 $Å^2$ of the lipid phytanyl chains were observed for the 1.55 Å resolution structure of bacteriorhodopsin (Luecke *et al*., 1999). In addition to reproducible B-factor distribution when comparing different datasets, an impressive superimposition of the phospholipid binding sites in the yeast cytochrome bc_1 complex was observed, including head group specificity and structurally resolved length of acyl chains. Even inter-species conserved 'kinks' of tightly bound acyl chains were demonstrated when comparing the lipids identified in the X-ray structures of the bovine enzyme with yeast (Fig. 30). This reproducibility of lipid binding clearly indicates tight and specific protein-lipid interactions. Furthermore, the primary ligands of phospholipids head groups in the yeast cytochrome bc_1 complex are highly conserved (see Lange *et al*., 2001, Palsdottir *et al*., 2003), supporting a functional role of these lipid binding sites.

Interestingly, the identified lipid filled cavities coincide with those demonstrated in the photosynthetic cytochrome b_6f complexes (Kurisu *et al*., 2003; Stroebel *et al*., 2003) and even homologous primary ligands of the lipid head groups were identified. Conserved features were especially observed in the cavity at the dimer interface (Fig. 29 and Fig. 30), including truncated acyl chains, in contrast to well defined head groups as illustrated by the binding mode of an endogenous sulfolipid in the structure of the photosynthetic cytochrome b_6f complex from alga (Stroebel *et al*., 2003), which coincides with the binding site the cardiolipin (L7) described here (see *section* 2.5.3) (Fig. 30).

The unresolved density in the structure of the enzyme with HHDBT bound at the Q_o site provokes speculations (see *section 2.5*). It could be derived from a lipid fragment sticking there, because no high affinity substance is there to replace it. The specific stabilization of the stigmatellin side chain would replace any non-specifically adhering substance. Similarly, in the structure of CoQ_9 depleted RC with empty Q_B site a detergent molecule was found to bind at the isoprenoid tail binding site (Lancaster and Michel, 1997). Importantly, these observations provoke the

conclusions drawn from inhibitor titration studies to estimate Q_o site occupancy (Bartoschek *et al*., 2001). The observation that Q_o site specific inhibitor replaces substrate molecules does not prove that they were replaced from the active site, as the structures show ample opportunities for substrate molecules to bind in the lipophilic cavity at the dimer interface.

The importance of this lipid enriched cavity for structural integrity of the homodimer is illustrated in the structure determination of the homologous cyanobacterial enzyme (Kurisu *et al*., 2003). The stability of this preparation was enhanced by addition of exogenous lipids (Zhang *et al*., 2003), two of which were retained and refined in this cavity. Also, studies on *R. sphaeroides* showed that extensive delipidation and concomitant substrate depletion induced monomerization of the enzyme, which could be derived from a collapse of the delipidated frontal cavity (Montoya *et al*., 1999).

The observed lipid-detergent exchangeability (see *section 2.5.3*) provokes conflicting views. It is well known that excess detergent destabilizes membrane proteins. However, individual detergent molecules may assume a role of stabilizing interactions, as illustrated in the detergent-lipid exchangeability of the interhelical lipid, which has a proposed structural role for stable integration of Rieske in the complex (Lange *et al*., 2001). The observed lipid-detergent exchangeability could indicate that lipid binding sites of high and low affinity and different degree of specificity exist? The low affinity/specificity binding sites would be exposed in the much higher detergent concentration surrounding the transmembrane region in classical detergent solubilized purification-crystallization procedure.

The stably refined lipids in the structures could then present high affinity binding sites? It can be concluded that sites with affinity for lipid molecules exist, where specific binding is illustrated in reproducibly identified and even cross-species conserved lipid binding sites. The controversial questions about the functional/structural role of tightly bound phospholipids awaits further analysis through for instance structure-based-mutagenesis approach.

3.7.Concluding remarks

X-ray structural analysis of the cytochrome bc_1 complex from the yeast *Saccharomyces cerevisiae* with the inhibitor HHDBT bound at the quinol oxidation site was carried out. Previous crystallographic studies on UHDBT binding were not successful in providing high resolution structural information (Kim *et al.*, 1998). A shorter chain variant of UHDBT, heptyl-HDBT, was here successfully co-crystallized and a 2.5 Å crystal structure was obtained (Palsdottir *et al.*, 2003). Importantly, HHDBT binds in its ionized form in contrast to previous reports claiming that an ionized compound cannot bind at the active site (Zhang *et al.*, 1999).

Structural resemblance and competitive inhibition of Q_o site catalysis by HHDBT support its recognition as a substrate analog. The binding mode of this hydroxyquinone-derivative was therefore discussed in functional context. The observed binding mode of stigmatellin (Hunte *et al.*, 2000) and HHDBT, support a single occupancy model for ubiquinol oxidation (Hunte *et al.*, 2003). FTIR spectroscopic analysis was initiated to address functional aspects of the proposed mechanistic models (Ritter *et al.*, 2004). Preliminary results from theoretical investigation of protonation probabilities of catalytic residues are presented (see *Appendix A2*).

Importantly, the yeast *S. cerevisiae* was selected as a model system, because this organism permits site-directed mutagenesis approaches to address the enzyme mechanism in molecular detail. Understanding the relationships between structure and function of the cytochrome bc_1 complex is not only of fundamental research interest in the field of cellular bioenergetics, it is also of medicinal and agricultural importance. Certain human diseases are caused by molecular defects of this central enzyme in energy transduction. The catalytic subunits of the enzyme are highly conserved and these human mutations may therefore be modeled into the yeast enzyme to permit kinetic characterization of variants (Fisher *et al.*, 2004).

A number of compounds block the catalysis of this vital enzyme in a species-specific manner. For instance, the hydroxynaphthoquinone derivative atovaquone is used therapeutically to treat *Plasmodium falciparum* malaria, *Pneumocystis carinii* pneumonia, and *Toxoplasma gondii* toxoplasmosis. Atovaquone binds more efficiently to the cytochrome bc_1 complex of the respective pathogens and blocks their function, while not disturbing the activity of the human enzyme. Atovaquone is structurally similar to HHDBT and stigmatellin. The orientation of these inhibitors in

the X-ray structures, as well as the observed Q_o site occupancy-induced conformational flexibility of the enzyme, therefore served as criteria to model the binding of the drug at the Q_o site, thus providing the first molecular description of atovaquone binding to the cytochrome bc_1 complex (Kessl *et al*., 2003). Subsequently, the molecular basis for acquired resistance to atovaquone in fungal pathogens that cause pneumonia was investigated (Kessl *et al*., 2004).

Finally, a structural analysis of lipid binding to the cytochrome bc_1 complex was performed. The protein purification scheme was modified to enrich the lipid content of the preparation. Accordingly, the isolated enzyme exhibited higher turnover numbers and two new phospholipids were identified in the X-ray structure, in addition to previously assigned tightly bound lipids (Lange *et al*., 2001). A phospholipid stabilized at the surface of the Q_o site marks the intermembrane space leaflet of the lipid bilayer. Together with the previously identified matrix leaflet lipids this lipid permitted vertical positioning of the enzyme in the membrane. Notably, the tightly bound lipids were strategically positioned at subunit interfaces pointing to a structural role in gluing this multisubunit enzyme. Also, the lipids were reproducibly identified in data sets derived from different preparations, even faithfully reproducing the acyl chain lengths resolved in the electron density maps. Strikingly, cross-species conserved lipid binding sites and cavities provoke ongoing research regarding the structural and functional roles of tightly bound lipids in membrane protein structures.

4. MATERIALS AND METHODS

4.1 Suppliers

Amersham Biosciences (http://www.amershambiosciences.com)

Biomol (http://www.biomol.de/inhalt.php)

Biosepra (http://www.ciphergen.com/products/biosepra)

Biotrace/Difco (http://www.intlbioproducts.com/FrameSet.htm)

Calbiochem (http://www.emdbiosciences.com/html/CBC/home.html)

Gerbu (http://www.gerbu.de)

Invitrogen (http://invitrogen.com)

Merck KGaA (http://www.merck.de)

Roth (http://www.carl-roth.de)

Sigma-Aldrich & Fluka (http://www.sigmaaldrich.com)

4.2 Chemicals

2-(N-morpholino) ethane sulfonic acid (MES)	Biomol
3-(N-morpholino)propane sulfonic acid (MOPS)	Biomol
5-Brom-4-Chlor-3-indolyl-phosphate (BCIP)	Biomol
Bovine Serum Albumin (BSA)	Biomol
Calcium chloride ($CaCl_2$)	Roth
D-biotin	Sigma
Desthiobiotin	Sigma
Dimethylsulfoxide (DMSO)	Biomol
di-Potassiumhydrogenphosphate trihydrate ($K_2HPO_4 \cdot 3H_2O$)	Roth
di-Sodium hydrogen phosphate dihydrate ($Na_2HPO_4 \cdot H_2O$)	Roth
Ethylenediamine-tetraacetic acid disodium salt(EDTA)	Gerbu
Formaldehyde, 36.5 %	Fluka
Glutaraldehyde, 25 %	Sigma
Hydrochloric acid (HCl) (37%)	Roth
Lithium dodecyl sulfate (LDS)	Sigma
n-dodecyl-b-D-maltopyranoside (DDM)	Glycon
Nitro Blau Tetrazolium (NBT)	Biomol
n-undecyl-b-D-maltopyranoside (UM)	Glycon

Phenyl-methyl-sulfonyl fluoride (PMSF)	Gerbu
Polyethylene glycol 4000 (PEG4000) (50 % w/v)	Hampton research
Polyoxyethylene-sorbitan-monolaurate (Tween20)	Koch
Potassiumdihydrogenphosphate (KH_2PO_4)	Merck
Silver nitrate ($AgNO_3$)	Roth
Sodium azide (NaN_3)	Merck
Sodium carbonate (Na_2CO_3)	Merck
Sodium chloride (NaCl)	Gerbu
Sodium dodecylsulfate (SDS)	Gerbu
Sodium hydroxide (NaOH)	Merck
Sodium thiosulphate 5-hydrate ($Na_2S_2O_3 \cdot 5H_2O$)	Sigma-Aldrich
Sucrose (purity 97.995 %)	Gerbu
Tetramethylrhodamine-5-maleimide (TMR5M)	Molecular Probes
Tris-hydroxymethyl-9-aminomethane (Tris)	Roth

4.2.1 Chromatography materials

Activated thiol sepharose 4B	Amersham Biosciences
CH activated sepharose 4B	Amersham Biosciences
Diethylaminoethyl (DEAE) Fast flow sepharose	Amersham Biosciences
HyperD Diethylaminoethyl (DEAE)	Biosepra
NHS activated sepharose Fast Flow (FF)	Amersham Biosciences
PD10 (Sephadex G-25)	Amersham Biosciences
Superdex 75 PC 3.2/30	Amersham Biosciences
Superose 6 PC 3.2/30	Amersham Biosciences
TSK4000	TosoHaas

4.2.2 Proteins

Anti-myc-tag monoclonal antibody 9E10	hybridoma supernatant
Avidin	Fluka
Cytochrome bc_1 complex from *R. capsulatus*	Prof. F. Daldal
Cytochrome bc_1 complex from bovine heart	Prof. U. Brandt
Cytochrome bc_1 complex from *P. denitrificans*	Prof. B. Ludwig
Cytochrome *c* from horse heart	Sigma-Aldrich
Gel filtration HMW calibration kit	Amersham Bioscience

Gel filtration LMW calibration kit	Amersham Bioscience
Goat anti-mouse IgG alkaline phosphatase conjugate	Sigma-Aldrich
LMW calibration Kit for SDS	Amersham Bioscience
Pre-stained protein marker	Invitrogen
Streptavidin-coupled alkaline phosphatase	Amersham Bioscience

4.2.3 Strains

Bacteria

E. coli-K12 JM83 transformed with pASK68$_{18E11}$	Dr. C. Hunte
E. coli-K12 JM83 transformed with pASK68$_{78+79}$	

Yeast

FGY3 wildtype *S. cerevisiae*	Prof. M. Greenberg
Baker's yeast	*Wieninger*

4.2.4 Inhibitors

Undecyl stigmatellin (UST)	Dr. H. Miyoshi
^{13}C-UST	
Methoxyiminoacetamide (MIA)	
^{13}C-MIA	
Stigmatellin	Sigma-Aldrich
Ubiquinone-2	
5-*n*-heptyl-6-hydroxy-4,7-dioxobenzothiazole (HHDBT)	Prof. B. Trumpower

4.2.5 Other materials

MPG® Streptavidin coated magnetic beads	CPG Inc.
Step-tactin coated magnetic beads 5%	IBA
Bicinichoninic acid (BCA) Assay Reagent A and B	Uptima
Streptavidin coated M-PVA SAV2 Dynabeads	Chemagen
NuPAGE® 4-12% Bis-Tris Gel	Invitrogen
EXtrelut®NT1 glass column	Merck

4.3 Solutions

Gel electrophoresis and staining

20x Running buffer for NuPAGE Novex precast gels (pH 7.3): 1.0 M MES, 1.0 M Tris, 69.3 mM SDS and 20.5 mM EDTA

LDS Sample Buffer for gel electrophoresis: 3 % LDS, 10 % (w/v) glycerol, 50 m*M* Tris (8.5), 0.075 % (v/v) Serva Blue-G250, 0.025% (v/v) Phenol Red, 50 mM dithiothreitol

Coomassie stain solution: 0.25 % (w/v) Coomassie Brilliant Blue R250, 50 % (v/v) methanol and 10 % (v/v) acetic acid

Coomassie destaining: 40 % (v/v) methanol, 10 % (v/v) acetic acid

Storage solution: 7 % (v/v) acetic acid, 2 % (v/v) glycerin

Silver stain fixation solution: 30% ethanol and 10% acetic acid

Silver stain conditioning solution: 0.5 M sodiumacetate trihydrate, 0.01 M $Na_2S_2O_3 \cdot 5H_2O$, 0.125 % glutaraldehyde and 30 % ethanol

Silver stain solution: 6 mM $AgNO_3$ and 0.025 % formaldehyde

Silver stain developing solution: 0.24 M Na_2CO_3 and 0.04 % formaldehyde

Western blotting

Phosphate buffered saline (PBS) buffer : 2.7 mM KCl, 1.5 mM KH_2PO_4, 13 mM Na_2HPO_4 and 13.7 mM NaCl

PBS-T buffer: PBS containing 0.1 % Tween20

Semi-dry transfer buffer: 1x running buffer with 20 % methanol

Blocking buffer: PBS with 0.5% (v/v) Tween20 and 20 µg/ml avidin.

Washing buffer: PBS with 0.1% (v/v) Tween20

Color development solution: 33 µl NBT and 66 µl BCIP in 10 ml of 100 mM Tris/HCl(9.5), 100 mM NaCl, 5 mM $MgCl_2$

Fv fragment preparation

LB medium(1L): 10 g NaCl, 10 g bactotryptone, 5 g yeast extract

Periplasmic extraction buffer: 0.5 M sucrose, 100 mM Tris(8.0), 1 mM EDTA

Equilibration buffer: 0.05 M Tris(8.0)

Elution buffer: 0.05 M Tris(8.0), 2.5 mM desthiobiotin

Column storage buffer: 0.02% NaN_3, 1 mM EDTA

Column cleaning-in-place solution: equilibration buffer with 0.02% SDS

Fluorescent labeling of Fv

Labeling buffer: 50 mM KP_i (7.0) (carefully deoxygenated)

Magnetic beads pull down assay

Assay buffer: add 0.1% BSA (w/v) to SEC buffer (20 mM KP_i(7.5), 250 mM NaCl, 0.05% UM)

Elution buffer: 20 mM biotin in SEC buffer

Enzyme activity assay

Activity assay buffer: 250 mM sucrose, 50 mM KH_2PO_4/K_2HPO_4 at pH 7.3 - *i.e.* 50 mM KP_i(7.3), 0.2 mM EDTA, 1 mM NaN_3, 0.1 % BSA, 0.05% UM

Membrane preparation

Sorbitol solution: 1.2 M D-sorbitol, 0.01 M $CaCl_2 \cdot 2H_2O$, 0.1 M Tris, adjust pH with HCl to 7.5 and used immediately

Mannitol buffer: 50 mM KP_i(7.4), 650 mM D-mannit, 5 mM EDTA, and 2 g/L BSA

Solubilization buffer: 50 mM KH_2PO_4/K_2HPO_4 KP_i(7.3), 325 mM NaCl, 1.5 % DDM, 0.01 % PMSF

DEAE FF chromatography

Equilibration buffer: 50 mM KP_i(6.9), 350 mM NaCl, 0.015% DDM

Gradient high salt: 50 mM KP_i(6.9), 500 mM NaCl, 0.015% DDM, 0.01 % PMSF

Gradient low salt: 50 mM KP_i(6.9), 380 mM NaCl, 0.015% DDM, 0.01 % PMSF

Wash buffer: 10 mM KP_i(7.3), 1 M NaCl, 0.015% DDM

Storage buffer: 20 mM KP_i(7.3), 0.02 % NaN_3

Sample dilution buffer: 50 mM KP_i(6.9), 0.015% DDM

HyperD DEAE chromatography

Column packing buffer: 0.1 M KP_i(6.8), 0.25 M NaCl

Equilibration buffer: 50 mM KP_i(6.9), 150 mM NaCl, 0.015% DDM

Gradient high salt: 50 mM KP_i(6.9), 1 M NaCl, 0.015% DDM

Gradient low salt: 50 mM KP_i(6.9), 0.015% DDM

Storage buffer: 20% ethanol, 1 M NaCl

Size exlusion chromatography (SEC)

SEC buffer: 20 mM KP_i(7.5), 250 mM NaCl, 0.05% UM

3-D crystallization

Inhibitor stock solutions: Inhibitors were dissolved to 20 mM in DMSO

Solution for crystallization: 100 mM Tris/HCl(8.5/8.0 at 4°C), 0.05% UM, PEG4000(6-12%), x µM inhibitor

Reservoir solution: 100 mM Tris/HCl(8.5/8.0 at 4°C), 0.05% UM, PEG4000(5%)

Crystal storage solution: 100 mM Tris/HCl(8.5/8.0 at 4°C), 0.05% UM, PEG4000(8%), x µM inhibitor

Solution for cryoprotection: 0.2-1.2 M sucrose, 100 mM Tris/HCl(8.0), 0.05% UM, PEG4000(8-14%)

4.4 Equipment

ÄKTA purifier updated as explorer	Amersham Biosciences
Analytical SMART station	Pharmacia Biotech
Avanti J-20XPI	Beckmann Coulter
Biosys2000	Beckmann Instruments
Centricon (2 ml), Centriprep (15 ml)	Amicon
Centrisart (1.5 ml)	Sartorius AG
Desintegrator S	Bernd Euler
Diode array spectrophotometer	Agilent
Dual-wavelength UV/ vis Lambda40	Perkin-Elmer
DYNO-MILL	W. A. Bachofen AG
ELISA reader	PowerWave X, Bio-Tek Inst.
Eppendorf microfuge 5415C	Eppendorf
NuPAGE Novex XCell Mini Cell	Invitrogen
Sorvall RC-5B (rotors SS34 and GSA)	Du Pont de Nemours
Table centrifuge 4 K 10	Sigma-Aldrich
Ultrospec2100 UV/visible	Amersham pharmacia
UZ Optima LE-80K (rotor Ti45)	Beckmann Coulter
Vivaspin	Vivascience
Western blot apparatus	"semi-dry" system at MPI

4.5 Software

Windows, UNIX and SGI platforms. Windows based software for graphical presentation and curve fitting of kinetic data was Origin 7 (http://www.originlab.com) and KaleidaGraph (http://www.synergy.com), respectively. Unicorn software for Windows was used to control the ÄKTA purifier. Image processing, data scaling and reduction of X-ray data was performed with the HKL suite of programs. Refinement and model building was performed with CNS1.0 and Program O, respectively. Coordinate analysis, structural alignment, estimation of accessibility and evaluation of atomic contacts were performed with diverse program packages from the Uppsala Software Facility (http://xray.bmc.uu.se/usf). Other programs used were Naccess, LSQMAN, Profit, and HBPlus. For graphical presentation of X-ray structures, Ligplot, Molscript, Bobscript, and Raster3D were used.

4.6 Preparation of crystallization-grade material of the cytochrome bc_1 complex

All procedures were carried out at 4°C to prevent proteolytic degradation and denaturation of the probes. Preparation the cytochrome bc_1 complex was performed as described (Palsdottir and Hunte, 2003), with adjustments to the procedures listed below.

4.6.1 Preparation of membranes from Saccharomyces cerevisiae

The preparation was scaled up to accommodate more material by breaking the cells in the large DYNO-MILL (W. A. Bachofen AG, Maschinenfabrik). The yeast cells were either baker´s yeast (prepare by *Wieninger*, i.e. "fresh" supermarket yeast stored at 4°C) or FGY3 strain *Saccharomyces cerevisiae* (stored at -80 °C). 1,350 g of yeast cells were resuspended in 4 L of 10 mM EDTA and sedimented by spinning at 5000 rpm (7300 *g*) for 10 min in an Avanti J-20 centrifuge. The cells were resuspended in 4 L sorbitol solution. After second round of sedimentation, the wet weight of the cell sediment was estimated (ca. 1 kg). Effective cell breakage was ensured under hypertonic conditions where a 35 % (w/v) suspension of cells was carefully adjusted in mannitol buffer. To avoid clogging, the cell suspension was filtered through a nylon cloth (200 µm), prior to loading into the glass bead mill. The serine protease inhibitor phenylmethylsulfonyl fluoride (PMSF) was pre-dissolved in a small volume of dimethylsulfoxide and added to the suspension at a final concentration of 1 mM. The cell suspension was pumped through the mill at an approximate flow rate of 20

ml/min and the stirring adjusted to 2000 rpm. Successful cell breakage was monitored by microscopic analysis of the resulting specimen. More than 50% of the cells should be disrupted after the first run. The passage was repeated 3 times for complete disruption with addition of PMSF before every round of cell breakage. After diluting the broken cells with mannitol-free extraction buffer [1:10 (v/v)], cell debris and residual intact cells were sedimented 6200 rpm (5900 *g*) for 25 min using GSA rotor. The supernatant was subjected to ultracentrifugation at 43,000 rpm (~150,000 *g*) for 90 min. The membrane preparation was frozen at -80°C and was not stable for long term storage as noticed in reduced yield and enzyme activity of preparations stored for more than 6 months.

4.6.2 Solubilization of membranes

Resuspend 25 ml of crude membranes in 1.5 % *n*-dodecyl-b-D-maltoside (DDM), 350 mM NaCl, 50 mM KP_i 7.3, and 0.01% PMSF in a final volume of 210 ml. After incubation with stirring for 45 minutes, the solubilisate was subjected to ultracentrifugation at 150,000 *g* for 35 minutes.

4.6.3 Anion exchange chromatography

Purification of the enzyme is based on two consecutive chromatographic steps using the weak anion exchanger diethylaminoethyl (DEAE)-material, in line with moderately acidic average pI of the extramembraneous subunits (see Table 1). The intrinsic absorbance of cytochromes in the visible range assists in their detection during purification. Distinct dark red fractions clearly distinguished the target protein from the green-yellowish cytochrome *c* oxidase eluting in neighboring fractions. The multiple wavelength systems provided by the ÄKTA and Biosys chromatography systems permitted monitoring of the absorbance at 280 nm for total protein content and at 413 nm to specifically monitor heme absorbance. The membrane extract was loaded on a DEAE fast flow (FF) CL-6B resin and the eluted fractions were applied to the ceramic HyperD DEAE column.

4.6.3.1 DEAE FF anion exchange chromatography

The DEAE FF column (~100 ml, diameter of 5 cm) was operated by a peristaltic pump and equilibrated with several column volumes (CVs) of equilibration buffer. After loading the sample, the majority of weakly bound contaminants was removed by applying 1.5 CVs equilibration buffer. An elution gradient of 380-500 mM NaCl in

equilibration buffer was applied.The pooled fractions were diluted 2.4-fold with salt-free elution buffer to ensure efficient binding to the next anion-exchange chromatography column.

4.6.3.2 HyperD DEAE anion exchange chromatography

The capacity of the second anion exchange step was increased by scaling up the geometry of the column. The hyperdiffusion ceramic HyperD DEAE resin (50 µm bead size) was packed in high-pressure-resistant empty column holder. To recreate identical operating conditions, the linear flow rate was changed according to the increase in inner diameter of column and length. The chromatographic run was operated using the ÄKTA system at a flow rate of 4.5 ml/min. The scaled up column with a size of 7 cm x 10 mm permitted the purification of up to 40 mg of the cytochrome bc_1 complex. The resin was equilibrated with several CVs of buffer. A detergent exchange step from DDM to UM (3 CV) was performed. For elution a two-step salt gradient was applied: 150-300 mM NaCl (3 CVs), hold step (3 CVs), and 300-500 mM NaCl (8 CVs). The target protein eluted at ~35 mS in the first gradient. The cytochrome bc_1 complex containing fractions were pooled and concentrated using ultrafiltration devices with a molecular mass cut-off at 30 kDa. Notably, the chosen cutoff value of 30 kDa confers enrichment of the detergent. To ensure reproducible 3-D crystallization of this membrane protein preparation, the subsequent steps for protein concentration were standardized with respect to buffer volumes and choice of ultrafiltration devices.

4.7 Preparation and isolation of the Fv fragment 18E11

Fv fragment production was performed using a bacterial periplasmic expression system. Periplasmic expression of the Fv fragment was made in *E. coli*-K12 strain JM83 transformed with pASK68, as described by Kleywegt *et al.* (1995). A C-terminal strep-tag on Fv fragment heavy chain was used in one step streptavidin affinity chromatography, as described (Schmidt and Skerra, 1994; Kleymann *et al.*, 1995; Voss and Skerra, 1997). For immunodetection in Western blots C-terminal myc-tags were inserted in the Fv fragment light chain. Streptavidin-coupled alkaline phosphatase permitted enzymatic detection of heavy chain.

4.7.1 Streptavidin preparation

Streptavidin was prepared in inclusion bodies as described (Schmidt and Skerra, 1994). Correctly folded material was monitored by running SDS PAGE of reduced and non-reduced material. The latter was separated in the gel as a tetramer (4 x 13.3 kDa). The yield from one preparation was 720 mg/10 L culture in a spectroscopic determination where streptavidin has an extinction coefficient of ε_{280} 35.6 $mM^{-1}cm^{-1}$ for monomer. The BCAssay for total protein content yielded 960 mg/10 L culture. Streptavidin was coupled to the column material according to manufacturers instructions.

4.7.2 Streptavidin affinity chromatography

The periplasmic extract was avidin-treated to block biotinylated proteins: 40 µl avidin/10 mL periplasma, 30 min incubation at 4°C and centrifugation at 17000 rpm SS34 for 30 min. The streptavidin coupled columns were equilibrated with Tris-HCl (pH 8.0).The streptavidin coupled CH activated sepharose 4B was operated at a flow rate of 0.7 ml/min. The NHS activated sepharose FF material was operated at 1.3 ml/min. After loading with periplasmic extract, the equilibration buffer applied and this step was strictly monitored and stopped when 10 % of the peak height was until baseline. Elution was performed with 2.5 mM desthiobiotin (DTB) in equilibration buffer. After purification, the Fv fragment was concentrated to 1 ml using a vivaspin (15 ml) ultrafiltration device with molecular mass cut off at 10 kDa, washed with 2 x 5 ml Tris-HCl (pH 8.0) and finally concentrated to < 500 µl (~10 mg/ml), sterile filtered and 1 mM EDTA was added to the probe. A typical yield from wildtype Fv18E11 preparation was ~ 4.5 mg/120 mL periplasmic extract, as estimated by the BCAssay. The estimated shelf-life of functional Fv-fragment was ~3 weeks at 4°C. Notably, O/N incubation in diluted state in the DTB elution buffer caused destabilization and disassembly of the preparation. Therefore, immediate rebuffering and concentration of Fv fragment was required.

4.7.3 Fluorescent labeling of Fv fragment with engineered cysteine

The Fv18E11 plasmid was modified by introducing a cysteine on the light chain C-terminus just before the myc-tag, $pFv6_{oligos\ 78+79}$ (*provided by D. Vinzens*) for fluorescent labeling with thiol reactive probes. All buffers were carefully

deoxygenated to prevent oxidation of the free sulfhydryl groups. In this light sensitive labeling procedure the reaction tubes were wrapped in aluminium foil. Both a 20- and a 2-fold molar excess of 10 mM TMR-5M stock solution in DMSO were added to 1 mg/ml solution of the protein in 50 mM KP_i (7.0). After 1 hour incubation at RT (or O/N at 4°C) the reaction was stopped by adding 1 mM N-Acetylcysteine. Excess label was removed by PD10-Sephadex G-25 desalting column. Labeling efficiency was probed spectrophotometrically and was in the range of 20-40 % mol dye/mol protein. Tetramethylrhodamine-5-maleimide (TMR-5M) in 20 mM MOPS (adj. w. NaOH to 7.0) has an extinction coefficient of ε_{541} 91$mM^{-1}cm^{-1}$.

4.8 Size-exclusion chromatography (SEC)

The isolated enzyme is a homodimer with a molecular mass > 500 kDa (i.e. M_r 233.4 kDa per monomer plus detergent micelle). The co-complex with Fv fragment for 3-D crystallization of the detergent solubilized enzyme was formed with excess Fv fragment at a molar ratio of 1:1.4, as described (Hunte *et al*., 2000).

4.8.1 Isolation of the Fv-cytochrome bc_1 co-complex

For preparative size exclusion chromatography the high-resolution silica-based column material TSK-G4000SW (0.75 cm x 60.0 cm, *Toso Haas)* was equilibrated with SEC buffer at a flow rate of 0.45 ml/min. The pooled and concentrated fractions of the DEAE-HyperD eluate were loaded and separated using the same buffer. The capacity of the column allowed maximum of five mg of protein in 1 mL injected volume per run. The co-complex eluted with a retention time of ~46 minutes at a flow rate of 0.45 ml/min. The retention volumes for thyroglobulin (669 kDa), ferritin (440 kDa), catalase (232 kDa), and aldolase (158 kDa) were 16.9 ml, 20.3 ml, 21.6 ml, and 21.9 ml. Chymotrypsinogen (25 kDa) co-eluted with ribonuclease (13.7 kDa) at 25.5 ml. The elution volume for 1 mg/ml Blue dextran was used to estimate the void volume of ~12 ml.

4.8.2 Analytical gel filtration of Fv fragment

The Fv fragment assembly was monitored by gel filtration chromatography using Sephadex 75 column mounted on the SMART system. This method permits separation at analytical scale or ~50 µg protein. A single symmetric elution peak

indicated purity and stability of the sample. The column was operated at a flow rate of 50 µl/min in 50 mM Tris (pH 8.0). The column was calibrated as follows: Albumin (67 kDa) eluted in the void volume. Ovalbumin (43 kDa), chymotrypsinogen (25 kDa), and ribonuclease (13.7 kDa) eluted at 1.1 ml, 1.3 ml, and 1.5 ml, respectively. The void volume was estimated at 0.9 ml with blue dextran.

4.8.2.1 TCA precipitation

TCA precipitation was performed for gel electrophoretic detection of the eluted fractions with AU280 < 0.1. The probe was vortexed and incubated in 1% deoxycholate for 15 min at RT, after which it was incubated for 20 min in 12 % TCA (4°C) and spun down at 13,000 RPM in a table centrifuge. The pellet was solubilized by shaking in 20-100 µl 2.5% SDS at 37° C for 10 min.

4.9 Protein Determination

Determination of protein content was performed for the total protein content of probe using the BCAssay or specifically for the *b*-type hemes by taking advantage of the redox-properties of the heme cofactors for spectral characterization.

4.9.1 BCAssay

The total protein content was estimated using a modified Lowry procedure, the BCAssay protein quantification kit, according to instructions. This colorimetric assay, which is read at 562 nm-595 nm, is based on the bicinchoninic acid method introduced by Smith (Smith *et al*., 1985) and is especially suitable for measuring protein concentration in detergent containing samples.

4.9.2 Spectroscopic Quantification

The extinction coefficient for cytochrome *b* with respect to the difference absorption spectra of the dithionite-reduced minus the ferricyanide-oxidized sample is 28.5 $mM^{-1}cm^{-1}$(562-575 nm) (Vanneste, 1966). The concentration of cytochrome bc_1 complex equals half the concentration calculated for heme *b*. Cytochrome c_1 concentration was determined by difference absorption spectra of the ascorbate-reduced minus the ferricyanide-oxidized sample using an extinction coefficient of 17.1 mM^{-1} cm^{-1} (553-540 nm) (Yu *et al*., 1974).

4.10 SDS-PAGE Analysis

Ready-made polyacrylamide gels (4-12 % BisTris NuPAGE gel) of the Invitrogen system were used. Samples were prepared in LDS sample buffer and incubated for 30 min at 40°C. The moderate heat treatment is important to prevent the hydrophobic subunits from aggregating. The precast gel was fixed in the electrophoresis chamber XCell sureLock and filled with MES running buffer until the gel tray was covered. 20 µl sample was loaded per well and the gel run at 100-125 mA constant current per gel for 1 hour. The more soluble LDS in sample buffer, instead of SDS, yielded less diffusion and better focusing of bands.

4.10.1 Gel staining

For Coomassie staining the gel was incubated for 1 hour in stain solution and then destained for few hours or until background was colorless. Sensitivity of this staining procedure depends on the dye-binding capacity of the protein (>1 µg). For increased sensitivity silver staining permits detection of nanogram amounts of proteins. The gel was soaked in silver stain fixation solution for 15 min, after which it was incubated for 15 min in conditioning solution. After incubating (3 x 5 min) with dH2O, incubation for 20 min in silver solution was followed by a short incubation (3 x 10 s) in dH2O. Addition of developing solution yielded rapid detection of bands (< 5 min) and was stopped by washing with dH2O and incubating with 5% acetic acid.

4.10.2 Western Blot

The protein transfer from the gel onto a nitrocellulose membrane was performed by semidry blotting. The transfer took 1 hour with 50 mA at 4°C. The membrane was incubated with blocking buffer for 30 minutes at RT (or O/N at 4°C) in order to reduce non-specific interactions and then washed with the same buffer (3 x 5 minutes). For strep-tag detection a streptavidine conjugated alkaline phosphatase (1:1000 in washing buffer) was incubated for one hour at 4°C, followed by washing (3 x 10 min). For myc-tag detection, the mouse monoclonal antibody 9E10 was used as primary antibody and the alkaline phosphatase conjugated polyclonal goat anti-mouse IgG as secondary antibody. Substrates for alkaline phosphatase (i.e. BCIP/NBT) were used for color development and the enzymatic reaction was visualized in a purple stained bands.

4.11 Determination of cytochrome bc_1 complex activity

For steady-state activity determination the reduction of cytochrome *c* by the cytochrome bc_1 complex was followed with a spectrophotometric assay at 550 nm. The extinction coefficient of cytochrome *c* is 18.5 $mM^{-1}cm^{-1}$ (550-540 nm) (Clejan and Beattie, 1986). The assay was performed according to (Snyder *et al*., 2000) with slight modifications. An assay volume of 1 ml was used. The reaction mixture contained ~1 nmol cytochrome $b\,c_1$ complex, estimated by spectroscopic quantification of the *b* type hemes (see section 4.9.2), and 50 nmol horse cytochrome *c* in assay buffer (50 mM KP_i 7.3, 0.2 mM EDTA, 1mM NaN_3, 250 mM sucrose, and 0.05 % UM). The reaction was started by addition of 80 nmol decylubiquinol. The reaction was followed for 1-3 min at 550 nm. The activity was calculated from the initial linear reduction rate of cytochrome *c*. The background of non-enzymatic cytochrome *c* reduction was subtracted. Turnover numbers refer to mol cytochrome *c* reduced per mol cytochrome bc_1 complex per second under conditions of continuous turnover, where the catalytic reaction is zero order with respect to decylubiquinol and cytochrome *c*. Specific activity was calculated as µmol cytochrome *c* reduced per min per mg total protein.

4.11.1 Procedure for the two-electron reduction of decylubiquinone

The chemically inert and pH resistant (1-13) EXtrelut columns consist of a wide-pore kieselguhr and are therefore ideal for analysing lipophilic substances. This procedure avoids the time-consuming use of a separatory funnel and permits one step liquid-liquid extraction, with minimized sample loss. The principle of separation is as follows, the aqueous solution acts as stationary phase and elution takes place in organic solvent (cyclohexane) which is non-miscible with water. 150 mg Na-Dithionite ($Na_2S_2O_4$) were dissolved in 1 ml degassed N_2-saturated water and applied to the column, which was equilibrated for 10 min. 10 mg of substrate were dissolved in 1 ml of N_2-saturated cyclohexane. The substrate solution was reduced during flow through (~1 ml) and for quantitative recovery the column was incubated with at least 4-5 ml of cyclohexane. A color change from yellow (oxidized) to colorless ubiquinol roughly reflected the extent of reduction. The eluted sample was dried by flushing with N_2. A 20 mM stock solution was prepared in ethanol with 10mM HCl and stored at -80ºC.

4.12 Magnetic beads assay

The streptavidin/streptactin-magnetic beads assay was optimized for efficient pull down of Fv18E11-cytochrome bc_1 complex. All steps were carried out at 4°C. The assay is based on the strep-tag technology. Here, strep-tag I was irreversibly replaced by biotin elution buffer. Streptactin is optimized for efficient interactions with strep tag II, but successful pulldown of strep tag I coupled to Fv18E11 is also feasible. Typically, 100 µl beads suspension (50 mg/ml) were used per assay tube. The theoretical capacity of beads is typically ~100 pmol/mg or 500 pmol strep tag II fusion protein per assay tube, which means that the sensitivity of the assay for co-complex pulldown is >10 µg Fv18E11. A comfortable working range was ~10-fold higher or 100 µg Fv18E11 and 400 µg bc_1 complex. The assay buffer was the same as used in size-exclusion chromatography of the co-complex, i.e. SEC buffer, and was supplemented with 0.1% BSA to reduce unspecific binding. The molecular mass of 67 kDa for BSA, does not interfere with detection of cytochrome bc_1 polypeptides in gel electrophoretic analysis. Beads were activated and washed with 4 x 1 mL assay buffer and equilibrated on ice for 15 min. 250 µl of pre-formed co-complex (~2 mg/ml) was incubated with beads for at least 1 hour, gently dispersing beads every 10 minutes. 4 x 500 µl washing within a time span of 10 minutes, was followed by elution with 25 µl elution buffer.

4.13 Structure determination of cytochrome bc_1-Fv co-complex with inhibitors

Co-crystallization with HHDBT bound at the Q_o site was successful and led to X-ray structure determination at 2.5 Å resolution.

4.13.1 Crystallization with HHDBT

HHDBT (20 mM DMSO) was added in ~30 fold molar excess to the diluted enzyme or a final concentration of 100 µM in 3 ml solution of 3.6 µM enzyme. The Fv-enzyme-inhibitor co-complex was subsequently concentrated to ~200 µM (50 mg/ml) for 3-D crystallization. The amount of stigmatellin (20 mM DMSO) applied for co-crystallization was a factor of 10 less, due to its comparatively stronger inhibitory potency. The crystals were obtained in a hanging drop arrangement by vapor diffusion against 5 % polyethylene glycol 4000 at 4°C in 24-well Linbro plates. Larger size crystals were obtained by microseeding in a sitting drop arrangement. The protein

solution (50 mg/ml) was mixed in a ratio of 2 volumes protein solution per 1 volume precipitating agent (5% polyethylene glycol 4000, Tris-HCl pH 7.5 (adjusted at RT), 0.05% UM, 10 μM HHDBT). Final conditions in crystallization drop: 17 mM Tris (pH 8.0, 4 °C), 33 mM KPi (pH 7.5), 167 mM NaCl, and 0.05% UM, or a 0.5 pH unit lower than the conditions where the crystals of the stigmatellin-inhibited enzyme were obtained (Hunte *et al.*, 2000). For structural comparison, a data set with stigmatellin bound was collected at the same pH.

4.13.2 Cryoprotection trials

Conditions for cryoprotection of the crystals were probed. Among additives tested for suitability were lithium salts (LiCl, $LiSO_4$ and $LiCHO_2$), PEG400, glycerol, DMSO and sucrose. Sucrose turned out to be the most successful candidate for further optimization. Sucrose enhances solubility of the protein and therefore the amount of precipitating agent had to be increased accordingly. Screens were made to monitor the feasibility of growing crystals in sucrose containing buffers at final concentration of 250 mM and 500 mM. Subsequently, stepwise soaking with the aim to increase sucrose content was found to confer successful cryoprotection. The first images of a cryoprotected yeast cytochrome bc_1 complex were obtained at the DESY beamline (Hamburg). Although not of sufficient quality for data collection these trials provided useful hints for future directions in development of cryoconditions (S. Solmaz and C. Hunte, *work in progress*).

4.13.3 X-ray data collection

Diffraction data was collected at The European Synchrotron Radiation Facility, Grenoble, France (http://www.esrf.fr). A charge-coupled device detector (marCCD, mar USA, Evanston, IL) was used to register the reflections and the ProDC program was used to control the goniometer and detector through Spec and the MAR software, respectively. The HHDBT data set was collected at 180 mm detector-to-crystal distance, permitting theoretical resolution of 2.18 Å, using wavelength ~0.92994 Å at ID14EH3, ESRF (Grenoble). Data collection was performed at 4°C. To minimize radiation damage the beam intensity was attenuated (~2-5 photons/sec). Data collection was optimized for 20 seconds per pass and 3 passes/frame, meaning exposure time of 1 minute per frame in the oscillation range of $\Delta\varphi$ of 1 degree.

4.13.4 X-ray data processing

Data were processed with the program DENZO and merged using SCALEPACK from the HKL package (HKL Research, Charlottesville, NC) (Otwinowski and Minor, 1997). DENZO and XdisplayF were used to visualise, index, integrate diffraction maxima and refine crystal and detector parameters. SCALEPACK was used for finding relative scale factors between measurements and for merging and statistical analysis of measurements. Large crystals (>0.5 mm side length) permitted translation of the crystal in steps of 0.1 mm. The best dataset of the stigmatellin inhibited enzyme from the modified preparation was obtained from a single crystal with final dimensions of ~ 1 x 0.5 x 0.5 mm side lengths. The crystal was translated along the longest axis (1 mm). Data collection was performed in regulated steps of irradiation followed by translation from one end to the other, leaving mosaics of 0.05 mm areas not targeted by the beam. In this way more than 100 % completeness from one crystal was obtained. However, the last set of reflections were of low intensity and for refinement the data were truncated to 98% completeness to ensure quality of the experimental density map (Table 4). The crystals of the HHDBT inhibited enzyme were smaller and 7 crystals had to be scaled together to reach more than 90% completeness of data of acceptable quality.

4.13.5 Refinement and model building

Energy minimization and B-factor refinement were performed using the CNS program package (version 1.0) (Brunger *et al*., 1998) and applying the maximum likelihood function as the target for refinement. The high resolution stigmatellin-inhibited enzyme was in used as a model (PDB entry 1KB9), excluding all non-protein molecules. Phospholipids, Q_o and Q_i site ligands, water molecules and the detergent molecule were independently added in stepwise rounds of refinement. Subsequently, stepwise improvement of the model was observed as decreasing R/R_{free} factors. The model was improved based on F_o-F_c and $3F_o$-$2F_c$ electron density maps, using the program O (version 8.0.4). Simulated annealing omit maps were calculated in the areas of interest. Amino acid displacements were manually adjusted and in 1P84.pdb a displaced loop segment was manually repositioned based on the difference density, followed by a refinement cycle. Topology and parameter files were generated using the program Xplo2d and torsion data blocks prepared with the program Moleman2 (X-

UTIL package) (Kleywegt and Jones, 1997). The difference electron density map (F_o-F_c) confirmed the presence of 5 previously assigned tightly bound phospholipids and detergent molecule (Lange *et al*., 2001) and importantly two new phospholipids were identified and refined. Water molecules were included according to peaks observed in the F_o-F_c electron density map contoured at 3s. New water molecules were numbered as starting from Wat^{500}. Assignment of flexible and poorly resolved side chains was aided by alanine substitution using Program O, followed by a refinement cycle. At the given resolution the refinement of alternate conformation was not suitable. The side chains of buried Asn, Gln, and His were oriented as judged from hydrogen bond criteria (McDonald and Thornton, 1995). The estimation of acyl chain lengths was based on the extent of visibility in the experimental difference electron density (F_o-F_c) maps.

4.13.6 Coordinate analysis

4.13.6.1 Hydrogen bond analysis

Here, hydrogen bond angle is denoted as θ (X-H···A) and the bending angle at the acceptor atom as ϕ (H···A-C). The program HBPlus was to analyse neighboring atoms and hydrogen bond interactions (McDonald and Thornton, 1994). Atomic contacts were evaluated based on contact legitimacy of hydrophobic-hydrophilic properties of the interacting atoms using the Ligand-Protein Contacts (LPC) software link from the Protein Databank (http://www.rcsb.org/). For the identification of weak hydrogen bonds estimation of hydrogen atom position was made by generating a structural model with hydrogens added using CNS (v.1.0) (Brunger *et al*., 1998). Criteria for identifying weak hydrogen bonds were extracted from Desiraju and Steiner (1999). PROCHECK (v.3.2) analysis verified the stereochemical quality of the coordinates (Laskowski *et al*., 1993).

4.13.6.2 Estimation of surface accessible residues

Estimation of accessibility of amino acid residues in the X-ray structures and buried surface calculations were performed using the program NACCESS (Hubbard *et al*., 1991)(http://wolf.bms.umist.ac.uk/naccess/).

4.13.6.3 Buried surface area calculations

The calculated interfacial area in Fv-epitope and cytochrome *b*-Rieske interactions is the area of accessible surface area on both interaction partners, that becomes

inaccessible to solvent due to protein-protein contacts (Lo Conte *et al*., 1999). Interfacial surface area was calculated with NACCESS by calculating accessibility of the interacting polypeptides A and B as a complex (AB), as well as for A and B separately and according to the equation: A+B-AB. In this way an estimation of buried surface area ($Å^2$), i.e. interfacial area, was carried out. Accordingly, the distribution of polar and non-polar interactions could be estimated.

4.13.6.4 Structural alignment

Differences between two homologous protein structures were estimated by the root mean square deviation criteria (RMSD, Å) in terms of atomic positions after superimposition of the Cα atoms. The structures were superimposed using explicit least squares option in LSQMAN (Dejavuu package) and inspected in Program O. Analysis of $RMSD_{all}$ of the X-ray structures from the yeast enzyme (*i.e.* PDB entries 1KB9 and 1P84) with ProFit V2.2 (http://www.bioinf.org.uk/software/profit). Stigmatellin-inhibited enzyme was crystallized at the same pH as the HHDBT containing enzyme. The control data-set was collected with 2.8 Å resolution, 93 % completeness and R_{sym} 5.8 %. Refinement resulted in final R factor of 20.8 % and R_{free} 24.5 %. Lowering the pH by 0.5 unit did not affect the structure of the catalytic subunits of the stigmatellin inhibited enzyme, as judged by positional root mean square deviation (RMSD, Å) of superimposed atoms with LSQMAN yielding $RMSD_{all}/RMSD_{C_a}$ of 0.142/0.098, 0.175/0.118 and 0.204/0.133 for cytochrome *b*, cytochrome c_1 and the Rieske protein respectively.

4.13.7 Graphical presentation of results

Figures were prepared using the programs O (Jones *et al*., 1991), LIGPLOT version 4.0 (Wallace *et al*., 1995), MolScript version 1.4 (Kraulis, 1991), BobScript (Esnouf, 1999), and Raster3D (Merritt and Murphy, 1994).

4.14 Multiple sequence alignment of cytochrome *b*

Multiple sequence alignment was performed with the BCM search launcher (http://searchlauncher.bcm.tmc.edu/multi-align/multi-align.html) and ClustalW1.8 using default parameters. For presentation of the alignment, the amino acid sequences were shaded according to similarity using the BOXSHADE 3.21 server (http://www.ch.embnet.org/software/BOX_form.html) (see *Appendix A1*). Consensus

symbols were displayed by default. Sequences were retrieved from ExPASy Molecular Biology Server (http://www.expasy.org/) for *Homo sapiens* (CYB_HUMAN), *Bos taurus* (CYB_BOVIN), *Saccharomyces cerevisiae* (CYB_YEAST), *Plasmodium falciparum* (CYB_PLAFA), *Plasmodium bergheii (*CYB_PLABE), *Rhodobacter sphaeroides* (CYB_RHOSH), *Rhodobacter capsulatus* (CYB_RHOCA), *Paracoccus denitrificans* (CYB_PARDE). The sequence for *Gallus Gallus* cytochrome *b* was taken from PDB entry 1BCC.pdb. Likewise, sequences for cytochrome *b*6 and subunit IV of cytochrome b_6f complexes (Plastohydroquinone : Plastocyanin Oxidoreductase) were used as submitted with the PDB entries from *Chlamydomonas Reinhardtii* (1OQ9.pdb) and *Mastogladicus Laminosus* (1UM3.pdb). Given the number of a residue in the yeast sequence (used throughout text), the number of the corresponding residue in chicken (*i.e. G. gallus*) is found by adding 2 if the number is less than 114. For residues 114 and later, the numbering is the same. The number of the corresponding residue in the bovine sequence is found by subtracting 1 from the number in the chicken sequence after the first five residues. For comparative analysis of parasite and yeast cytochrome *b* subtraction of 6 residues in the *cd* loop and subtraction of 11 residues in the *ef* loop generates the corresponding position in the *Plasmodium* sequences.

4.15 FTIR Spectroscopy of the yeast cytochrome bc_1 complex

To supplement the X-ray structural data, mechanistic insight into redox dependent protonation behaviour of the sample, was pursued with Fourier-Transfer Infrared Spectroscopy (FTIR). The FTIR spectra were recorded by Dr. Michaela Ritter and interpretation of data was carried out under the supervision of Dr. Petra Hellwig.

4.15.1 Preparation of protein sample

The cytochrome bc_1 complex eluting from the HyperD DEAE column was used for measurements. The detergent exchange buffer (300 mM NaCl, 50 mM KP_i (pH 6.9), 0.05% UM) was used as working buffer in the electrochemical and spectroscopic studies. Inhibitors (*e.g.* HHDBT, stigmatellin, UST, ^{13}C-UST, MIA, ^{13}C-MIA and UK2A) were added at a final concentration of 1 µM to the cytochrome bc_1 complex in diluted state of the protein of ~ 30 µM. After adding the inhibitors the enzyme was concentrated in a centrifugal spin device with molecular mass cutoff of 30 kDa to a final concentration of 0.3-0.5 mM.

4.15.2 FTIR measurements

FTIR and UV/vis difference spectra were simultaneously recorded as a function of the applied potential using a setup combining an IR beam from the interferometer (modified IFS 25, Bruker, Germany) for the 4000-1000 cm^{-1} range and a dispersive spectrometer for the 400-900 nm range as described (see M. Ritter, *PhD thesis*). First, the protein was equilibrated at an initial electrode potential and a single-beam spectrum was recorded. Then the final potential was applied, and a single-beam spectrum was again recorded after equilibration. Equilibration generally took less than 4 min for the full potential step from -0.292 to +0.708 V as followed by the difference signals in the visible spectral range. Infrared difference spectra as presented here were calculated from two single-beam spectra, with the initial spectrum taken as reference.

REFERENCES

Baciou, L. and Michel, H. (1995) Interruption of the water chain in the reaction center from Rhodobacter sphaeroides reduces the rates of the proton uptake and of the second electron transfer to QB. Biochemistry, 34:7967-7972.

Bartoschek, S., Johansson, M., Geierstanger, B.H., Okun, J.G., Lancaster, C.R.D., Humpfer, E., Yu, L., Yu, C.A., Griesinger, C., and Brandt, U. (2001) Three molecules of ubiquinone bind specifically to mitochondrial cytochrome bc1 complex. J Biol Chem, 276:35231-35234.

Baymann, F., Robertson, D. E., Dutton, P. L., and Mantele, W. (1999) Electrochemical and spectroscopic investigations of the cytochrome bc1 complex from Rhodobacter capsulatus. Biochemistry, 38:13188-13199.

Beattie, D. S., Wang, Y., and Obungu, V.H. (1999) The role of various domains of the iron-sulfur protein in the assembly and activity of the cytochrome bc1 complex of yeast mitochondria. J Bioenerg Biomembr, 31:215-224.

Beckmann, J. D., Ljungdahl, P.O., and Trumpower, B.L. (1989) Mutational analysis of the mitochondrial Rieske iron-sulfur protein of Saccharomyces cerevisiae. I. Construction of a RIP1 deletion strain and isolation of temperature-sensitive mutants. J Biol Chem, 264:3713-3722.

Behr, J., Hellwig, P., Mantele, W., and Michel, H. (1998) Redox dependent changes at the heme propionates in cytochrome c oxidase from Paracoccus denitrificans: direct evidence from FTIR difference spectroscopy in combination with heme propionate 13C labeling. Biochemistry, 37:7400-7406.

Behr, J., Michel, H., Mantele, W., and Hellwig, P. (2000) Functional properties of the heme propionates in cytochrome c oxidase from Paracoccus denitrificans. Evidence from FTIR difference spectroscopy and site-directed mutagenesis. Biochemistry, 39:1356-1363.

Berry, E.A. and Trumpower, B.L. (1985) Isolation of ubiquinol oxidase from Paracoccus denitrificans and resolution into cytochrome bc1 and cytochrome c-aa3 complexes. J Biol Chem, 260:2458-2467.

Berry, E.A., Huang, L.S., and DeRose, V.J. (1991) Ubiquinol-cytochrome c oxidoreductase of higher plants. Isolation and characterization of the bc1 complex from potato tuber mitochondria. J Biol Chem, 266:9064-9077.

Berry, E.A., Guergova, K., Huang, L.S., and Crofts, A.R. (2000) Structure and function of cytochrome bc complexes. Annu Rev Biochem, 69:1005-1075.

Berry, E.A. and Huang, L.S. (2003) Observations concerning the quinol oxidation site of the cytochrome bc1 complex. FEBS Lett, 555:13-20.

Berry, S. (2002) The chemical basis of membrane bioenergetics. J Mol Evol. 54:595-613.

Bogdanov, M., and Dowhan, W. (1995). Phosphatidylethanolamine is required for in vivo function of the membrane-associated lactose permease of Escherichia coli. J Biol Chem: 270:732-739.

Bogdanov, M., and Dowhan, W. (1998) Phospholipid-assisted protein folding: phosphatidylethanolamine is required at a late step of the conformational maturation of the polytopic membrane protein lactose permease. EMBO J. 17:5255-5264.

Boumans, H., Grivell, L.A., and Berden, J.A. (1998) The respiratory chain in yeast behaves as a single functional unit. J Biol Chem, 273:4872-4877.

Bowyer, J.R., Edwards, C.A., and Trumpower, B.L. (1981) Involvement of the iron-sulfur protein of the mitochondrial cytochrome b-c1 complex in the oxidant-induced reduction of cytochrome b. FEBS Lett, 126:93-97.

Bowyer, J.R., Edwards, C.A., Ohnishi, T., and Trumpower, B.L. (1982) An analogue of ubiquinone which inhibits respiration by binding to the iron-sulfur protein of the cytochrome b-c1 segment of the mitochondrial respiratory chain. J Biol Chem, 257:8321-8330.

Brandt, U., Uribe, S., Schägger, H., and Trumpower, B.L. (1994) Isolation and characterization of QCR10, the nuclear gene encoding the 8.5-kDa subunit 10 of the Saccharomyces cerevisiae cytochrome bc1 complex. J Biol Chem, 269:12947-12953.

Brandt, U. (1996) Bifurcated ubihydroquinone oxidation in the cytochrome bc1 complex by proton-gated charge transfer. FEBS lett, 387: 1-6.

Brandt, U. and Okun, J.G. (1997) Role of deprotonation events in ubihydroquinone:cytochrome c oxidoreductase from bovine heart and yeast mitochondria. Biochemistry, 36:11234-11240.

Brandt, U. (1998) The chemistry and mechanics of ubihydroquinone oxidation at center P (Qo) of the cytochrome bc1 complex. Biochim Biophys Acta, 1365:261-268.

Brasseur, G., Saribas, A.S., and Daldal, F. (1996) A compilation of mutations located in the cytochrome b subunit of the bacterial and mitochondrial bc1 complex. Biochim Biophys Acta, 1275:61-69.

Brasseur, G., Bruscella, P., Bonnefoy, V., and Lemesle, M. (2002) The bc1 complex of the iron-grown acidophilic chemolithotrophic bacterium Acidithiobacillus ferrooxidans functions in the reverse but not in the forward direction. Is there a second bc1 complex? Biochim Biophys Acta, 1555:37-43.

Brasseur, G., Lemesle-Meunier, D., Reinaud, F., and Meunier, B. (2004) Qo site deficiency can be compensated by extragenic mutations in the hinge region of the Iron-Sulfur Protein in the bc1 complex of Saccharomyces cerevisiae. J Biol Chem. 23:24203-11

Bruel, C., Brasseur, R., and Trumpower, B.L. (1996) Subunit 8 of the Saccharomyces cerevisiae cytochrome bc1 complex interacts with succinate-ubiquinone reductase complex. J Bioenerg Biomembr, 28:59-68.

Brugna, M., Rodgers, S., Schricker, A., Montoya, G., Kazmeier, M., Nitschke, W., and Sinning, I. (2000) A spectroscopic method for observing the domain movement of the Rieske iron-sulfur protein. Proc Natl Acad Sci U S A, 97:2069-2074.

Brunger, A.T., Adams, P.D., Clore, G.M., DeLano, W.L., Gros, P., Grosse, K., Jiang, J.S., Kuszewski, J., Nilges, M., Pannu, N.S., Read, R.J., Rice, L.M., Simonson, T., and Warren, G.L. (1998) Crystallography & NMR system: A new software suite for macromolecular structure determination. Acta Crystallogr. Sect. D 54, 905–921

Carman, G.M. and Henry, S.A. (1989) Phospholipid biosynthesis in yeast. Annu Rev Biochem, 58:635-669.

Cartailler, J.P. and Luecke, H. (2003) X-ray crystallographic analysis of lipid-protein interactions in the bacteriorhodopsin purple membrane. Annu Rev Biophys Biomol Struct, 32:285-310.

Chambers, J.Q. (1988) Electrochemistry of quinones. The Chemistry of Quinonoid compounds. Vol II. S. Patai and Z. Rapporport, eds. John Wiley & sons Ltd. (USA) pp.719-757

Clejan, L., and Beattie, D.S. (1986). Preparation of complex III from yeast mitochondria and related methodology. Methods Enzymol. 126, 173-180.

Cooley, J.W., Roberts, A.G., Bowman, M.K., Kramer, D.M., and Daldal, F. (2004) The raised midpoint potential of the [2Fe2S] cluster of cytochrome bc1 is mediated by both the Qo site occupants and the head domain position of the Fe-S protein subunit. Biochemistry, 43: 2217-2227.

Covian, R. and Moreno-Sanchez, R. (2001) Role of protonatable groups of bovine heart bc1 complex in ubiquinol binding and oxidation. Eur J Biochem, 268:5783-5790.

Covian, R., Pardo, J.P., and Moreno-Sanchez, R. (2002) Tight Binding of Inhibitors to Bovine bc1 Complex Is Independent of the Rieske Protein Redox State. Consequences for semiquinone stabilization in the quinol oxidation site. J.Biol.Chem., 277:48449-48455.

Covian, R., Gutierrez-Cirlos, E.B., and Trumpower, B.L. (2004) Anti-cooperative oxidation of ubiquinol by the yeast cytochrome bc1 complex. J Biol Chem, 279:15040-15049.

Crofts, A.R. and Meinhardt, S.W. (1982) A Q-cycle mechanism for the cyclic electron-transfer chain of Rhodopseudomonas sphaeroides. Biochem Soc Trans, 10:201-203.

Crofts, A.R. and Wang, Z. (1989) How rapid are the internal reactions of the UQH2:cyt c2 oxidoreductase? Photosynth. Res. 22, 69-87

Crofts, A.R., Barquera, B., Gennis, R.B., Kuras, R., Guergova-Kuras, M., and Berry, E.A. (1999a) Mechanism of ubiquinol oxidation by the bc1 complex: different domains of the quinol binding pocket and their role in the mechanism and binding of inhibitors. Biochemistry, 38:15807-15826.

Crofts, A.R., Guergova, K., Huang, L., Kuras, R., Zhang, Z., and Berry, E.A. (1999b) Mechanism of ubiquinol oxidation by the bc1 complex: role of the iron sulfur protein and its mobility. Biochemistry, 38:15791-15806.

Crofts, A.R., Hong, S., Ugulava, N., Barquera, B., Gennis, R., Guergova-Kuras, M, and Berry, E.A. (1999c) Pathways for proton release during ubihydroquinone oxidation by the bc1 complex. Proc Natl Acad Sci U S A, 96:10021-10026.

Crofts, A.R., Hong, S., Zhang, Z., and Berry, E.A. (1999d) Physicochemical aspects of the movement of the rieske iron sulfur protein during quinol oxidation by the bc1 complex from mitochondria and photosynthetic bacteria. Biochemistry, 38:15827-15839.

Crofts, A.R., Guergova-Kuras, M., Kuras, R., Ugulava, N., Li, J., and Hong, S. (2000) Proton-coupled electron transfer at the Q(o) site: what type of mechanism can account for the high activation barrier? Biochim Biophys Acta, 1459:456-466.

Crofts, A.R., Shinkarev, V.P., Kolling, D.R., and Hong, S. (2003) The modified Q-cycle explains the apparent mismatch between the kinetics of reduction of cytochromes c1 and bH in the bc1 complex. J Biol Chem, 278:36191-36201.

Crofts, A.R. (2004) The cytochrome bc1 complex: function in the context of structure. Annu Rev Physiol, 66:689-733.

Cruciat, C.M., Brunner, S., Baumann, F., Neupert, W., and Stuart, R.A. (2000) The cytochrome bc1 and cytochrome c oxidase complexes associate to form a single supracomplex in yeast mitochondria. J Biol Chem, 275:18093-18098.

Darrouzet, E., Valkova-Valchanova, M., Moser, C.C., Dutton, P.L., and Daldal, F. (2000) Uncovering the [2Fe2S] domain movement in cytochrome bc1 and its implications for energy conversion. Proc Natl Acad Sci U S A, 97:4567-4572.

Darrouzet, E. and Daldal, F. (2002) Movement of the iron-sulfur subunit beyond the ef loop of cytochrome b is required for multiple turnovers of the bc1 complex but not for single turnover Qo site catalysis. J Biol Chem, 277:3471-3476.

Darrouzet, E., Valkova-Valchanova, M., and Daldal, F. (2002) The [2Fe-2S] cluster E(m) as an indicator of the iron-sulfur subunit position in the ubihydroquinone oxidation site of the cytochrome bc1 complex. J Biol Chem, 277:3464-3470.

Davies, D.R. and Cohen, G.H. (1996) Interactions of protein antigens with antibodies. Proc Natl Acad Sci U S A, 93:7-12.

de Vries, S. and Grivell, L.A. (1988) Purification and characterization of a rotenone-insensitive NADH:Q6 oxidoreductase from mitochondria of Saccharomyces cerevisiae. Eur J Biochem, 176:377-384.

de Vrije, T., de Swart, R.L., Dowhan, W., Tommassen, J., and de Kruijff, B. (1988) Phosphatidylglycerol is involved in protein translocation across Escherichia coli inner membranes. Nature 334:173-5.

Degli-Esposti, M., de Vries, S., Crimi, M., Ghelli, A., Patarnello, T., and Meyer, A. (1993) Mitochondrial cytochrome b: evolution and structure of the protein. Biochim Biophys Acta, 1143:243-271.

Deisenhofer, O., Epp, K., Miki, R., Huber, and H. Michel. (1985) Structure of the protein subunits in the photosynthetic reaction center of Rhodopseudomonas viridis at 3 Å resolution. Nature 318: 618–624.

Deisenhofer, J. and Michel, H. (1989) Nobel lecture. The photosynthetic reaction centre from the purple bacterium Rhodopseudomonas viridis. EMBO J, 8:2149-2170.

Deisenhofer, J., Epp, O., Sinning, I., and Michel, H. (1995) Crystallographic refinement at 2.3 A resolution and refined model of the photosynthetic reaction centre from Rhodopseudomonas viridis. J Mol Biol, 246:429-457.

Denke, E., Merbitz, Z., Hatzfeld, O.M., Snyder, C.H., Link, T.A., and Trumpower, B.L. (1998) Alteration of the midpoint potential and catalytic activity of the rieske iron-sulfur protein by changes of amino acids forming hydrogen bonds to the iron-sulfur cluster. J Biol Chem, 273:9085-9093.

Desiraju, G. R. and Steiner, T. (1999) The Weak Hydrogen Bond, Oxford University Press, NY.

di Rago, J.P., Sohm, F., Boccia, C., Dujardin, G., Trumpower, B.L., and Slonimski, P.P. (1997) A point mutation in the mitochondrial cytochrome b gene obviates the requirement for the nuclear encoded core protein 2 subunit in the cytochrome bc1 complex in Saccharomyces cerevisiae. J Biol Chem, 272:4699-4704.

Ding, H., Daldal, F., and Dutton, P.L. (1995a) Ion pair formation between basic residues at 144 of the Cyt b polypeptide and the ubiquinones at the Qo site of the Cyt bc1 complex. Biochemistry, 34:15997-16003.

Ding, H., Moser, C.C., Robertson, D.E., Tokito, M.K., Daldal, F., and Dutton, P.L. (1995b) Ubiquinone pair in the Qo site central to the primary energy conversion reactions of cytochrome bc1 complex. Biochemistry, 34:15979-15996.

Ding, H., Robertson, D.E., Daldal, F., and Dutton, P.L. (1992) Cytochrome bc1 complex [2Fe-2S] cluster and its interaction with ubiquinone and ubihydroquinone at the Qo site: a double-occupancy Qo site model. Biochemistry, 31:3144-3158.

Dowhan, W. (1997) Molecular basis for membrane phospholipid diversity: why are there so many lipids? Annu Rev Biochem. 66:199-232.

Dutzler, R., Campbell, E.B., and MacKinnon, R. (2003) Gating the selectivity filter in ClC chloride channels. Science, 300:108-112.

Elbehti, A., Nitschke, W., Tron, P., Michel, C., and Lemesle, M. (1999) Redox components of cytochrome bc-type enzymes in acidophilic prokaryotes. I. Characterization of the cytochrome bc1-type complex of the acidophilic ferrous ion-oxidizing bacterium Thiobacillus ferrooxidans. J Biol Chem, 274:16760-16765.

Engel, W.D., Schägger, H., and von Jagow, G. (1980) Ubiquinol-cytochrome c reductase (EC 1.10.2.2). Isolation in triton X-100 by hydroxyapatite and gel chromatography. Structural and functional properties. Biochim Biophys Acta, 592:211-222.

Esnouf, R.M. (1999) Further additions to MolScript version 1.4, including reading and contouring of electron-density maps.Acta Cryst. D 55 (Pt 4), 938-940

Essen, L.O. and Skerra, A. (1993) Single-step purification of a bacterially expressed antibody Fv fragment by immobilized metal affinity chromatography in the presence of betaine. J Chromatogr A, 657:55-61.

Essen, L.O., Harrenga, A., Ostermeier, C., and Michel, H. (2003) 1.3 A X-ray structure of an antibody Fv fragment used for induced membrane-protein crystallization. Acta Crystallogr D Biol Crystallogr, 59:677-687.

Fisher, N. and Meunier, B. (2001) Effects of mutations in mitochondrial cytochrome b in yeast and man. Deficiency, compensation and disease. Eur J Biochem, 268:1155-1162.

Fisher, N., Bourges, I., Hill, P., Brasseur, G., and Meunier, B. (2004a) Disruption of the interaction between the Rieske iron-sulfur protein and cytochrome b in the yeast bc1 complex owing to a human disease-associated mutation within cytochrome b. Eur J Biochem, 271:1292-1298.

Fisher, N., Castleden, C.K., Bourges, I., Brasseur, G., Dujardin, G., and Meunier, B. (2004b) Human disease-related mutations in cytochrome b studied in yeast. J Biol Chem, 279:12951-12958.

Fivelman, Q.L., Butcher, G.A., Adagu, I.S., Warhurst, D.C., and Pasvol, G. (2002) Malarone treatment failure and in vitro confirmation of resistance of Plasmodium falciparum isolate from Lagos, Nigeria. Malar J, 1:1.

Frey, T.G. and Mannella, C.A. (2000) The internal structure of mitochondria. Trends Biochem Sci, 25:319-324.

Friedman, M.D., Stotter, P.L., Porter, T.H., and Folkers, K. (1973) Synthesis of alkyl-4,7-dioxobenzothiazoles with prophylactic antimalarial activity. J Med Chem 16:1314-1316

Friedrich, T. and Böttcher, B. (2004) The gross structure of the respiratory complex I: a Lego System. Biochim Biophys Acta 1608:1-9.

Fyfe, P.K., Isaacs, N.W., Cogdell, R.J., and Jones, M.R. (2004) Disruption of a specific molecular interaction with a bound lipid affects thermal stability of the purple bacterial reaction centre. Biochim Biophys Acta. 1608:11-22.

Gao, X., Wen, X., Yu, C., Esser, L., Tsao, S., Quinn, B., Zhang, L., Yu, L., and Xia, D. (2002) The Crystal Structure of Mitochondrial Cytochrome bc1 in Complex with Famoxadone: The Role of Aromatic-Aromatic Interaction in Inhibition. Biochemistry, 41:11692-11702.

Gao, X., Wen, X., Esser, L., Quinn, B., Yu, L., Yu, C.A., and Xia, D. (2003) Structural basis for the quinone reduction in the bc1 complex: a comparative analysis of crystal structures of mitochondrial cytochrome bc1 with bound substrate and inhibitors at the Qi site. Biochemistry, 42:9067-9080.

Gatti, D.L., Meinhardt, S.W., Ohnishi, T., and Tzagoloff, A. (1989) Structure and function of the mitochondrial bc1 complex. A mutational analysis of the yeast Rieske iron-sulfur protein. J Mol Biol, 205:421-435.

Gil, J.P., Nogueira, F., Stromberg, N., Lindberg, J., Carrolo, M., Casimiro, C., Lopes, D., Arez, A.P., Cravo, P.V., and Rosario, V.E. Detection of atovaquone and Malarone resistance conferring mutations in Plasmodium falciparum cytochrome b gene (cytb). Mol Cell Probes, 17:85-89.

Goffeau, A., Barrell, B.G., Bussey, H., Davis, R.W., Dujon, B., Feldmann, H., Galibert, F., Hoheisel, J.D., Jacq, C., Johnston, M., Louis, E.J., Mewes, H.W., Murakami, Y., Philippsen, P., Tettelin, H., and Oliver, S.G. (1996) Life with 6000 genes. Science, 274:546, 563-546, 567.

Gomez, B. and Robinson, N.C. (1999) Phospholipase digestion of bound cardiolipin reversibly inactivates bovine cytochrome bc1. Biochemistry, 38:9031-9038.

Gopta, O.A., Feniouk, B.A., Junge, W., and Mulkidjanian, A.Y. (1998) The cytochrome bc1 complex of Rhodobacter capsulatus: ubiquinol oxidation in a dimeric Q-cycle? FEBS Lett, 431:291-296.

Guergova-Kuras, M., Ugulava, N., Hadad, I., Kuras, R., and Crofts, A.R. (2000) Specific mutagenesis of the rieske iron-sulfur protein in Rhodobacter sphaeroides shows that both the thermodynamic gradient and the pK of the oxidized form determine the rate of quinol oxidation by the bc1 complex. Biochemistry, 39:7436-7444.

Gutierrez-Cirlos, E. and Trumpower, B.L. (2002) Inhibitory analogs of ubiquinol act anti-cooperatively on the Yeast cytochrome bc1 complex. Evidence for an alternating, half-of-the-sites mechanism of ubiquinol oxidation. J Biol Chem, 277:1195-1202.

Haines, T.H. (1983) Anionic lipid headgroups as a proton-conducting pathway along the surface of membranes: a hypothesis. Proc Natl Acad Sci U S A, 80:160-164.

Hill, P., Kessl, J., Fisher, N., Meshnick, S., Trumpower, B.L., and Meunier, B. (2003) Recapitulation in Saccharomyces cerevisiae of cytochrome b mutations conferring resistance to atovaquone in Pneumocystis jiroveci. Antimicrob Agents Chemother, 47:2725-2731.

Höfle, G., Kunze, B., Zorzin, C., and Reichenbach, H. (1984) Liebigs Ann. Chem. 8: 1883-1904

Hong, S., Ugulava, N., Guergova, K., and Crofts, A.R. (1999) The energy landscape for ubihydroquinone oxidation at the Q(o) site of the bc1 complex in Rhodobacter sphaeroides. J Biol Chem, 274:33931-33944.

Hubbard S.J. and Thornton J.M. 'Naccess',computer program - V.2.1.1. (1993) Dept. Biochemistry and Molecular Biology, University College, London

Hunte, C., Koepke, J., Lange, C., Rossmanith, T., and Michel, H. (2000) Structure at 2.3 A resolution of the cytochrome bc1 complex from the yeast Saccharomyces cerevisiae co-crystallized with an antibody Fv fragment. Structure Fold Des, 8:669-684.

Hunte, C. and Michel, H. (2002) Crystallisation of membrane proteins mediated by antibody fragments. Curr Opin Struct Biol, 12:503-508.

Hunte, C., Palsdottir, H., and Trumpower, B.L. (2003) Protonmotive pathways and mechanisms in the cytochrome bc1 complex. FEBS Lett, 545:39-46.

Iwaki, M., Giotta, L., Akinsiku, A.O., Schägger, H., Fisher, N., Breton, J., and Rich, P.R. (2003) Redox-induced transitions in bovine cytochrome bc1 complex studied by perfusion-induced ATR-FTIR spectroscopy. Biochemistry, 42:11109-11119.

Iwata, S., Ostermeier, C., Ludwig, B., and Michel, H. (1995) Structure at 2.8 A resolution of cytochrome c oxidase from Paracoccus denitrificans. Nature, 376:660-669.

Iwata, S., Saynovits, M., Link, T.A., and Michel, H. (1996) Structure of a water soluble fragment of the 'Rieske' iron-sulfur protein of the bovine heart mitochondrial cytochrome bc1 complex determined by MAD phasing at 1.5 A resolution. Structure, 4:567-579.

Iwata, S., Lee, J.W., Okada, K., Lee, J.K., Iwata, M., Rasmussen, B., Link, T.A., Ramaswamy, S, and Jap, B.K. (1998) Complete structure of the 11-subunit bovine mitochondrial cytochrome bc1 complex. Science, 281:64-71.

Izrailev, S., Crofts, A.R., Berry, E.A., and Schulten, K. (1999) Steered molecular dynamics simulation of the Rieske subunit motion in the cytochrome bc1 complex. Biophys J, 77:1753-1768.

Janssen, M.J., Koorengevel, M.C., de Kruijff, B., and de Kroon, A.I. (2000) The phosphatidylcholine to phosphatidylethanolamine ratio of Saccharomyces cerevisiae varies with the growth phase. Yeast, 16:641-650.

Jiang, F., Ryan, M.T., Schlame, M., Zhao, M., Gu, Z., Klingenberg, M., Pfanner, N., and Greenberg, M.L. (2000) Absence of cardiolipin in the crd1 null mutant results in decreased mitochondrial membrane potential and reduced mitochondrial function. J Biol Chem, 275:22387-22394.

Jiang, L. and Lai, L. (2002) CH···O hydrogen bonds at protein-protein interfaces. J Biol Chem, 277:37732-37740.

Jiang,Y., Lee,A., Chen,J., Ruta,V., Cadene,M., Chait,B.T., and MacKinnon,R. (2003) X-ray structure of a voltage-dependent K+ channel. Nature, 423:33-41.

Jones, T. A., Zou, J. Y., Cowan, S. W., and Kjeldgaard, M. (1991) Improved methods for building protein models in electron density maps and the location of errors in these models. Acta Cryst. A 47 (Pt 2), 110-119.

Joseph-Horne, T., Hollomon, D.W., and Wood, P.M. (2001) Fungal respiration: a fusion of standard and alternative components.Biochim Biophys Acta. 1504:179-95

Junemann, S., Heathcote, P., and Rich, P.R. (1998) On the mechanism of quinol oxidation in the bc1 complex. J Biol Chem, 273:21603-21607.

Katona, G., Andreasson, U., Landau, E.M., Andreasson, L.E., and Neutze, R. (2003) Lipidic cubic phase crystal structure of the photosynthetic reaction centre from Rhodobacter sphaeroides at 2.35A resolution. J Mol Biol, 331:681-692.

Keilin, D (1925) On cytochrome, a respiratory pigment common to animal, yeast, and higher plants. Proc. Roy. Soc., 98, 312-339.

Kessl, J.J., Lange, B.B., Merbitz-Zahradnik, T., Zwicker,K., Hill,P., Meunier,B., Palsdottir, H., Hunte, C., Meshnick, S., and Trumpower, B.L. (2003) Molecular basis for atovaquone binding to the cytochrome bc1 complex. J Biol Chem, 278:31312-31318.

Kessl, J.J., Hill, P., Lange, B.B., Meshnick, S.R., Meunier, B., and Trumpower, B.L. (2004) Molecular basis for atovaquone resistance in Pneumocystis jirovecii modeled in the cytochrome bc1 complex of Saccharomyces cerevisiae. J Biol Chem, 279:2817-2824.

Kim, C.H. and King, T.E. (1983) A mitochondrial protein essential for the formation of the cytochrome c1-c complex. Isolation, purification, and properties. J Biol Chem. 258:13543-51.

Kim, H., Xia,D., Yu, C.A., Xia, J.Z., Kachurin, A.M., Zhang, L., Yu, L., and Deisenhofer, J. (1998) Inhibitor binding changes domain mobility in the iron-sulfur protein of the mitochondrial bc1 complex from bovine heart. Proc Natl Acad Sci U S A, 95:8026-8033.

Kleymann, G., Ostermeier, C., Ludwig, B., Skerra, A., and Michel, H. (1995) Engineered Fv fragments as a tool for the one-step purification of integral multisubunit membrane protein complexes. Biotechnology (N Y), 13:155-160.

Kleywegt, G. J., and Jones, T. A. (1997) Software for handling macromolecular envelopes. Methods Enzymol. 277, 208–230

Korsinczky, M., Chen, N., Kotecka, B., Saul, A., Rieckmann, K., and Cheng, Q. (2000) Mutations in Plasmodium falciparum cytochrome b that are associated with atovaquone resistance are located at a putative drug-binding site. Antimicrob Agents Chemother, 44:2100-2108.

Kraulis, P.J. (1991) Molscript: a program to produce both detailed and schematic plots of protein structures. J Appl Cryst: 24:946-950.

Kunze, B., Kemmer, T., Hofle, G., and Reichenbach, H. (1984) Stigmatellin, a new antibiotic from Stigmatella aurantiaca (Myxobacterales). I. Production, physico-chemical and biological properties. J Antibiot (Tokyo), 37:454-461.

Kurisu, G., Zhang, H., Smith, J.L., and Cramer, W.A. (2003) Structure of the cytochrome b6f complex of oxygenic photosynthesis: tuning the cavity. Science, 302:1009-1014.

Lancaster, C.R.D. and Michel, H. (1997) The coupling of light-induced electron transfer and proton uptake as derived from crystal structures of reaction centres from Rhodopseudomonas viridis modified at the binding site of the secondary quinone, QB. Structure, 5:1339-1359.

Lange, C., Nett, J.H., Trumpower, B.L., and Hunte, C. (2001) Specific roles of protein-phospholipid interactions in the yeast cytochrome bc1 complex structure. EMBO J, 20:6591-6600.

Lange, C. and Hunte, C. (2002) Crystal structure of the yeast cytochrome bc1 complex with its bound substrate cytochrome c. Proc Natl Acad Sci U S A, 99:2800-2805.

Laskowski, R.A., MacArthur, M.W., Moss, D.S., and Thornton, J.M. (1993) PROCHECK: a program to check the stereochemical quality of protein structures. J. Appl.Cryst. 26, 283-291

Le Coutre, J., Tittor, J., Oesterhelt, D., and Gerwert, K. (1995) Experimental evidence for hydrogen-bonded network proton transfer in bacteriorhodopsin shown by Fourier-transform infrared spectroscopy using azide as catalyst. Proc Natl Acad Sci U S A 92:4962-6.

Lee, A.G. (2003) Lipid-protein interactions in biological membranes: a structural perspective. Biochim Biophys Acta, 1612:1-40.

Lee, S.Y., Hunte, C., Malaney, S., and Robinson, B.H. (2001) The N-terminus of the Qcr7 protein of the cytochrome bc1 complex in S. cerevisiae may be involved in facilitating stability of the subcomplex with the Qcr8 protein and cytochrome b. Arch Biochem Biophys, 393:215-221.

Lewis, B.A. and Engelman, D.M. (1983) Lipid bilayer thickness varies linearly with acyl chain length in fluid phosphatidylcholine vesicles. J Mol Biol, 166:211-217.

Link, T.A., Hagen, W.R., Pierik, A.J., Assmann, C., and von Jagow, G. (1992) Determination of the redox properties of the Rieske [2Fe-2S] cluster of bovine heart bc1 complex by direct electrochemistry of a water-soluble fragment. Eur J Biochem, 208:685-691.

Link, T.A. (1997) The role of the 'Rieske' iron sulfur protein in the hydroquinone oxidation (Q(P)) site of the cytochrome bc1 complex. The 'proton-gated affinity change' mechanism. FEBS Lett, 412:257-264.

Ljungdahl, P.O., Pennoyer, J.D., Robertson, D.E., and Trumpower, B.L. (1987) Purification of highly active cytochrome bc1 complexes from phylogenetically diverse species by a single chromatographic procedure. Biochim Biophys Acta, 891:227-241.

Ljungdahl, P.O., Beckmann, J.D., and Trumpower, B.L. (1989) Mutational analysis of the mitochondrial Rieske iron-sulfur protein of Saccharomyces cerevisiae. II. Biochemical characterization of temperature-sensitive RIP1- mutations. J Biol Chem, 264:3723-3731.

Lo Conte, L., Chothia, C., and Janin, J. (1999) The atomic structure of protein-protein recognition sites. J Mol Biol. 285:2177-2198.

Luecke, H., Schobert, B.,Richter, H.T.,Cartailler, J.P., and Lanyi, J.K. (1999) Structure of bacteriorhodopsin at 1.55 A resolution. J Mol Biol. 291:899-911.

Maarse, A.C., de Haan, M., Schoppink, P.J., Berden, J.A., and Grivell, L.A. (1988) Inactivation of the gene encoding the 11-kDa subunit VIII of the ubiquinol-cytochrome-c oxidoreductase in Saccharomyces cerevisiae. Eur J Biochem, 172:179-184.

Margulis, L. (1981) Symbiosis in Cell Evolution, 1st Edition. Freeman, New York.

Marres, C.A., de Vries, S., and Grivell, L.A. (1991) Isolation and inactivation of the nuclear gene encoding the rotenone-insensitive internal NADH: ubiquinone oxidoreductase of mitochondria from Saccharomyces cerevisiae. Eur J Biochem. 195:857-62.

Matsuura, K., Bowyer, J.R., Ohnishi, T., and Dutton, P.L. (1983) Inhibition of electron transfer by 3-alkyl-2-hydroxy-1,4-naphthoquinones in the ubiquinol-cytochrome c oxidoreductases of Rhodopseudomonas sphaeroides and mammalian mitochondria. Interaction with a ubiquinone-binding site and the Rieske iron-sulfur cluster. J Biol Chem, 258:1571-1579.

McDonald, I. K. and Thornton, J. M. (1994) Satisfying hydrogen bonding potential in proteins. J. Mol. Biol. 238, 777-793

Merbitz-Zahradnik, T., Zwicker, K., Nett, J.H., Link, T.A., and Trumpower, B.L. (2003) Elimination of the disulfide bridge in the Rieske iron-sulfur protein allows assembly of the [2Fe-2S] cluster into the Rieske protein but damages the ubiquinol oxidation site in the cytochrome bc1 complex. Biochemistry, 42:13637-13645.

Merritt, E.A., and Murphy, M.E.P. Raster 3D Version 2.0. A program for photorealistic molecular graphics. Acta Cryst D 1994: 50:869-873.

Michel, H. (1983) Crystallization of membrane proteins. Trends Biochem Sci 8: 56–59.

Mitchell, P. (1961) Coupling of phosphorylation to electron and hydrogen transfer by a chemi-osmotic type of mechanism. Naturwissenschaften 191:144-8.

Mitchell, P. (1975) The protonmotive Q cycle: a general formulation. FEBS Lett, 59:137-139.

Mitchell,P. (1976) Possible molecular mechanisms of the protonmotive function of cytochrome systems. Journal of Theoretical Biology, 62:327-367.

Montoya, G., Kaat, K., Rodgers, S., Nitschke, W., and Sinning, I. (1999) The cytochrome bc1 complex from Rhodovulum sulfidophilum is a dimer with six quinones per monomer and an additional 6-kDa component. Eur J Biochem, 259:709-718.

Mulkidjanian, A.Y. (1999) Conformationally controlled pK-switching in membrane proteins: one more mechanism specific to the enzyme catalysis? FEBS Lett, 463:199-204.

Muller, F.L., Roberts, A.G., Bowman, M.K., and Kramer, D.M. (2003) Architecture of the Qo site of the cytochrome bc1 complex probed by superoxide production. Biochemistry, 42:6493-6499.

Nagle, J.F. and Morowitz, H.J. (1978) Molecular mechanisms for proton transport in membranes. Proc. Natl. Acad. Sci. 75:298-302.

Nett, J.H., Hunte, C., and Trumpower, B.L. (2000) Changes to the length of the flexible linker region of the Rieske protein impair the interaction of ubiquinol with the cytochrome bc1 complex. Eur J Biochem, 267:5777-5782.

Obungu, V.H., Wang, Y., and Beattie, D.S. (1998) The role of charged amino acids in the alpha1-beta4 loop of the iron-sulfur protein of the cytochrome bc1 complex of yeast mitochondria. J Biol Chem, 273:11917-11922.

Obungu, V.H., Wang, Y., Amyot, S.M., Gocke, C.B., and Beattie, D.S. (2000) Mutations in the tether region of the iron-sulfur protein affect the activity and assembly of the cytochrome bc1 complex of yeast mitochondria. Biochim Biophys Acta, 1457:36-44.

Ostermeier, C., Iwata, S., Ludwig, B., and Michel, H. (1995) Fv fragment-mediated crystallization of the membrane protein bacterial cytochrome c oxidase. Nat Struct Biol, 2:842-846.

Ostermeier, C., Harrenga, A., Ermler, U., and Michel, H. (1997) Structure at 2.7 A resolution of the Paracoccus denitrificans two-subunit cytochrome c oxidase complexed with an antibody FV fragment. Proc Natl Acad Sci U S A, 94:10547-10553.

Osyczka, A., Moser, C.C., Daldal, F., and Dutton, P.L. (2004) Reversible redox energy coupling in electron transfer chains. Nature, 427:607-612.

Otwinowski, Z., and Minor, W. (1997) Processing of X-ray Diffraction Data Collected in Oscillation Mode. Methods Enzymol. 276, 307–326.

Oudshoorn, P., van Steeg, H., Swinkels, B.W., Schoppink, P., and Grivell, L.A. (1987) Subunit II of yeast QH2:cytochrome-c oxidoreductase. Nucleotide sequence of the gene and features of the protein. Eur J Biochem, 163:97-103.

Palade, G.E. (1952) The fine structure of mitochondria. Anat Rec. 114:427-51.

Palsdottir, H., Lojero, C.G., Trumpower, B.L., and Hunte, C. (2003) Structure of the yeast cytochrome bc1 complex with a hydroxyquinone anion Qo site inhibitor bound. J Biol Chem, 278:31303-31311.

Palsdottir, H. and Hunte, C. (2003) Purification of the cytochrome bc1 complex from yeast. In: Membrane Protein Purification and Crystallization-A practical guide. C. Hunte, G. von Jagow, and H. Schägger, eds. Academic Press, Elsevier Science (USA), pp. 191-203.

Palsdottir, H. and Hunte, C. Lipids in membrane protein structures in special issue on "Lipid-Protein Interactions", Biochem Biophys Acta (in press).

Peng, G., Fritzsch, G., Zickermann, V., Schägger, H., Mentele, R., Lottspeich, F., Bostina, M., Radermacher, M., Huber, R., Stetter, K.O., and Michel, H. (2003) Isolation, characterization and electron microscopic single particle analysis of the NADH:ubiquinone oxidoreductase (complex I) from the hyperthermophilic eubacterium Aquifex aeolicus. Biochemistry 42:3032-9.

Pfeiffer, K., Gohil, V., Stuart, R.A., Hunte, C., Brandt, U., Greenberg, M.L., and Schägger, H. (2003) Cardiolipin stabilizes respiratory chain supercomplexes. J Biol Chem, 278:52873-52880.

Phillips, J.D., Graham, L.A., and Trumpower, B.L. (1993) Subunit 9 of the Saccharomyces cerevisiae cytochrome bc1 complex is required for insertion of EPR-detectable iron-sulfur cluster into the Rieske iron-sulfur protein. J Biol Chem, 268:11727-11736.

Riccio, P., Schägger, H., Engel, W.D., and von Jagow, G. (1977) bc1-Complex from beef heart. One-step purification by hydroxyapatite chromatography in Triton X-100, polypeptide pattern and respiratory chain characteristics. Biochim Biophys Acta, 459:250-262.

Rich, P.R.(1984) Electron transfer through the isolated mitochondrial cytochrome b-c1 complex. Biochim. Biophys. Acta 768, 53–79.

Rich, P.R. and Harper, R. (1990) Partition coefficients of quinones and hydroquinones and their relation to biochemical reactivity. FEBS Lett, 269:139-144.

Rich, P.R. (2004) The quinone chemistry of bc complexes. Biochim Biophys Acta 1658:165-71.

Rieske, J.S. (1976) Composition, structure, and function of complex III of the respiratory chain. Biochim Biophys Acta, 456:195-247.

Riistama, S., Hummer, G., Puustinen, A., Dyer, R.B., Woodruff, W.H., and Wikstrom, M. (1997) Bound water in the proton translocation mechanism of the haem-copper oxidases.FEBS Lett. 414:275-80.

Ritter, M., Palsdottir, H., Abe, M., Mantele, W., Hunte, C., Miyoshi, H., and Hellwig, P. (2004) Direct Evidence for the Interaction of Stigmatellin with a Protonated Acidic Group in the bc1 Complex from Saccharomyces cerevisiae As Monitored by FTIR Difference Spectroscopy and (13)C Specific Labeling. Biochemistry, 43:8439-8446.

Ritter, M., Anderka, O., Ludwig, B., Mantele, W., and Hellwig, P. (2003) Electrochemical and FTIR spectroscopic characterization of the cytochrome bc1 complex from Paracoccus denitrificans: evidence for protonation reactions coupled to quinone binding. Biochemistry, 42:12391-12399.

Roth, M., Lewit-Bentley, A., Michel, H., Deisenhofer, J., Huber, R., and Oesterhelt, (1989) Detergent structure in crystals of a bacterial photosynthetic reaction centre. Nature 340: 659–662.

Saint-Georges, Y., Bonnefoy, N., di Rago, J.P., Chiron, S., and Dujardin, G. (2002) A pathogenic cytochrome b mutation reveals new interactions between subunits of the mitochondrial bc1 complex. J Biol Chem, 277:49397-49402.

Samoilova, R.I., Kolling, D., Uzawa, T., Iwasaki, T., Crofts, A.R., and Dikanov, S.A. (2002) The interaction of the Rieske iron-sulfur protein with occupants of the Qo-site of the bc1 complex, probed by electron spin echo envelope modulation. J Biol Chem, 277:4605-4608.

Saraste, M. (1999) Oxidative phosphorylation at the fin de siecle. Science, 283:1488-1493.

Saribas, A.S., Valkova-Valchanova, M., Tokito, M.K., Zhang, Z., Berry, E.A., and Daldal, F. (1998) Interactions between the cytochrome b, cytochrome c1, and Fe-S protein subunits at the ubihydroquinone oxidation site of the bc1 complex of Rhodobacter capsulatus. Biochemistry, 37:8105-8114.

Sarkhel, S. and Desiraju, G.R. (2004) N-H···O, O-H···O, and C-H···O hydrogen bonds in protein-ligand complexes: strong and weak interactions in molecular recognition. Proteins, 54:247-259.

Schägger, H., Hagen, T., Roth, B., Brandt, U., Link, T.A., and von Jagow, G. (1990) Phospholipid specificity of bovine heart bc1 complex. Eur J Biochem, 190:123-130.

Schägger, H. and Pfeiffer, K. (2000) Supercomplexes in the respiratory chains of yeast and mammalian mitochondria. EMBO J, 19:1777-1783.

Schägger, H. (2002) Respiratory chain supercomplexes of mitochondria and bacteria. Biochim Biophys Acta, 1555:154-159.

Schlame, M., Rua, D., and Greenberg, M.L. (2000) The biosynthesis and functional role of cardiolipin. Prog Lipid Res, 39:257-288.

Schmidt, T.G. and Skerra (1994). One-step purification of bacterially produced porteins by means of the Strep tag and immobilized recombinant core streptavidin. J. Chromatogr. 676, 337-345.

Schneiter, R., Brugger, B., Sandhoff, R., Zellnig, G., Leber, A., Lampl, M., Athenstaedt, K., Hrastnik, C., Eder, S., Daum, G., Paltauf, F., Wieland, F.T., and Kohlwein, S.D. (1999) Electrospray ionization tandem mass spectrometry (ESI-MS/MS) analysis of the lipid molecular species composition of yeast subcellular membranes reveals acyl chain-based sorting/remodeling of distinct molecular species en route to the plasma membrane. J Cell Biol, 146:741-754.

Schoepp, B., Brugna, M., Riedel, A., Nitschke, W., and Kramer, D.M. (1999) The Qo-site inhibitor DBMIB favours the proximal position of the chloroplast Rieske protein and induces a pK-shift of the redox-linked proton. FEBS Lett, 450:245-250.

Schopf, J.W. (1994) The early evolution of life: solution to Darwin's dilemma. Trends Ecol Evol. 9:375-7.

Schoppink, P.J., Berden, J.A., and Grivell, L.A. (1989) Inactivation of the gene encoding the 14-kDa subunit VII of yeast ubiquinol. Cytochrome c oxidoreductase and analysis of the resulting mutant. Eur J Biochem, 181:475-483.

Schultz, B.E. and Chan, S.I. (2001) Structures and proton-pumping strategies of mitochondrial respiratory enzymes. Annu Rev Biophys Biomol Struct. 30:23-65.

Schutz, M., Schoepp, C., Lojou, E., Woodstra, M., Lexa, D., Tron, P., Dolla, A., Durand, M.C., Stetter, K.O., and Baymann, F. (2003) The naphthoquinol oxidizing cytochrome bc1 complex of the hyperthermophilic knallgasbacterium Aquifex aeolicus: properties and phylogenetic relationships. Biochemistry, 42:10800-10808.

Sidhu, A. and Beattie, D.S. (1982) Purification and polypeptide characterization of complex III from yeast mitochondria. J Biol Chem, 257:7879-7886.

Siedow, J.N., Power, S., de la Rosa, F.F. and Palmer, G. (1978) The preparation and characterization of highly purified, enzymically active complex III from baker's yeast. J Biol Chem, 253:2392-2399.

Small, W.C. and McAlister-Henn, L. (1998) Identification of a cytosolically directed NADH dehydrogenase in mitochondria of Saccharomyces cerevisiae. J Bacteriol. 180:4051-5.

Smith, P.K., Krohn, R.I., Hermanson, G.T., Mallia, A.K., Gartner, F. H., Provenzano, M.D., Fujimoto, E.K., Goeke, N.M., Olson, B.J., and Klenk, D.C. (1985). Measurement of protein using bicinchoninic acid. Anal. Biochem. 150, 76-85.

Snyder, C.H., Merbitz, Z., Link, T.A., and Trumpower, B.L. (1999) Role of the Rieske iron-sulfur protein midpoint potential in the protonmotive Q-cycle mechanism of the cytochrome bc1 complex. J Bioenerg Biomembr, 31:235-242.

Snyder, C.H., Gutierrez-Cirlos, E.B., and Trumpower,B.L. (2000) Evidence for a concerted mechanism of ubiquinol oxidation by the cytochrome bc1 complex. J Biol Chem, 275:13535-13541.

Sperka-Gottlieb, C.D., Hermetter, A., Paltauf, F., and Daum,G. (1988) Lipid topology and physical properties of the outer mitochondrial membrane of the yeast, Saccharomyces cerevisiae. Biochim Biophys Acta, 946:227-234.

Srivastava, I.K., Morrisey, J.M., Darrouzet, E., Daldal, F., and Vaidya, A.B. (1999) Resistance mutations reveal the atovaquone-binding domain of cytochrome b in malaria parasites. Mol Microbiol, 33:704-711.

Stroebel, D., Choquet, Y., Popot, J.L., and Picot, D. (2003) An atypical haem in the cytochrome b(6)f complex. Nature, 426:413-418.

Sun, J. and Trumpower, B.L. (2003) Superoxide anion generation by the cytochrome bc1 complex. Arch Biochem Biophys, 419:198-206.

Syafruddin, D., Siregar, J.E., and Marzuki, S. (1999) Mutations in the cytochrome b gene of Plasmodium berghei conferring resistance to atovaquone. Mol Biochem Parasitol, 104:185-194.

Tandori, J., Sebban, P., Michel, H., and Baciou, L. (1999) In Rhodobacter sphaeroides reaction centers, mutation of proline L209 to aromatic residues in the vicinity of a water channel alters the dynamic coupling between electron and proton transfer processes. Biochemistry, 38:13179-13187.

Thierbach, G., Kunze B., Reichenbach, H. and Höfle, G. (1984) The mode of action of stigmatellin, a new inhibitor of the cytochrome b-c_1 segment of the respiratory chain. Biochim. Biophys. Acta 765, 227-235.

Tielens, A.G., Rotte, C., van Hellemond, J.J., and Martin,W. (2002) Mitochondria as we don't know them. Trends Biochem Sci, 27:564-572.

Trumpower, B.L. and Haggerty, J.G. (1980) Inhibition of electron transfer in the cytochrome b-c, segment of the mitochondrial respiratory chain by a synthetic analogue of ubiquinone. J Bioenerg Biomembr, 12:151-164.

Trumpower, B.L. (1990) The protonmotive Q cycle. Energy transduction by coupling of proton translocation to electron transfer by the cytochrome bc1 complex. J Biol Chem, 265:11409-11412.

Trumpower, B.L. (2002) A concerted, alternating sites mechanism of ubiquinol oxidation by the dimeric cytochrome bc1 complex. Biochim Biophys Acta, 1555:166-173.

Tsai, A.L., Kauten, R., and Palmer, G. (1985) The interaction of yeast Complex III with some respiratory inhibitors. Biochim Biophys Acta, 806:418-426.

Tuller, G., Nemec, T., Hrastnik, C., and Daum, G. (1999) Lipid composition of subcellular membranes of an FY1679-derived haploid yeast wild-type strain grown on different carbon sources. Yeast, 15:1555-1564.

Tzagoloff, A., Wu, M.A., and Crivellone, M. (1986) Assembly of the mitochondrial membrane system. Characterization of COR1, the structural gene for the 44-kilodalton core protein of yeast coenzyme QH2-cytochrome c reductase. J Biol Chem, 261:17163-17169.

Ugulava, N.B. and Crofts, A.R. (1998) CD-monitored redox titration of the Rieske Fe-S protein of Rhodobacter sphaeroides: pH dependence of the midpoint potential in isolated bc1 complex and in membranes. FEBS Lett, 440:409-413.

Ullmann, G.M., Noodleman, L., and Case, D.A. (2002) Density functional calculation of p K(a) values and redox potentials in the bovine Rieske iron-sulfur protein. J Biol Inorg Chem, 7:632-639.

van Klompenburg, W., Nilsson, I., von Heijne, G.,and de Kruijff, B. (1997) Anionic phospholipids are determinants of membrane protein topology. EMBO J 16:4261-4266.

Vanneste, W.H. (1966). Molecular proportion of the fixed cytochrome components of the respiratory chain of Keilin-Hartree particles and beef heart mitochondria. Biochim. Biophys. Acta 113, 175-178.

von Heijne, G. (1986) The Distribution of Positively Charged Residues in Bacterial Inner Membrane Proteins Correlates With the Trans-Membrane Topology. EMBO J. 5, 3021-3027

von Heijne, G. and Gavel, Y. (1988) Topogenic signals in integral membrane proteins. Eur J Biochem, 174:671-678.

von Jagow, G. and Link, T.A. (1986) Use of specific inhibitors on the mitochondrial bc1 complex. Methods Enzymol, 126:253-271.

von Jagow, G. and Ohnishi, T. (1985) The chromone inhibitor stigmatellin--binding to the ubiquinol oxidation center at the C-side of the mitochondrial membrane. FEBS Lett, 185:311-315.

Voss, S. and Skerra, A. (1997) Mutagenesis of a flexible loop in streptavidin leads to higher affinity for the Strep-tag II peptide and improved performance in recombinant protein purification. Prot. Engng. 10, 975-982.

Wallace, A. C., Laskowski, R. A., and Thornton, J. M. (1995) LIGPLOT: a program to generate schematic diagrams of protein-ligand interactions. Protein Eng. 8, 127-134

Weiss, H., Leonard, K., and Neupert, W. (1990) Puzzling subunits of mitochondrial cytochrome reductase. Trends Biochem Sci, 15:178-180.

Weiss, H., Linke, P., Haiker, H., and Leonard, K. (1987) Structure and function of the mitochondrial ubiquinol: cytochrome c reductase and NADH: ubiquinone reductase. Biochem Soc Trans, 15:100-102.

Wikstrom, M.K. and Berden, J.A. (1972) Oxidoreduction of cytochrome b in the presence of antimycin. Biochim Biophys Acta, 283:403-420.

Xia, D., Yu, C.A., Kim, H., Xia, J.Z., Kachurin, A.M., Zhang, L., Yu, L., and Deisenhofer,J. (1997) Crystal structure of the cytochrome bc1 complex from bovine heart mitochondria. Science, 277:60-66.

Xiao, K., Liu, X., Yu, C.A., and Yu, L. (2004) The extra fragment of the iron-sulfur protein (residues 96-107) of Rhodobacter sphaeroides cytochrome bc1 complex is required for protein stability. Biochemistry, 43:1488-1495.

Yan, J. and Cramer, W.A. (2003) Functional insensitivity of the cytochrome b6f complex to structure changes in the hinge region of the Rieske iron-sulfur protein. J Biol Chem, 278:20925-20933.

Yang, M. and Trumpower, B.L. (1994) Deletion of QCR6, the gene encoding subunit six of the mitochondrial cytochrome bc1 complex, blocks maturation of cytochrome c1, and causes temperature-sensitive petite growth in Saccharomyces cerevisiae. J Biol Chem, 269:1270-1275.

Yu, C.A., Yu, L., and King, T.E. (1974) Soluble cytochrome b-c1 complex and the reconstitution of succinate-cytochrome c reductase. J Biol Chem, 249:4905-4910.

Yu, C.A. and Yu, L. (1980) Structural role of phospholipids in ubiquinol-cytochrome c reductase. Biochemistry, 19:5715-5720.

Yu, C.A., Gu, L.Q., Lin, Y.Z., and Yu, L. (1985) Effect of alkyl side chain variation on the electron-transfer activity of ubiquinone derivatives. Biochemistry, 24:3897-3902..

Zara, V., Palmisano, I., Conte, L., and Trumpower, B.L. (2004) Further insights into the assembly of the yeast cytochrome bc1 complex based on analysis of single and double deletion mutants lacking supernumerary subunits and cytochrome b. Eur J Biochem, 271:1209-1218.

Zhang, H., Kurisu, G., Smith, J.L., and Cramer,W.A. (2003) A defined protein-detergent-lipid complex for crystallization of integral membrane proteins: The cytochrome b6f complex of oxygenic photosynthesis. Proc Natl Acad Sci U S A, 100:5160-5163.

Zhang, L., Snyder, C., Trumpower, B.L., Yu, L., and Yu, C.A. (1999) Determination of the binding rate constants of stigmatellin and UHDBT to bovine cytochrome bc1 complex by cytochrome c1 oxidation. FEBS Lett, 460:349-352.

Zhang, L., Tai, C.H., Yu, L., and Yu, C.A. (2000) pH-induced intramolecular electron transfer between the iron-sulfur protein and cytochrome c1 in bovine cytochrome bc1 complex. J Biol Chem, 275:7656-7661.

Zhang, Z., Huang, L., Shulmeister, V.M., Chi, Y.I., Kim, K.K., Hung, L.W., Crofts, A.R., Berry, E.A., and Kim, S.H. (1998) Electron transfer by domain movement in cytochrome bc1. Nature, 392:677-684.

Zhou, Y., Morais, C., Kaufman, A., and MacKinnon, R. (2001) Chemistry of ion coordination and hydration revealed by a K+ channel-Fab complex at 2.0 A resolution. Nature, 414:43-48.

Zickermann, V., Bostina, M., Hunte, C., Ruiz, T., Radermacher, M., and Brandt, U. (2003) Functional implications from an unexpected position of the 49-kDa subunit of NADH:ubiquinone oxidoreductase. J Biol Chem. 278:29072-8.

Zinser, E., Sperka, G., Fasch, E.V., Kohlwein, S.D., Paltauf, F., and Daum, G. (1991) Phospholipid synthesis and lipid composition of subcellular membranes in the unicellular eukaryote Saccharomyces cerevisiae. J Bacteriol, 173:2026-2034.

Zu, Y., Couture, M.M., Kolling, D.R., Crofts, A.R., Eltis, L.D., Fee, J.A., and Hirst, J. (2003) Reduction potentials of Rieske clusters: importance of the coupling between oxidation state and histidine protonation state. Biochemistry, 42:12400-12408.

ABBREVIATIONS

μM	micromolar
A	absorption
AC	ADP/ATP carrier
ATP	adenosine triphosphate
AU	absolute units
B6F	cytochrome b_6f complex
BC1	cytochrome bc_1 complex
BCA	bicinichoninic acid
BCIP	bromochloroindolyl phosphate
b_H	high potential *b*-type heme
b_L	low potential *b*-type heme
BR	bacteriorhodopsin
BSA	bovine serum albumin
CDR	complementarity determining region
CL	cardiolipin
Cobp	cytochrome *b*
CoQ	coenzyme Q
Cor1p	core 1 protein
COX	cytochrome *c* oxidase
CV	cyclic voltammetry
Cyt1p	cytochrome c_1
ddH20	doubly distilled water
DDM	*n*-dodecyl-β-D-maltopyranoside
DEAE	diethylaminoethyl
DG	phosphatidylglycerophospholipid
DMSO	dimethylsulfoxide
DNA	deoxyribonucleic acid
E.	*Escherichiae*
EDTA	ethylene diamine tetraacetic acid
EPR	electron paramagnetic resonance
ESR	electron spin resonance
Fdh-N	formate dehydrogenase N
FTIR	Fourier transform infrared
Fv	antibody fragment, variable
FvH	Fv fragment heavy chain
FvL	Fv fragment light chain
g	gram
IMM	inner mitochondrial membrane
IMS	intermembrane space
kDa	kilodalton
kg	kilogram
Mr	molecular mass
nm	nanometer
NMR	nuclear magnetic resonance
O/N	overnight
OMM	outer mitochondrial membrane
P.	*Paracoccus*
PA	phosphatidic acid

PAGE	polyacrylamide gel electrophoresis
PC	phosphatidyl choline
PDB	protein databank
PE	phosphatidyl ethanolamine
PG	phosphatidyl glycerol
PI	phosphatidyl inositol
PMF	protonmotive force
PS	phosphatidylserine
PSI	photosystem I
Q	quinone
QCR10p	subunit 10
QCR2p	core 2 protein
QCR6p	subunit 6, hinge protein
QCR7p	subunit 7
QCR8p	subunit 8
QCR9p	subunit 9
QH_2	quinol
Q_i site	quinone reduction site
Q_o site	quinol oxidation site
R.	*Rhodobacter*
RC	reaction center
Rip1p	Rieske
RMSD	root mean square deviation
RPM	rotations per minute
RT	room temperature
s	seconds
S.	*Saccharomyces*
SEC	size exclusion chromatography
SHE‘	standard hydrogen electrode (for pH 7)
SL	sulfolipid
SQR	Succinate:Quinone Oxidoreductase
UM	*n*-undecyl-β-D-maltopyranoside
UQ6	coenzyme Q_6
UST	undecylstigmatellin
UV/vis	ultraviolet/visible
w/v	weight per volume (g/100 ml)
WT	wildtype
ε	extinction coefficient

APPENDIX 1

A.1. Multiple sequence alignment of cytochrome *b*

Multiple amino acid sequence alignment was performed as described in *section 4.14*. Careful analysis of regions of homology provided the necessary fundament for discussing cross-species structural differences. The sequence-based structural differences were discussed with respect to the binding behavior of ligands targeted to the active site.

A.1.1. Sequence alignment of mitochondrial, bacterial and photosynthetic enzymes. *The mitochondrial (H. sapiens, B. taurus, G. gallus, S. cerevisiae, P. jiroveci, P. berghei, P. falciparum) and bacterial (P. denitrificans, R. sphaeroides, R. capsulatus) cytochrome b were aligned with cytochrome b_6 and subunit IV (the first 10 amino acids underlined) from cyanobacteria (M. laminosus) and thylakoids of alga (C. reinhardtii).*

```
H.sapiens            1 --------------MTPMRKINPLMKLINHSFIDLPTPSNISAWWNFGSLLGACLILQIT
B.taurus             1 --------------MTNIRKSHPLMKIVNNAFIDLPAPSNISSWWNFGSLLGICLILQIL
G.gallus             1 -------------MAPNIRKSHPLLKMINNSLIDLPAPSNISAWWNFGSLLAVCLMTQIL
S.cerevisiae         1 ---------------MAFRKSNVYLSLVNSYIIDSPQPSSINYWWNMGSLLGLCLVIQIV
P.jiroveci           1 ----------------------------------------YLWNYGSLSGLCLIIQII
P.denitrificans      1 MAGIPHDHYEPKTGFERWLHRRLPIVSLVYDTLMIPTPKNLNWWWIWGIVLAFCLVLQIA
R.sphaeroides        1 -SGIPHDHYEPRTGIEKWLHSRLPIVALAYDTIMIPTPRNLNWMWIWGVVLAFCLVLQIV
R.capsulatus         1 -SGIPHDHYEPKTGIEKWLHDRLPIVGLVYDTIMIPTPKNLNWWWIWGIVLAFTLVLQIV
P.berghei            1 -------------------MNYNSINLVKTHLINYPCPLNINFLWNYGFLLGIIFFIQIL
P.falciparum         1 -------------------MNFYSINLVKAHLINYPCPLNINFLWNYGFLLGIIFFIQII
C.reinhardtii        1 -----------MSKVYDWFEERLEIQAIADDITSKYVPPHVNIFYCIGGITFTCFLVQVA
M.laminosus          1 -----------MANVYDWFQERLEIQALADDVTSKYVPPHVNIFYCLGGITLTCFLIQFA
consensus            1              .  . . .. . ..   .. .. . .........* .........*..

H.sapiens           47 TGLFLAMHYSPDASTAFSSIAHITRDVNYGWIIRYLHANGASMFFICLFLHIGRGLYYGS
B.taurus            47 TGLFLAMHYTSDTTTAFSSVTHICRDVNYGWIIRYMHANGASMFFICLYMHVGRGLYYGS
G.gallus            48 TGLLLAMHYTADTSLAFSSVAHTCRNVQYGWLIRNLHANGASFFFICIFLHIGRGLYYGS
S.cerevisiae        46 TGIFMAMHYSSNIELAFSSVEHIMRDVHNGYILRYLHANGASFFFMVMFMHMAKGLYYGS
P.jiroveci          19 TGVTLAMHYIPSIDLAFLSVEHIMWDVNYGWLIRYIHSNTASFFFLFVYIHIAWGIYYGS
P.denitrificans     61 TGIVLVMHYTPHVDLAFASVEHIMRDVNGGYMLRYLHANGASLFFLAVYIHIFRGLYYGS
R.sphaeroides       60 TGIVLAMHYTPHVDLAFASVEHIMRNVNGGFMLRYLHANGASLFFIAVYLHIFRGLYYGS
R.capsulatus        60 TGIVLAMHYTPHVDLAFASVEHIMRDVNGGWAMRYIHANGASLFFLAVYIHIFRGLYYGS
P.berghei           42 TGVFLASRYSPEISYAYYSIQHILRELWSGWCFRYMHATGASLVFFLTYLHILRGLNYSY
P.falciparum        42 TGVFLASRYTPDVSYAYYSIQHILRELWSGWCFRYMHATGASLVFLLTYLHILRGLNYSY
C.reinhardtii       50 TGFAMTFYYRPTVAEAFASVQYIMTDVNFGWLIRSIHRWSASMMVLMMVLHVFRVYLTGG
M.laminosus         50 TGFAMTFYYKPTVTEAYASVQYIMNEVSFGWLIRSIHRWSASMMVLMMILHVFRVYLTGG
consensus           61 **. ....*.. ...*. *. .........*...*..*...**.... ...*. .......

H.sapiens          107 FLYS--ETWNIGIILLLATMATAFMGYVLPWGQMSFWGATVITNLLSAIPYIGTDLVQWI
B.taurus           107 YTFL--ETWNIGVILLLTVMATAFMGYVLPWGQMSFWGATVITNLLSAIPYIGTNLVEWI
G.gallus           108 YLYK--ETWNTGVILLLTLMATAFVGYVLPWGQMSFWGATVITNLFSAIPYIGHTLVEWA
S.cerevisiae       106 YRSPRVTLWNVGVIIFTLTIATAFLGYCCVYGQMSHWGATVITNLFSAIPFVGNDIVSWL
P.jiroveci          79 YRTPRILVWSIGVVIFLIMIVTAFLGYVLPFGQMSLWGATVITNLMSAIPWIGNDIVNFI
P.denitrificans    121 YKAPREVTWIVGMLIYLMMMGTAFMGYVLPWGQMSFWGATVITGLFGAIPGVGEAIQTWL
R.sphaeroides      120 YKAPREVTWIVGMLIYLAMMATAFMGYVLPWGQMSFWGATVITGLFGAIPGIGHSIQTWL
R.capsulatus       120 YKAPREITWIVGMVIYLLMMGTAFMGYVLPWGQMSFWGATVITGLFGAIPGIGPSIQAWL
P.berghei          102 LYLP--LSWISGLIIFALFIVTAFIGYVLPWGQMSYWGATVITNLLSGIP----SLVIWL
P.falciparum       102 MYLP--LSWISGLILFMIFIVTAFVGYVLPWGQMSYWGATVITNLLSSIP----VAVIWI
C.reinhardtii      110 FKRPRELTWVTGVIMAVCTVSFGVTGYSLPWDQVGYWAVKIVTGVPDAIPGVGGFIVELL
M.laminosus        110 FKKPRELTWISGVILAVITVSFGVTGYSLPWDQVGYWAVKIVSGVPEAIPVVGVLISDLL
consensus          121 .. .. ..*..*.............**.....*...*........ ..** ..  .. ..
```

```
H.sapiens          165 WGGYSVDSPTLTRFFTFH-FILPFIIAALATLHLLFLHETGSNNPLGITSHS--------
B.taurus           165 WGGFSVDKATLTRFFAFH-FILPFIIMAIAMVHLLFLHETGSNNPTGISSDV--------
G.gallus           166 WGGFSVDNPTLTRFFALH-FLLPFAIAGITIIHLTFLHESGSNNPLGISSDS--------
S.cerevisiae       166 WGGFSVSNPTIQRFFALH-YLVPFIIAAMVIMHLMALHIHGSSNPLGITGNL--------
P.jiroveci         139 WGGFSVNHATLNWFFSLH-YLLPFVLLALVVAHLISLHVHGSSNPLGVTGNS--------
P.denitrificans    181 LGGPAVDNPTLNRFFSLH-YLLPFVIAALVVVHIWAFHTTGNNNPTGVEVRRG-------
R.sphaeroides      180 LGGPAVDNATLNRFFSLH-YLLPFVIAALVAIHIWAFHSTGNNNPTGVEVRRT-------
R.capsulatus       180 LGGPAVDNATLNRFFSLH-YLLPFVIAALVAIHIWAFHTTGNNNPTGVEVRRT-------
P.berghei          156 CGGYTVSDPTIKRFFVLH-FILPFVALCIVFIHIFFLHLHGSTNPLGYDTAL--------
P.falciparum       156 CGGYTVSDPTIKRFFVLH-FILPFIGLCIVFIHIFFLHLHGSTNPLGYDTAL--------
C.reinhardtii      170 RGGVGVGQATLTRFYSLHTFVLPLLTAVFMLMHFLMIRKQGISGPLMSVTKKPDLSDPVL
M.laminosus        170 RGGSSVGQATLTRYYSAHTFVLPWLIAVFMLLHFLMIRKQGISGPLMATLKKPDLSDPKL
consensus          181  **..*.. *. .....* ...*.........*.. .. .*...*......

H.sapiens          216 --------DKITFHPYYTIKDALGLLLFLLSLMTLTLFSPDLLGDPDNYTLANPLNTPPH
B.taurus           216 --------DKIPFHPYYTIKDILGALLLILALMLLVLFAPDLLGDPDNYTPANPLNTPPH
G.gallus           217 --------DKIPFHPYYSFKDILGLTLMLTPFLTLALFSPNLLGDPENFTPANPLVTPPH
S.cerevisiae       217 --------DRIPMHSYFIFKDLVTVFLFMLILALFVFYSPNTLGHPDNYIPGNPLVTPAS
P.jiroveci         190 --------DRLPFHPYFSFKDLVTVFLFLLALSFFVFYAPNVLGHSDNYIMANPMATPPS
P.denitrificans    233 -SKEEAKKDTLPFWPYFVIKDLFALAVVLVVFFAIVGFMPNYLGHPDNYIEANPLVTPAH
R.sphaeroides      232 -SKAEAQKDTVPFWPYFIIKDVFALAVVLLVFFAIVGFMPNYLGHPDNYIEANPLSTPAH
R.capsulatus       232 -SKADAEKDTLPFWPYFVIKDLFALALVLLGFFAVVAYMPNYLGHPDNYVQANPLSTPAH
P.berghei          207 ---------KIPFYPNLLSLDVKGFNNILILFLIQSIFGVIPLSHPDNAIVVNTYVTPLQ
P.falciparum       207 ---------KIPFYPNLLSLDVKGFNNVIILFLIQSLFGIIPLSHPDNAIVVNTYVTPSQ
C.reinhardtii      230 KAKLAKGMGHNTYGEPAWPNDLLYMFPVVILGTFACVIGLSVLDPAAMGEPANPFATPLE
M.laminosus        230 RAKLAKGMGHNYYGEPAWPNDLLYVFPVVIMGTFACIVALSVLDPAMVGEPANPFATPLE
consensus          241         ..... .... .*.... ......  ........*....... .*.. ** .

H.sapiens          268 IKPEWYFLFAYTILRSVPN------------------KLGGVLALLLSILILAMIP----
B.taurus           268 IKPEWYFLFAYAILRSIPN------------------KLGGVLALAFSILILALIP----
G.gallus           269 IKPEWYFLFAYAILRSIPN------------------KLGGVLALAASVLILFLIP----
S.cerevisiae       269 IVPEWYLLPFYAILRSIPD------------------KLLGVITMFAAILVLLVLP----
P.jiroveci         242 IVPEWYLLPFYAILWSISN------------------KLFGVVAMLAAILILFVLP----
P.denitrificans    292 IVPEWYFLPFYAILRAFTADVWVVMLVNWLSFGIIDAKFFGVIAMFGAILVMALVP----
R.sphaeroides      291 IVPEWYFLPFYAILRAFTADVWVVQIANFISFGIIDAKFFGVLAMFGAILVMALVP----
R.capsulatus       291 IVPEWYFLPFYAILRAFAADVWVVILVDGLTFGIVDAKFFGVIAMFGAIAVMALAP----
P.berghei          258 IVPEWYFLPFYAMLKTIPS------------------KNAGLVIVIASLQLLFLLAEQRN
P.falciparum       258 IVPEWYFLPFYAMLKTVPS------------------KPAGLVIVLLSLQLLFLLAEQRS
C.reinhardtii      290 ILPEWYFYPVFQILRVVPN------------------KLLGVLLMAAVPAGLITVP----
M.laminosus        290 ILPEWYLYPVFQILRSLPN------------------KLLGVLLMASVPLGLILVP----
consensus          301 *.****.......*.....                  *. *.... . .... ...

H.sapiens          306 ILHMSKQQSMMFRPLSQSLYWLLAADLLILTWIGGQPVSYPFTIIGQVASVLYFTTILIL
B.taurus           306 LLHTSKQRSMMFRPLSQCLFWALVADLLTLTWIGGQPVEHPYITIGQLASVLYFLLILVL
G.gallus           307 FLHKSKQRTMTFRPLSQTLFWLLVANLLILTWIGSQPVEHPFIIIGQMASLSYFTILLIL
S.cerevisiae       307 FTDRSVVRGNTFKVLSKFFFFIFVFNFVLLGQIGACHVEVPYVLMGQIATFIYFAYFLII
P.jiroveci         280 FVDLSWIWGSAFRPLSKFFFWIFVTNFFLLMFVGSQHVEEPFVTLGQYATFFYFFYFLVV
P.denitrificans    348 WLDTSRVRSGQYRPLFKWWFWLLAVDFVVLMWVGAMPAEGIYPYIALAGSAYWFAYFLII
R.sphaeroides      347 WLDTSPVRSGRYRPMFKIYFWLLAADFVILTWVGAQQTTFPYDWISLIASAYWFAYFLVI
R.capsulatus       347 WLDTSKVRSGAYRPKFRMWFWFLVLDFVVLTWVGAMPTEYPYDWISLIASTYWFAYFLVI
P.berghei          300 LTTIIQFKMVFSAREYSVPIIWFMCSFYALLWIGCPLPQDIFILYGRLFIILFFSSGLFS
P.falciparum       300 LTTIIQFKMIFGARDYSVPIIWFMCAFYALLWIGCQLPQDIFILYGRLFIVLFFCSGLFV
C.reinhardtii      328 FIESINKFQNPYRRPIATILFLLGTLVAVWLGIGSTFPIDISLTLGL------------
M.laminosus        328 FIENVNKFQNPFRRPVATTIFLFGTLVTIWLGIGAALPLDKTLTLGLF------------
consensus          361 ... .  ..  ....    .....  .......*..  . ... .. ...  ..   ...

H.sapiens          366 MPTISLIENKMLKWA----------------------
B.taurus           366 MPTAGTIENKLLKW-----------------------
G.gallus           367 FPTIGTLENKMLNY------------------------
S.cerevisiae       367 VPVISTIENVLFYIGRVNK--------------------
P.jiroveci         340 IPLVGII-----------------------------
P.denitrificans    408 LPLLGIIEKPDAMPQTIEEDFNAHYGPETHPAE-----
R.sphaeroides      407 LPILGAIEKPVAPPATIEEDFNAHYSPATGGTKTVVAE
R.capsulatus       407 LPLLGATEKPEPIPASIEEDFNSHYGNPAE--------
P.berghei          360 LVQNKKTHYDYSSQANI----------------------
P.falciparum       360 LVHYRRTHYDYSSQANI----------------------
C.reinhardtii          ---------------------------------------
M.laminosus            ---------------------------------------
consensus          421 .. .. ..      . .
```

APPENDIX 2

A.2. Theoretical investigation of the Q_o site mechanism

In this study the protonation behavior of the yeast cytochrome bc_1 complex was investigated by continuum electrostatics calculations. This work was carried out by diploma student Astrid Klingen under the supervision of Prof. Dr. Matthias Ullmann using the atomic models of the HHDBT (pdb entry 1P84) and stigmatellin (pdb entry 1KB9) inhibited cytochrome bc_1 complex (see *diploma thesis, Astrid Klingen*).

A.2.1. Protonation probabilities of catalytic residues

The transmembrane part of the enzyme was estimated from the position of tightly bound phospholipids in the X-ray structures. The titration behavior of enzyme residues was investigated before and after adding the membrane model. It was not surprising to find that addition of the membrane model affected the protonation probabilities of residues located at the membrane-aqueous interface. More specifically, 29 of 550 titratable residues per monomer displayed different titration behavior upon addition of the membrane. Calculations were also carried out on the structures with and without the antibody fragment Fv18E11 bound. The protonation behavior of the residues $Asp133^{Rip1p}$ and $Asp149^{Rip1p}$ was affected by removal of Fv18E11. These residues were shown by structural analysis to participate directly in antibody-antigen interactions (see Table 3, *section 2.2.4*).

Protonation probabilities of residues in the X-ray structures of the enzyme with stigmatellin or HHDBT bound at the Q_o site were compared. Initial calculations showed that, except for the catalytic residue Glu272, the other residues suggested in the proposed proton exit pathway from the Q_o site (see *section 3.3*) did not change their protonation pattern. Furthermore, the heme b_L propionate A was found to be deprotonated in the oxidized enzyme. Interestingly, the titration behavior of the structurally resolved phospholipids, suggested that the phosphates stably carry a negative charge and the lipid head groups did not appear to titrate.

The titration behavior of the catalytic residue Glu272, the primary ligand of stigmatellin, was highly sensitive to Q_o site occupancy. The protonation probability of Glu272 was lower when it was rotated into the binding site to form a hydrogen bond to stigmatellin. In the stigmatellin inhibited enzyme, Glu272 titrated with a pK_a of 6.8

and the protonation profile was not influenced by addition of the membrane model. On the other hand, in the HHDBT inhibited enzyme, the carboxylate side chain of Glu272 is rotated away from the active site and points towards a more hydrophilic environment, where it forms a hydrogen bond to the imidazole ring of His253. Without the membrane model, Glu272 was found to be deprotonated and His253 titrated with a pK_a of ~11. However, after adding the membrane, the protonation probability of Glu272 increased, whereas His253 appeared stable in the singly protonated imidazolate form.

Furthermore, Q_o site occupancy affected the titration behavior of $His343^{Cobp}$ that was especially sensitive to the exchange of HHDBT against the modeled substrate, ubiquinol. In structural context, $His343^{Cobp}$ is close to the Q_o site and forms contacts to cytochrome c_1 residues. Interestingly, $His343^{Cobp}$ is within *van der Waals* distance to $Ser268^{Cobp}$, which is in contact with the intermembrane space lipid (L6) (see *section 2.5.1*).

In agreement with spectroscopic and X-ray structural evidence (Palsdottir *et al.*, 2003), the titration curve of HHDBT when bound at the Q_o site showed that it is likely to be deprotonated at all the investigated pH values.

A.2.2. Theoretical treatment of the reaction mechanism

Studies on model compounds suggest that oxidation of QH_2 to QH_2^+ or deprotonation of QH_2 to QH^- (pKa ~ 11.3) are unlikely first events in catalysis at the Q_o site (Rich, 1984). In contrast, the ubisemiquinone radical ($QH^{\cdot}$) appears readily deprotonated (pK_a~5.9) to form the ubisemiquinone anion ($Q^{\cdot -}$), which is a strong reductant.

Here, reaction energies for the first events in quinol oxidation were calculated at pH 8.0. Ubiquinol was modeled into the site based on the mechanistic scheme of single occupancy (see Hunte *et al.*, 2003). Preliminary results showed that stabilization of a fully deprotonated semiquinone anion ($Q^{\cdot -}$) at the Q_o site is energetically feasible. The binding mode of HHDBT at the Q_o site is proposed to mimic this reaction intermediate (Palsdottir *et al.*, 2003).

The obtained reaction energies will serve as inputs for Marcus theory based methods to obtain rate constants for the reactions involved in Q_o site catalysis (A. Klingen, *in progress*).

APPENDIX 3

A.3 Structural analysis of the Rieske-cytochrome *b* interface in the yeast X-ray structures

A structural study of the catalytically important interface of cytochrome *b* and Rieske was carried out to characterize the atomic interactions within and between monomers A and B of the functional homodimer (A-B).

Comparison of the Rieske-cytochrome *b* interfaces in the structures of the HHDBT (PDB entry 1P84) and stigmatellin (PDB entry 1KB9) inhibited enzymes showed no major differences in the outcome of buried surface area calculations (see *section 4.13.6*). The area of Rieske-cytochrome *b* interaction within monomer A, was 1135.9 $Å^2$ for the stigmatellin inhibited enzyme and roughly the same, or 2.3 $Å^2$ greater when HHDBT was bound. The surface area of interaction between cytochrome *b* from monomer A and Rieske protein from the other monomer B (Rieske*) was 2292.0 $Å^2$ when stigmatellin was bound, and similar or 46.5 $Å^2$ greater when HHDBT was bound. This is still a negligible difference and corresponds to half the surface area of a free Gly residue (80 Å).

Table A3 Structural study of polar interactions between Rieske and cytochrome b. *Rieske and cytochrome b residues from the same monomer (A-A) contact at the „linker", i.e. a stretch of amino acids that connects the Rieske soluble domain to its transmembrane region. Polar interactions between cytochrome b from monomer A and Rieske* from the other monomer B in a homodimer (A-B), i.e. in a functional unit, occur both at the docking interface that is called „crater" on cytochrome b (the site of quinol oxidation), as well as at the linker where Rieske is tethered in the enzyme. Structural water molecules (Wat) that form hydrogen bond bridges at the interface are marked with the arrow pointing to cytochrome b residues (>).*

Monomer A Rieske linker	**Monomer A Cytochrome *b* (Pivot point)**	**Monomer B Rieske***	**Monomer A Cytochrome *b* (Crater)**
Thr77(O)	Asn74(Nδ2)	Cys159(O)	Wat338>Wat383>Lys288(Nz)
Ser80(Oγ)	Asn74(Nδ2)	His161(O)	Lys288(Nz)
Ser81(O)	His53(Nε2)>Wat17	His161(Nε2)	Wat16>Lys288(O)
	Wat66>His73(N)	Leu162(O)	Asn149(Nδ2)
Ser81(O)	Wat66>His73(Nε2)	Val165(N)	Thr265(Oγ1)
Thr83(O)	Wat66>His73(N)	Cys180(O)	Tyr279(OH)
Thr83(Oγ1)	His73(Cδ2)	Pro195(O)	Wat292>Lys288(N)
Thr85 (N)	Wat262>Wat15	Wat16	Wat264>Leu282(O)
Thr85 (Oγ)	Wat15>Wat17	Wat16	Wat264>Ile285(O)
Asp84(O)	His73(Nε2)	**Rieske*linker**	**Cytochrome *b* (Pivot point)**
Ala86(N)	Asp71(O)	Ile79(O)	Trp164(Nε1)
Asp87(Oδ1)	His67(Cε1)>Wat17	Met82(O)	Arg178(NH1/NH2)
Wat17	Wat53>Met52(O)	Ala84 (N)	Wat252>Ser163(O)

The interface of cytochrome *b* from one monomer (A) and Rieske* from the other monomer (B) in a functional unit is characterized by a number of nonpolar forces and a few polar interactions (Table A3) contributed by residues that reside in two regions of catalytic importance, namely the *cd* loop (W142, T145, V146, N149, L150, W164, G167, F169, R178) and the *ef* loop (P262, L263, T265, P266, A267, I269, Y279, L282, R283, P286, K288, V344) of cytochrome *b*. The Rieske* residues that contribute at the interface are either in the linker region (I79, M82, A84, A90, M91) or at the tip of the soluble domain that encloses the site of quinol oxidation (P115, T160, H161, L162, G163, C164, V165, I167, P179, C180, H181, G194, P195).

Particularly interesting at the catalytic cytochrome *b*-Rieske* interface are the polar interactions of $Cys180^{Rip1p*}$ and the [2Fe-2S] cluster ligand $His161^{Rip1p*}$ with cytochrome *b* residues. The conserved $Cys180^{Rip1p*}$ is involved in the disulfide bond, which stabilizes the fold of the Rieske domain (Cys180~Cys164) at the [2Fe-2S] cluster containing tip. Disruption of that disulfide bond is detrimental to quinol oxidation reaction.

APPENDIX 4

A.4 Structural comparison of cytochrome bc_1 complex from bovine and yeast

Structural alignment of the high resolution X-ray structures of the cytochrome bc_1 complex from yeast (Hunte *et al.*, 2000; Palsdottir *et al.*, 2003) and bovine (Gao *et al.*, 2002; Gao *et al.*, 2003) was carried out. For comparison of main chain displacements, superimposition of the Cα trace was performed. Based on sequence alignment, species-specific structural differences were distinguished from ligand induced conformational changes (see sequence alignment in *Appendix A.1*). The highly conserved *cd* (residues 138-166) and *ef* (residues 246-288) loops display Q_o site occupancy-induced structural differences in their main chain conformation (Fig. A4). The polypeptide region from residues ~200-250, on the other hand, probably exhibits species-specific structural differences, due to a less conserved stretch of amino acids, and the fact that the residues in this segment do not directly contact the Q_o site occupant. Interestingly, the flexible loop, which exhibits greatest displacement when comparing the structures of the HHDBT and stigmatellin inhibited yeast enzymes (see *section 2.3.6*), also turns out to be the site of major displacement in this cross-species structural comparison.

Structural alignment of the bovine enzymes with different ligands and substrate analogs bound, showed that Q_i site occupancy did not markedly induce great conformational changes. For instance, structural alignment of native (*i.e.* Q_o site empty) and antimycin inhibited bovine enzymes, showed a displacement of ~1.1 Å at His267 (corresponds to Ser268 *in yeast*) and His221 (His222 *in yeast*). Likewise, when comparing the structures of the bovine enzyme with antimycin and CoQ_2 bound, the only pronounced displacement was ~1.2 Å for these same residues. Comparison of the native bovine enzyme to the structure of the enzyme with NQNO bound, revealed displacements in the conserved residues: Val145, Ile146, and His221 (bovine numbering).

In the case of the Q_o site occupied with CoQ_2 and NQNO, respectively, displacements were observed at the conserved *cd* loop residues: Val145 and Leu149. Residues that contact NQNO are the conserved residues: Met138, Gly142, Leu145, Ile146, Pro270 and Phe274. These residues all contact HHDBT and stigmatellin, in the

structures of the yeast enzyme (see *section 2.3.3*). Interestingly, comparison of famoxadone inhibited and native bovine structures ($RMSD_{C\alpha}$ 0.508Å^2) shows greatest main chain displacement at Gly251-Asn255 and His267-Glu271. The latter region of conformational flexibility coincides with the most pronounced main chain displacement when comparing the structures of the stigmatellin and HHDBT inhibited yeast enzyme (Fig. 21). Notably, the greatest side chain displacement when comparing native and famoxadone inhibited bovine enzyme was observed for Asp252, which corresponds to yeast residue His253 (see *Appendix A.1*). Strikingly, His253 also shows the most pronounced side chain displacement when comparing the structures of stigmatellin and HHDBT inhibited yeast enzymes (Fig.21).

The key conclusion from this comparative X-ray structural analysis is that the regions of greatest main chain and also the most pronounced side chain displacements coincide. Thus, these observations point to conserved features in conformational flexibility of the enzyme.

Table A4 Main chain displacements in structural alignment of cytochrome b

PDB entry*	Inhibitor	Å	RMSD (Å^2)	Main chain displacement (max Å)
S.cerevisiae				
1KB9	Q_o, stigmatellin	2.3	-	-
1P84	Q_o, HHDBT	2.5	0.234	A267-V270 (1.7)
B.Taurus				
1LON	Native	2.6	0.790	V146-T148(1.7), V157(1.8), I161-S170(1.9), L230-T232(1.4), H253-N256(3.3), A267-P271(2.5), L302-L305(1.1), E345-Y348(1.4), A361-L364(1.7), P367-P368(1.6)
1LOL	Q_o, famoxadone	2.4	0.693	G143-T148(1.2), I154-V157(1.5), F169-V171(1.5), G260(1.9), S268-I269(2.8), 304-F307(1.4), A361-F363(1.6)
1NTM	Native	2.4	0.716	V146-Thr148(1.4), I154-G158(1.5), V162-W164(1.0), F169(1.7), L238-L240(1.7), S268-P271(1.9), L300-L302(1.1), H343-P347(1.9), A361-L364(1.8)
1NTK	Q_i, antimycin	2.6	0.757	V146-T148 (1.6), I154-G158(1.3), F169(1.7), L238-L240(1.5), A267-P271(3.0), L303-L305(1.3),H343-Y348(1.6)
1NTZ	Q_o/Q_i, CoQ_2 (partial)	2.6	0.728	V146-T148(1.2), V162-W164(1.1), F169(2.0), L230-T232(1.1), I239(1.7), S268-P271(2.3), A341-P347(2.0), A361-L364(1.7)
1NU1	Q_o/Q_i, NQNO (partial)	3.2	0.755	P155-G158(1.5), F169 (1.5), L230-T232(1.3), L238-242(1.9), A267-V270(2.1), L300-D309(1.5), E345-V346(2.1), A361-L364(1.9)

*Differences are displayed according to the criteria of spatial separation of more than 1 Å over a span of more than 2 amino acids, except where single residue Cα-trace displacement exceeds 1.5 Å. *1KB9: Hunte et al., 2000; 1P84: Palsdottir et al., 2003; 1LOX: Gao et al., 2002; 1NXX: Gao et al., 2003.*

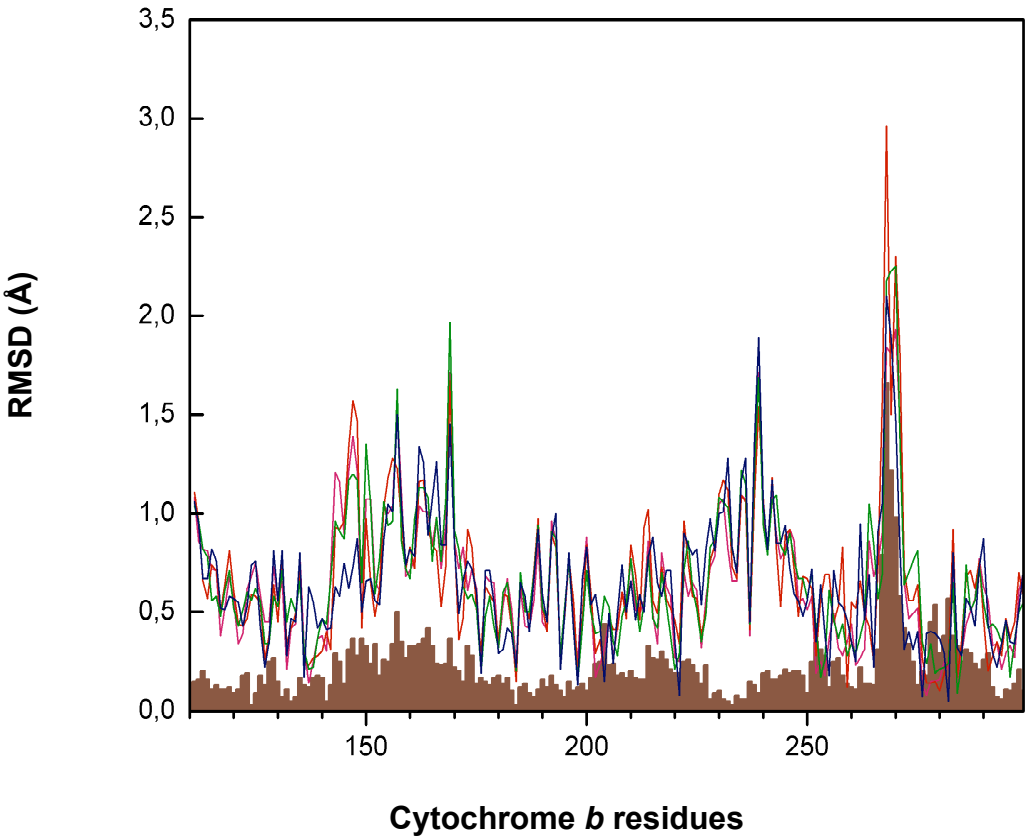

Fig. A4 Conformational flexibility of cytochrome b. *Cα trace displacement is depicted as RMSD (Å^2) for the span of residues from cytochrome b amino acids 50-300. The observed differences in main chain conformation may be derived from ligand induced changes shown as brown columns for the structural comparison of stigmatellin and HHDBT inhibited yeast cytochrome bc_1 complex. Cross-species comparison has to take into account sequence specific variations. Shown here is structural superimposition of the stigmatellin inhibited yeast enzyme with the X-ray structures from the bovine enzyme, drawn as lines (see Table A4 for details); magenta (native), red (antimycin), green (CoQ_2), and blue (NQNO). Note that only partial occupancy was obtained for CoQ_2 and NQNO.*

APPENDIX 5

A.5 Stabilizing interactions with the phosphodiester moiety of tightly bound phospholipids identified in X-ray structures of integral membrane proteins

Preferential stabilization of phospholipids at the *negative* side of the membrane was observed. A first attempt to identify lipid head group specific binding motifs was made (from Palsdottir and Hunte, *in press*).

Table A5 Ligands of the anionic head group of tightly bound phospholipids in X-ray structures of integral membrane proteins. *Amino acid side chains that contact the phoshodiester group of tightly bound phospholipids are shown. Residues within 4.5 Å distance from the phosphodiester group are listed. Primary ligands with atomic contacts at a distance of less than 3 Å are marked with bold. The abbreviations n and p denote the negative and positive leaflet of the bilayer, respectively. Also shown are ligands of a sulfolipid (SL).*

Lipid	Amino acid	Protein		Species	PDB entry	Res.(Å)
PE	KT	BC1	*n*, annular	*G.gal.*	1BCC	3.2
PE	**Y**QT	BC1	*n*, same binding site as L4	*G.gal.*	1BCC	3.2
PE	**Y**NYQK	BC1	*n*, annular, **L4**	*S.cer.*	1KB9	2.3
PE	**N**	BC1	*n*, dimer interface, **L2**	*S.cer.*	1KB9	2.3
PE(4)	**R**HS;**R**W;**R**; K	COX	*n*	*R.sph.*	1M56	2.3
PE(2)	**R**; **K**R	COX	*n*	*B.tau.*	1V54	1.8
PE	**KY**R	RC	*n*	*T.tep.*	1EYS	2.2
PE	KK	SDH	*n*	*E.col.*	1NEK	2.6
PE(2)	**Q**HK; **Y**Q	COX	*p*	*R.sph.*	1M56	2.3
PE(1)	**T**	COX	*p*	*B.tau.*	1V54	1.8
PC	**S**	BC1	*n*, cavity at dimer interface, **L1**	*S.cer.*	1KB9	2.3
PC	**R**HE	COX	*n*	*P.den.*	1QLE	3.0
PC	H	COX	*n*	*B.tau.*	1V54	1.8
PC(3)	T	AC	*n*	*B.tau.*	1OKC	2.2
PC	**H**S	BC1	*p*	*S.cer.*	1P84	2.5
PC	**R**D	COX	*p*	*P.den.*	1QLE	3.0
PI	**K**ST	BC1	*p*, integral protein lipid, **L3**	*S.cer.*	1KB9	2.3
PG(3)	**R**HS; **RW**	COX	*n*	*B.tau.*	1V54	1.8
PG(3)	**RN**RD; **RS**	PSI	*n*	*S.elo.*	1JBO	2.5
CL	**K, R**H	BC1	*n*, cavity at dimer interface, **L7**	*S.cer.*	*Here*	2.5
CL	**KYK, Y**HN	BC1	*n*, near Q_i site (proton uptake), **L5**	*S.cer.*	1KB9	2.3
CL	RKYD**, H**KK	COX	*n*	*B.tau.*	1V54	1.8
CL	**HR**, KW	RC	*n*	*R.sph.*	1M3X	2.55
CL	**H**RN, **WH**	RC	*n*, lipidic cubic phase	*R.sph*	1OGV	2.4
CL(2)	**S**	AC	*n*	*B.tau.*	1OKC	2.2
CL	NDY**, HN**	COX	*p*	*B.tau.*	1V54	1.8
CL	**NT**, NS	FDH	*p*, interface of adjacent monomers	*E.col.*	1KQF	1.6
DG	**K**S	BR	*n*, important for trimer formation	*H.hal.*	1BM1	3.5
SL	**RK**N	B6F	*n*, sulfolipid, cavity at dimer interface, same position as **L1** and **L4**	*C.rei.*	1Q90	3.1

Resolution, Res.; Cytochrome bc_1 complex, BC1; Cytochrome b_6f complex, B6F; Cytochrome c oxidase, COX; Photosynthetic reaction center, RC; Photosystem I, PSI; Bacteriorhodopsin, BR; ADP/ATP carrier, AC; Formate dehydrogenase, FDH; Succinate dehydrogenase, SDH; Phosphatidyl ethanolamine, PE; Phosphatidyl choline, PC; Phosphatidyl inositol, PI; Phosphatidyl glycerol, PG; Cardiolipin, CL; Phosphatidylglycerophospholipid, DG; Phosphatidic acid, PA; phosphatidylserine, PS; sulfolipid, SL.

Lebenslauf

Hildur Pálsdóttir

Born October 10th 1973 in Copenhagen, Denmark

Academic record

1979-1983	Elementary school, Snælandsskóli, Reykjavík.
1983-1985	Elementary school, Melaskóli, Reykjavík.
1985-1989	Junior High School, Hagaskóli, Reykjavík.
	One term freshman in Gainesville High School, Florida.
1989-1993	Junior college, Menntaskólinn í Reykjavík. Natural Science Line I.
	One term junior in Corvallis High School, Oregon.
1994-1995	Biochemistry, University of Iceland.
1995-1998	B. Sc. Institute of Molecular and Structural Biology University of Århus, Denmark. Supervisor: Kim K. Mortensen.
1998-2000	M. Sc. Institute of Molecular and Structural Biology and Department of Medical Biochemistry, University of Århus, Denmark. External supervisor: Prof. Dr. Julio E. Celis. Internal supervisor: Prof. Dr. Peter Andreasen.
2000-2004	Ph. D. Department of Biochemistry, Johann Wolfgang Goethe-University and Max-Planck Institute of Biophysics. External supervisor: Prof. Dr. Hartmut Michel. Internal supervisor: Prof. Dr. Bernd Ludwig.

Scholarships

1998-1999 Danish Government Sholarship for foreign nationals.

1999-2000 Research scholarship from the Danish Cancer Society.

Selected Meetings

2004 Molecular Bioenergetics Sonderforschungsbereich 472, Feb. 23-25.

2003 Poster at the Gordon Research Conference on Molecular & Cellular Bioenergetics, June 22-27.

2002 2 posters at the 12th European Bioenergetics Conference, Sept. 10-15.
9th International Conference on the Crystallization of Biological Macromolecules, March 23-28.

1999 Poster at VII Danish Cancer Society Symposium, August 22-25.
Meeting of Center for Molecular Gerontology/Aging Research, Dec. 6-7.
Talk at meeting of The Danish Centre for Molecular Gerontology, April 9.

1998 Poster at EMBO Workshop: Talking Proteins, Sept. 16-19.
Poster at 25th Silver Jubilee FEBS Meeting, July 5-10.

1997 EMBO workshop: Frontiers of Molecular Biology, Oct. 26-28.
EMBL summer school for Denmark, May 13-15.

ACKNOWLEDGEMENTS

I would like to thank all the current and former members of the Max-Planck Institute of Biophysics, with whom I shared these invigorating four years of my life:

Prof. Dr. Hartmut Michel for giving me the opportunity to join the Department of Molecular Membrane Biology, for his support, and for his profoundly interesting discussions on so many diverse topics.

Dr. Carola Hunte for her supervision, for giving me the opportunity to participate in exciting interdisciplinary projects, for expanding my horizons, and for stimulating discussions.

Prof. Dr. Bernd Ludwig for his academic support and for taking the responsibility of external supervision.

Dr. Petra Hellwig and Dr. Michaela Ritter for a memorable journey through the maze of bands and a very pleasant collaboration.

Dr. Hideto Myioshi for providing the labeled inhibitors for the FTIR studies.

Prof. Dr. Matthias Ullmann and Astrid Klingen for carrying out the electrostatic calculations, for introducing me to theoretical thinking, and for an enjoyable collaboration.

Oliver Anderka and Thomas Kleinschroth for their interesting viewpoints and for vivid discussions.

Prof. Dr. Bernhard Trumpower and his team for a fruitful collaboration and an enjoyable visit to Dartmouth.

Prof. Dr. Etana Padan and Prof. Dr. Wolfgang Junge for inspiration.

Prof. Dr. Julio Celis and his group for their ongoing support.

Thanks to Christian and Daniela for getting me started, Sofia for always helping out, Hanne and Conny for their patient assistance. Roy, Ulli and Eberhard for the crystallographic advice. Also, thanks to Ian, Inge, Vinoth, Björn, Sabine, Christiane, Nils, Miro, Syed, Sozanne, Shweta, Sebastian, Tina, Marc, Emiliano, Paolo, Cécile, Nicolas, Christoph(s), Stephen, Danka, Darui, Guohong, Ankita(s), Vasundara, Arun, Sachin, Chitra, Alex, Elena(s), Lucia, Kerstin, Kristina, Hanno, Tomaso, Dagmar, Eva(s), and my splendid office mate Mauro.

Special thanks to Paolo, Günther, Barbara, and Lutz, for their sincere and truthful support, and to Solveigh and Rosemarie for their moral support in the library during

the writing of this thesis. Surely, I forgot to mention many, so I hereby apologize and thank you, too.

Particular thanks to Gregor for his solid and immeasurable support, for cheering me on, and for adding an exhilarating chapter to my memoirs.

Life outside the lab would be nothing without my heartfelt friends: my dear Luana, Matteo, Emanuela, Gianni, Sladjana, Mihnea, Laura and Elena, Rene, Nadine and Leo. Thank you for all the moments of deep joy and happiness, and for your friendship in times that demanded self-exploration and maturation. To Mihnea for encouraging me to explore the paths of lower resolution. To the brave Ana and to Lena for their kind hospitality during the Niederrad days.

Unique thanks to my wonderful friend Fulga, for her deep friendship, infinite support, and for the many inspiring magical moments. To Bata for patiently sharing his views on arts, politics, and philosophy. Thanks to Branko, Clara, Vladi and the unborn Marianov for good vibrations, and especially to Dora, who provided the fuel to succeed. Thanks to my friends from far away, Sesselja for artistic input, Nanna, Vala and the sewing club, Steini, Krissi, Ricardo and Nos. Thanks to Manfred, Michaela and Natasha for the kind welcome to Berkeley. Also, thanks to Francis, Patrick, Jhoanna, Stephanie and Sophia for their congenial spirits.

Exceptional thanks to Terry for his tireless encouragement, his wisdom and warmth.

Most heartfelt thanks to my family for their love, patience, and understanding.

Very special thanks to Mr. Okandan for his high quality printing and kind help.

Finally, I would like to thank the Max-Planck Society and the German Research Foundation (SFB 472) for their generous financial support.